

**PROTON TUNNELLING IN RIBOSOMAL PEPTIDE BOND  
FORMATION**

**HADIEH MONAJEMI**

**FACULTY OF SCIENCE  
UNIVERSITY OF MALAYA  
KUALA LUMPUR**

**2018**

PROTON TUNNELLING IN RIBOSOMAL PEPTIDE BOND  
FORMATION

HADIEH MONAJEMI

THESIS SUBMITTED IN FULFILMENT OF THE  
REQUIREMENTS FOR THE DEGREE OF  
DOCTOR OF PHILOSOPHY

DEPARTMENT OF PHYSICS  
FACULTY OF SCIENCE  
UNIVERSITY OF MALAYA  
KUALA LUMPUR

2018

UNIVERSITI MALAYA

**ORIGINAL LITERARY WORK DECLARATION**

Name of Candidate: **HADIEH MONAJEMI**

Registration/Matric No: **SHC110039**

Name of Degree: **DOCTOR OF PHILOSOPHY**

Title of Project Paper/Research Report/Dissertation/Thesis (“this Work”):

**PROTON TUNNELLING IN RIBOSOMAL PEPTIDE BOND FORMATION**

Field of Study: **COMPUTATIONAL BIOPHYSICS AND BIOCHEMISTRY**

I do solemnly and sincerely declare that:

- (1) I am the sole author/writer of this Work;
- (2) This Work is original;
- (3) Any use of any work in which copyright exists was done by way of fair dealing and for permitted purposes and any excerpt or extract from, or reference to or reproduction of any copyright work has been disclosed expressly and sufficiently and the title of the Work and its authorship have been acknowledged in this Work;
- (4) I do not have any actual knowledge nor do I ought reasonably to know that the making of this work constitutes an infringement of any copyright work;
- (5) I hereby assign all and every rights in the copyright to this Work to the University of Malaya (“UM”), who henceforth shall be owner of the copyright in this Work and that any reproduction or use in any form or by any means whatsoever is prohibited without the written consent of UM having been first had and obtained;
- (6) I am fully aware that if in the course of making this Work I have infringed any copyright whether intentionally or otherwise, I may be subject to legal action or any other action as may be determined by UM.

Candidate’s Signature

Date: **28.03.2018**

Subscribed and solemnly declared before,

Witness’s Signature

Date: **28.03.2018**

Name:

Designation:

# PROTON TUNNELLING IN RIBOSOMAL PEPTIDE BOND FORMATION

## ABSTRACT

Proton transfer reactions are simple yet important reactions which have been immensely investigated in different studies due to their dominance in many chemical and biochemical systems. The dual wave-particle nature of protons enables them to tunnel through classically high potential energy barriers. Being temperature independent, proton tunnelling can occur at any temperature. Hence, many studies have suggested that some enzymatic reactions with high energy barriers go through proton tunnelling. However, the occurrence of tunnelling has not yet been investigated in one of the most puzzling enzymatic reactions, i.e. the process of peptide bond formation in a large complex enzyme called the ribosome. A large part of this study aims to investigate the tunnelling behaviour in this mechanism using computational quantum chemistry tools and theoretical methods. We proposed three novel proton transfer mechanisms for this reaction which are based on three different crystallographic structures. Using density functional theory, we first obtained the structural and physical information about these reaction mechanisms. The rate of these reactions were then calculated using reaction rate theories with classical motion approximation. Ultimately, the tunnelling correction was calculated numerically and added to the classical reaction rate to investigate the tunnelling behaviour of proton. The results show that in one of our novel proposed mechanisms, the ribosome induces tunnelling by thinning the energy barrier width through shortening the proton donor-acceptor distance. This explains the unexpectedly high rate of ribosomal peptide bond formation. Using this idea, we attempted to induce tunnelling in a synthetic reaction and increase its efficiency. For this purpose, we studied the reaction of boronic acid with diols which is important in designing an efficient non-enzymatic glucose sensor for blood glucose monitoring applications. The

results indicate that one way to induce tunnelling through decreasing the donor-acceptor distance is to increase the electronegativity of the R-group. The transition structure for the highest electronegative R-group exhibits the shortest proton path from boronic acid to diol. The direct correlation of the electronegativity and the tunnelling corrected reaction rate further supports the importance of the lower donor-acceptor distance in inducing tunnelling.

**Keywords:** Quantum Biology, Proton Tunnelling, Chemical Kinetics, Ribosomal Peptide Bond Formation, Boronic Acid Glucose Sensor.

University of Malaya

***PENEROWONGAN PROTON DALAM PEMBENTUKAN IKATAN PEPTIDA DI  
DALAM RIBOSOM***

**ABSTRAK**

Tindak balas pemindahan proton adalah tindakbalas yang mudah namun penting dan telah banyak dikaji disebabkan ia banyak mendominasi tindakbalas di dalam pelbagai sistem kimia dan biokimia. Sifat dwi gelombang-zarah proton membolehkannya untuk menjalani proses penerowongan melalui halangan tenaga keupayaan yang tinggi secara klasik. Tindakbalas ini bebas daripada pengaruh suhu dan boleh berlaku pada sebarang suhu. Oleh itu, banyak kajian telah mencadangkan beberapa tindak balas enzim yang mempunyai halangan tenaga keupayaan yang tinggi berlaku melalui penerowongan proton. Namun begitu, proses penerowongan masih belum dikaji secara mendalam dan tindakbalas yang paling bermasalah adalah proses pembentukan ikatan peptid dalam enzim kompleks yang besar yang dipanggil ribosom. Sebahagian besar dari kajian ini mempunyai matlamat untuk mengkaji tingkah laku penerowongan dalam mekanisme ini dengan menggunakan kaedah teori pengkomputan secara kimia kuantum. Berdasarkan kajian ini, kami mengesyorkan tiga mekanisme pemindahan proton untuk tindak balas berdasarkan tiga struktur kristalografi yang berbeza. Menggunakan teori fungsi ketumpatan, maklumat struktur dan fizikal mengenai mekanisme tindak balas ini dapat diperolehi. Kelajuan tindak balas ini dikira menggunakan teori kadar tindak balas dengan gerakan penghampiran klasik. Akhirnya, pembetulan penerowongan dikira secara berangka dan ditambah kepada kelajuan tindak balas klasik untuk mengkaji tingkah laku penerowongan proton. Keputusan menunjukkan bahawa dalam salah satu dari mekanisme baru yang dicadangkan, ribosom mengaruhkan penerowongan proton melalui penipisan kelebaran halangan tenaga keupayaan dan ini memendekkan jarak antara proton penderma dan penerima. Ini menjelaskan kadar pembentukan ikatan

peptid di dalam ribosom yang tinggi. Menggunakan idea ini, kami telah mencuba untuk menginduksi penerowongan dalam sebuah tindak balas sintetik untuk meningkatkan efisiensinya. Untuk tujuan ini, kami mengkaji tindak balas asid boronik dengan diol yang cukup penting dalam mereka bentuk sensor bukan-enzim glukosa untuk aplikasi pemantauan glukosa darah. Dapatan kajian menunjukkan cara untuk mendorong terowong adalah melalui pengurangan jarak penderma-penerima untuk meningkatkan elektronegatifan kumpulan R. Struktur peralihan yang mempunyai keelektronegatifan R-kumpulan yang tinggi mempamerkan laluan proton yang singkat dari asid boronik ke diol. Korelasi keelektronegatifan dan kelajuan penerowongan menunjukkan tindakbakas terkait rapat dengan jarak penderma-penerima dalam mendorong penerowongan.

**Kata Kunci:** Biologi Kuantum, Penerowongan Proton, Kinetik Kimia, Pembentukan Ikatam Peptida Ribosom, Sensor Glukosa Asid Boron.

## ACKNOWLEDGEMENT

It is not easy to show the depth of my gratitude towards my supervisors and mentors Prof. Wan Ahmad Tajuddin Wan Abdullah, Prof. Sharifuddin Mohammad Zain and my advisor Dr. Toshimasa Ishida. I am deeply grateful for all the thoughtful toughness and hardship that I received from Prof. Wan without which, I wouldn't have had the insight I am having today. I thank him for all the difficult and challenging discussions we had which led me to a unique way of thinking and solving problems. I am deeply grateful for Prof. Sharifuddin's invaluable advice and guidance which illuminated my path towards a bright future. The path he showed me was not a short or easy path, but a path full of challenges which taught me a lot of new things. I am deeply grateful to my advisor Dr. Toshimasa who taught me how to do research in an ideal and perfect manner and patiently guided me towards a deeper understanding of science.

I would like to show my greatest appreciation to Prof. Yatimah Alias for advising me in Boronic Acid research and providing me with the financial support from High Impact Research Grant UM.C/625/1/HIR/MOE/F00004-21001 of Ministry of Education Malaysia. I would also like to thank the Institute of Research Management and Consultancy of University of Malaya (PS018-2012A), and University of Malaya Fundamental Research Grant Scheme (FP047-2016) for giving me financial support and providing me with research facilities. I thank Pusat Teknologi Maklumat, Data Intensive Computing Centre and Puan Sania Ariffin for providing the computer resources. A special thanks to my friends and lab mates with whom I had progressive discussions on various topics, Sidiq, Anuar, Ephrence, Mirah, Jannah...

I dedicate this thesis to my father, my love, my life, my everything...

## TABLE OF CONTENTS

<b>ABSTRACT.....</b>	<b>iii</b>
<b>ABSTRAK.....</b>	<b>v</b>
<b>ACKNOWLEDGEMENT.....</b>	<b>vii</b>
<b>TABLE OF CONTENTS.....</b>	<b>viii</b>
<b>LIST OF FIGURES.....</b>	<b>xi</b>
<b>LIST OF SCHEMES.....</b>	<b>xiv</b>
<b>LIST OF TABLES.....</b>	<b>xvi</b>
<b>LIST OF SYMBOLS AND ABBREVIATIONS.....</b>	<b>xvii</b>
<b>CHAPTER 1: QUANTUM BIOLOGY.....</b>	<b>1</b>
1.1 Introduction.....	1
1.2 Challenges.....	7
1.3 Objectives.....	10
1.4 Thesis.....	11
<b>CHAPTER 2: PROTON TRANSFER REACTIONS-A REVIEW.....</b>	<b>12</b>
2.1 Chemical Kinetics and Reaction Rate Theories.....	12
2.1.1 Calculation of the PES .....	13
2.1.1.1 $H\Psi=E\Psi$ .....	14
2.1.1.2 Density Functional Theory.....	17
2.1.2 Chemical kinetics.....	19

2.1.2.1	Conventional Transition State Theory (CTST).....	20
2.1.2.2	Generalized Transition State Theory (GTST).....	24
2.1.2.3	Quantum Transition State Theory (QTST).....	26
2.2	Proton transfer reactions.....	29
2.2.1	The Central Dogma of Biology.....	31
2.2.2	Boronic Acid as Glucose Sensor.....	45
2.3	Summary.....	48
<b>CHAPTER 3: CALCULATING THE REACTION RATE.....</b>		<b>49</b>
3.1	<i>In Vitro</i> Crystallographic Structures.....	49
3.1.1	Theozyme.....	50
3.2	<i>In Silico</i> Calculations of Reaction Mechanism.....	53
3.2.1	Simulation of the Reaction of Peptide Bond formation.....	54
3.2.2	Simulation of the Reaction of Boronic Acid With Diol.....	56
3.2.3	Model chemistry.....	58
3.2.3.1	The DFT Functionals.....	58
3.2.3.2	Basis Sets.....	63
3.2.3.3	Medium.....	68
3.2.4	Response theory: Gradients, Hessians and Reaction Paths.....	70
3.3	Calculating the Reaction Rates.....	74
3.3.1	Conventional Transition State Theory (CTST).....	75
3.3.2	Tunnelling Corrected Reaction Rate.....	80

<b>CHAPTER 4: RESULTS AND DISCUSSION.....</b>	<b>88</b>
4.1 The important role of P-site A-76 2'-OH as a peptidyl shuttle.....	88
4.1.1 Calculations based on old mechanisms.....	89
4.1.2 Three novel mechanisms proposed in this study.....	97
4.1.2.1 P-I mechanism.....	97
4.1.2.2 P-II mechanism.....	102
4.1.2.3 P-III mechanism.....	105
4.1.3 Ribosomal catalytic role.....	108
4.1.4 Quantum tunnelling in proton transfer reaction during peptide bond formation.....	110
4.2 Mechanistic study of boronic acid's reaction with diols.....	124
4.2.1 Kinetic study of $\text{CH}_3\text{-B(OH)}_2$ and $\text{CH}_3\text{-BOOH}^-$ in reaction with 1,2-ethanediol.....	125
4.2.2 Kinetic study of $\text{CF}_3\text{-B(OH)}_2$ and $\text{CF}_3\text{-BOOH}^-$ in reaction with 1,2-ethanediol.....	130
4.2.3 Comparing the reactivity of $\text{CH}_3\text{-B(OH)}_2$ and $\text{CF}_3\text{-B(OH)}_2$ towards 1,2-ethanediol.....	133
4.2.4 The R-group which results in a better sensor.....	135
4.2.5 Tunnelling effect on proton transfer reaction of boronic acid with diol.....	137
4.2.6 The R-group which results in a better tunnelling.....	145
<b>CHAPTER 5: PROTON TUNNELLING IN BIOCHEMISTRY - A CONCLUSION .....</b>	<b>148</b>
<b>REFERENCES.....</b>	<b>152</b>
<b>LIST OF PUBLICATIONS AND PAPERS PRESENTED.....</b>	<b>173</b>

## LIST OF FIGURES

- Figure 1.1 : The double potential well illustrating the bending motion of the  $\text{NH}_3$  molecule. Following the classical laws of motion, the hydrogen atoms have to go through the transition state which requires a certain amount of energy. However, under certain conditions, the molecules on the left can instantly become the molecule on the right without requiring the energy to reach the transition structure. The only explanation for this phenomenon is quantum tunnelling..... 2
- Figure 1.2 : A) The DNA bases where the adenine pairs with thymine and guanine pairs with cytosine in a normal state. B) The tautomerized states of the DNA bases where the protons went through an intramolecular proton tunnelling in which case, the base pairs are not complementary to one another like those in A..... 3
- Figure 1.3 : The Arrhenius plot indicating the dependence of the rate of reaction on the temperature. A) Divergence from classical behaviour is observed at lower temperatures where the reaction is independent of the temperature. B) Large KIE where there is an apparent gap between the deuterium and hydrogen transfer reaction rates..... 6
- Figure 1.4 : The central dogma of biology: From the top left, the DNA genetic code in the nucleus unwinds  $\rightarrow$  mRNA transcription  $\rightarrow$  protein synthesis in the ribosome..... 6
- Figure 2.1 : The reaction coordinate profile where the  $E_0$  indicates the zero point corrected energy of activation and  $E_c$  indicates the classical energy of activation (Steinfeld, 1999)..... 22
- Figure 2.2 : The schematic view of the trajectories of crossing from the dividing surface over the saddle point (a) and an alternative dividing surface (b) (Laidler, 1984)..... 25
- Figure 2.3 : The A) 3-D and B) 2-D structure of the tRNA molecule..... 32
- Figure 2.4 : The schematic view of the translation cycle: initiation step, elongation cycle, termination step, and recycling (Agirrezabala & Frank, 2010)..... 34
- Figure 2.5 : A) The 50S ribosome (LRS) with proteins in blue, RNA in orange, and the active site in red. B) The protein L27 in blue and the rest of the 50S ribosome (LRS) in grey (PDB: 4W2H). It can be seen that the tail of this protein is extended to the active site which was thought to be directly involved in the reaction..... 35

Figure 2.6 : The structure of the A2451 rRNA residue, located in the active centre (green) of the 50S ribosome with the 23S ribosomal RNA in orange, the 5S ribosomal RNA in yellow and the ribosomal proteins in blue.....	36
Figure 2.7 : The interaction of the N3 of A2451 with the attacking amine in a) (Hansen et al., 2002) and b) (Voorhees et al., 2009) crystallographic structures.....	37
Figure 3.1 : The radial characteristic of the STOs and GTOs, indicating a correct cusp behaviour near the nuclei for the STOs and a wrong cusp behaviour for the GTOs.....	66
Figure 3.2 : The three dimensional PES of the energy change with respect to displacement along two directions.....	71
Figure 3.3 : Minimum energy path profile (Laidler, 1984).....	75
Figure 3.4 : The endothermic potential barrier.....	82
Figure 3.5 : The symmetric Eckart potential barrier.....	84
Figure 3.6 : Transmission coefficient vs. the energy where:	
$\begin{cases} \text{if } E > U_{\ell_{im}} \rightarrow T(E) \approx 1 \\ \text{if } E \leq U_{\ell_{im}} \rightarrow 0 < T(E) < 1 \end{cases}$	86
Figure 4.1 : The transition state coordinates of the stepwise mechanism based on Steitz crystallographic structure (Schmeing et al., 2005) with direct participation of two water molecules and the A2451 ribose in the active site (The schematic view of this mechanism can be observed in Scheme 3.2). Some key interactions of the pre- and post- peptidyl transfer structures are different from the original structure of Steitz after optimization.....	100
Figure 4.2 : The transition state coordinates based on the crystallographic structure of Ramakrishnan and collaborators (Voorhees et al., 2009) for the 6-membered transition structure. (The schematic view of this mechanism can be observed in Scheme 3.2., TS6).....	103
Figure 4.3 : The transition state coordinate for a stepwise mechanism proposed in our study based on the crystallographic structure of Polacek and collaborators (Lang et al., 2008). (The schematic view of this mechanism can be observed in Scheme 3.2. TS1-6 $\rightarrow$ TS2-4).....	107
Figure 4.4 : The Arrhenius plot of the reaction rate of TS4, SW(TS2-4) and P-III mechanism from 53.15 K to 308.15 K. H stands for hydrogen and D stands for deuterium.....	115

Figure 4.5 : The plot of the kinetic isotope effect for the TS4, SW(TS2-4) and P-III mechanism from 53.15 K to 308.15 K.....	119
Figure 4.6 : The Arrhenius plot of the reaction rate of TS4, SW(TS2-4) and P-III mechanism from 253.15 K to 308.15 K.....	120
Figure 4.7 : The plot of the kinetic isotope effect of the reaction rate of TS4, SW(TS2-4) and P-III mechanisms from 253.15 K to 308.15 K.....	121
Figure 4.8 : The Arrhenius plot of reaction rate for the proton and deuterium transfer reaction of $\text{CH}_3\text{-B(OH)}_2$ , $\text{Cl}_3\text{-B(OH)}_2$ , $\text{CBr}_3\text{-B(OH)}_2$ , $\text{CCl}_3\text{-B(OH)}_2$ , and $\text{CF}_3\text{-B(OH)}_2$ with diol from 203.15 K to 308.15 K.....	140
Figure 4.9 : The Arrhenius plot of reaction rate for the proton and deuterium transfer reaction of $\text{CH}_3\text{-B(OH)}_2$ , $\text{Cl}_3\text{-B(OH)}_2$ , $\text{CBr}_3\text{-B(OH)}_2$ , $\text{CCl}_3\text{-B(OH)}_2$ , and $\text{CF}_3\text{-B(OH)}_2$ with diol from 253.15 K to 308.15 K.....	142
Figure 4.10 : The plot of kinetic isotope effect for the proton and deuterium transfer reaction of $\text{CH}_3\text{-B(OH)}_2$ , $\text{Cl}_3\text{-B(OH)}_2$ , $\text{CBr}_3\text{-B(OH)}_2$ , $\text{CCl}_3\text{-B(OH)}_2$ , and $\text{CF}_3\text{-B(OH)}_2$ with diol from 53.15 K to 308.15 K.....	143
Figure 4.11 : The plot of the kinetic isotope effect for proton and deuterium transfer reactions of $\text{CH}_3\text{-B(OH)}_2$ , $\text{Cl}_3\text{-B(OH)}_2$ , $\text{CBr}_3\text{-B(OH)}_2$ , $\text{CCl}_3\text{-B(OH)}_2$ , and $\text{CF}_3\text{-B(OH)}_2$ with diol from 253.15 K to 308.15 K.....	144
Figure 4.12 : The transition structure of boronic acid in reaction with diol in five different R-groups at room temperature. The numbers represent the distance between boron and the oxygen of incoming diol at the first step of reaction.....	146

## LIST OF SCHEMES

Scheme 2.1: Previously proposed concerted and stepwise mechanisms, indicated in valence and core of the scheme respectively. A) Both TS4 and TS6 correspond to the concerted 4-membered and 6-membered mechanisms. TS1-4→TS2-4 corresponds to a 4-membered mechanism in both steps. TS1-4→TS2-6 corresponds to a 4-membered mechanism in the first step and a 6-membered mechanism in the second step, and so on. B) TS8 corresponds to a concerted 8-membered mechanism, while TS1-6→TS2-8 corresponds to a 6-membered one in the first step and an 8-membered one in the second step.....	41
Scheme 2.2: Two possible conjugates of a) trigonal, and b) tetrahedral boronate ion.....	47
Scheme 3.1: Different conditions of constructing a theozyme according to the available information in the enzymes' crystallographic data.....	52
Scheme 3.2: The three mechanisms proposed in this study. The reactant and products are taken from the pre- and post-peptidyl chrystallographic structures of Steitz on the left (Schmeing et al., 2005-b), Ramakrishnan in the middle (Voorhees et al., 2009) and Polacek on the right (Lang at al., 2008).....	55
Scheme 3.3: The five different proposed reaction mechanisms for the reaction of boronic acid with diol.....	57
Scheme 3.4: The self consistent field procedure in Kohn-Sham density functional theory geometry optimization.....	64
Scheme 4.1: The most well-known mechanisms for the formation of peptide bond: a) The concerted TS-4 mechanism, b) The stepwise mechanism with formation of a tetrahedral carbonyl carbon as a central atom binding to both the attacking nucleophile (N <sub>1</sub> ) and the leaving 3'O (O <sub>1</sub> ), c) The concerted 6-member mechanism with the A76 2'-OH as a proton shuttle between (N <sub>1</sub> ) and (O <sub>1</sub> ), d) An 8-member mechanism with three protons <i>in flight</i> : the H <sub>1</sub> from N <sub>1</sub> , the H <sub>2</sub> from 2'-O and the H <sub>3</sub> from water.....	96
Scheme 4.2: Five stepwise reaction mechanisms for methylboronic acid in interaction with 1,2-ethanediol.....	127
Scheme 4.3: Five different reaction mechanisms for trifluoromethylboronic acid in interaction with 1,2-ethanediol.....	131

Scheme 4.4: Different possibilities of the reactivity of boronic acid with diols in different medium and different electronegative R-groups..... 136

Scheme 4.5: Different possibilities of the reactivity of boronate ion with diols in different mediums and different electronegative R-groups..... 137

University of Malaya

## LIST OF TABLES

Table 4.1: The calculated activation free energies and the reaction rates for old mechanisms calculated in this study and other studies. The rate in the SW reaction corresponds to the rate determining step.....	91
Table 4.2: The different transition state coordinates for previously proposed 4-member, 6-member, 8-member and stepwise mechanisms of peptide bond formation in this study.....	95
Table 4.3: The free energies of activation and reaction rates for the three novel proposed reaction mechanisms.....	108
Table 4.4: The tunnelling correction factor ( $\Gamma$ ), width parameter ( $\ell$ ) and tunnelling rate for all proposed mechanisms of peptide bond formation in room temperature.....	112
Table 4.5: The thermodynamic data of the five mechanisms between $\text{CH}_3\text{-B(OH)}_2$ and 1,2-ethanediol.....	126
Table 4.6: The thermodynamic data of the five mechanisms between $\text{CF}_3\text{-B(OH)}_2$ and 1,2-ethanediol.....	130
Table 4.7: The tunnelling correction ( $\Gamma$ ), width parameter ( $\ell$ ) and tunnelling rate for reaction of $\text{CH}_3\text{B(OH)}_2$ with 1,2-ethanediol.....	139
Table 4.8: The tunnelling correction ( $\Gamma$ ), width parameter ( $\ell$ ) and tunnelling rate for reaction of $\text{CF}_3\text{B(OH)}_2$ with 1,2-ethanediol.....	139
Table 4.9: The calculated barrier width for the energy barrier of mechanism M-I-I for all five R-groups.....	145

## LIST OF SYMBOLS AND ABBREVIATIONS

$\Psi$	:	Molecular wavefunction
$\psi_i$	:	Molecular orbital
$H$	:	Molecular Hamiltonian
$h$		Planck's constant
$\hbar$		Planck's constant
$k_B$		Boltzmann constant
$q_{\ddagger}$	:	Activated complex partition function without vibrational motion
$q^{\ddagger}$	:	Activated complex partition function with vibrational motion
$\Delta G^{\ddagger}$	:	Free energy of activation
$\Gamma$	:	Tunnelling component
$\nu$	:	Vibrational frequency of the TS along the reaction
$T(E)$	:	Transmission coefficient
$\ell$	:	Characteristic length of the potential barrier
$\sigma$	:	Imaginary wave number
$\varepsilon$	:	square diagonal matrix of the orbital energies
aa-tRNA	:	aminoacyl-transfer Ribonucleic Acid
BO	:	Born-Oppenheimer
DFT	:	Density Functional Theory
DNA	:	Deoxyribonucleic Acid
CC	:	Coupled Cluster

CI	:	Configuration Interaction
CTST	:	Conventional Transition State Theory
GGA	:	Generalized Gradient Approximation
GTO	:	Gaussian Type Orbital
HF	:	Hartree Fock
IEFPCM	:	Integral Equation Formalism for the Polarizable Continuum Model
KIE	:	Kinetic Isotope Effect
LCT	:	Large Curvature Tunnelling
LDA	:	Local Density Approximation
LRS	:	Larger Ribosomal Subunit
MBPT	:	Many Body Perturbation Theory
MCSCF	:	Multiconfigurational self-consistent field
MD	:	Molecular Dynamics
MEP	:	Minimum Energy Path
mRNA	:	messenger Ribonucleic Acid
PCM	:	Polarizable Continuum Model
PES	:	Potential Energy Surface
PT	:	Proton Tunnelling
PTC	:	Peptidyl Transferase Centre
QTST	:	Quantum Transition State Theory
QST	:	Quadratic Synchronous transit
RRKM	:	Rice–Ramsperger–Kessel–Marcus

SCF	:	Self Consistent Field
SCT	:	Small Curvature Tunnelling
SE	:	Schrödinger Equation
SMD	:	Solvation Model based on Density
SRS	:	Small Ribosomal Subunit
STQN	:	Synchronous Transit Quasi-Newton
STO	:	Slater Type Orbital
TST	:	Transition State Theory
TS	:	Transition Structures
VTST	:	Variational Transition State Theory
YADH	:	Yeast Alcohol Dehydrogenase
ZCT	:	Zero Curvature Tunnelling

# CHAPTER 1

## QUANTUM BIOLOGY

### 1.1 Introduction

The fundamental laws of quantum mechanics, which govern the behaviour of subatomic particles, though rather counter-intuitive to common experience, should however form the basis for the understanding of all macroscopic phenomena. In fact, these laws have started to provide answers to some of the persisting problems in biology (Pullman & Pullman, 1963; Löwdin, 1963, 1965; McFadden & Al-Khalili, 1999; Matta, 2010; Al-Khalili & McFadden, 2014), whereas biological phenomena have always generally been described in classical terms. The wave-particle duality characteristic of subatomic particles (which gave birth to the theory of quantum mechanics) is among those strange behaviour that stands contrary to common sense but is able to explain many strange phenomena.

An important result of this characteristic is a phenomenon known as *quantum tunnelling* which, as an example, can be observed in the bending motion of the  $\text{NH}_3$  molecule. The configurational changes in this motion is a result of 'tunnelling' through the energy barrier of a double potential energy well (Figure 1.1). In quantum mechanics it is allowed to borrow energy  $\Delta E$  for a short time  $\Delta t$  which obeys the Heisenberg uncertainty principle,  $\Delta E \Delta t \sim \hbar$ , where  $\hbar$  is the Planck's constant.

Tunnelling occurs when there is an overlap between the wavefunction of a particle in two minima on the potential energy surface. Lighter particles have a larger de-Broglie wavelength and as a result, a larger overlap which increases the probability of their

existence in the classically forbidden region of the energy barrier (Figure 1.1, the yellow area under the curve). Heavier particles on the other hand, have less or no overlap due to their smaller de-Broglie wavelength. They are not light enough to follow quantum mechanical laws of motion and the only way for them to appear at the other side of the potential energy curve is to follow the classical laws of motion and overcome the energy barrier. This behaviour might sound *counter-intuitive* in a classical system, but it is a common experience for a quantum particle in subatomic systems.

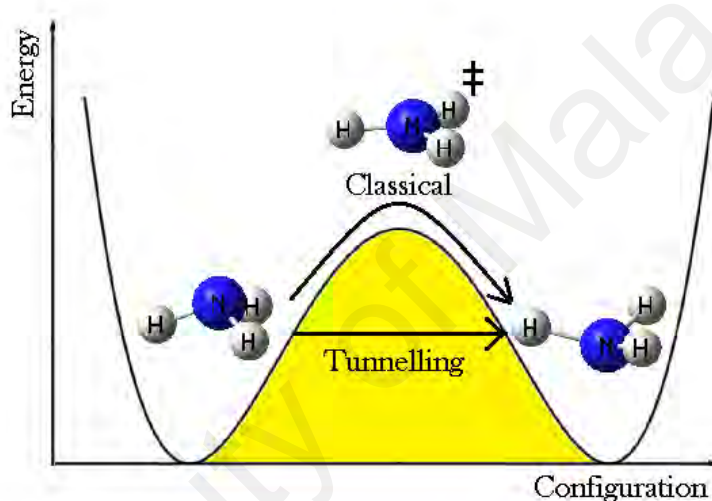


**Figure 1.1: The double potential well illustrating the bending motion of the  $\text{NH}_3$  molecule. Following the classical laws of motion, the hydrogen atoms have to go through the transition state which requires a certain amount of energy. However, under certain conditions, the molecules on the left can instantly become the molecule on the right without requiring the energy to reach the transition structure. The only explanation for this phenomenon is quantum tunnelling.**

Fundamentally, everything is governed by the laws of quantum mechanics and classical mechanics is only a special case of quantum mechanics where the quantum state of the system collapses into classical certainty due to quantum decoherence. Decoherence occurs through the interaction of a quantum system with its surroundings which can be anything from an observer to the hot and noisy biological environment.

Even though the occurrence of quantum behaviour in biological systems might sound contradictory to common sense, there are still some biochemical phenomena that cannot be explained by anything other than quantum effects. For example, in the kinetics of some enzymatic reactions, rates which do not correspond to classical laws of motion have been observed. This can only be explained by considering quantum tunnelling effects in the biochemical reactions. In fact, some biological phenomena have been associated with various quantum mechanical behaviour (Pullman & Pullman, 1963; Matta, 2010).

It was first argued by Erwin Schrödinger in his lectures, published in 1944 that the transfer of genetic information from one generation to the other is quantum mechanical in nature (Schrödinger, 1944). Two decades later, a Swedish physicist named Per-Olv Löwdin introduced a model in which the DNA bases (Deoxyribonucleic Acid) were in a superposition of both tautomerized (Figure 1.2-B) and normal (Figure 1.2-A) states where the proton tunnelling has either occurred or not occurred respectively (Löwdin, 1963, 1965).

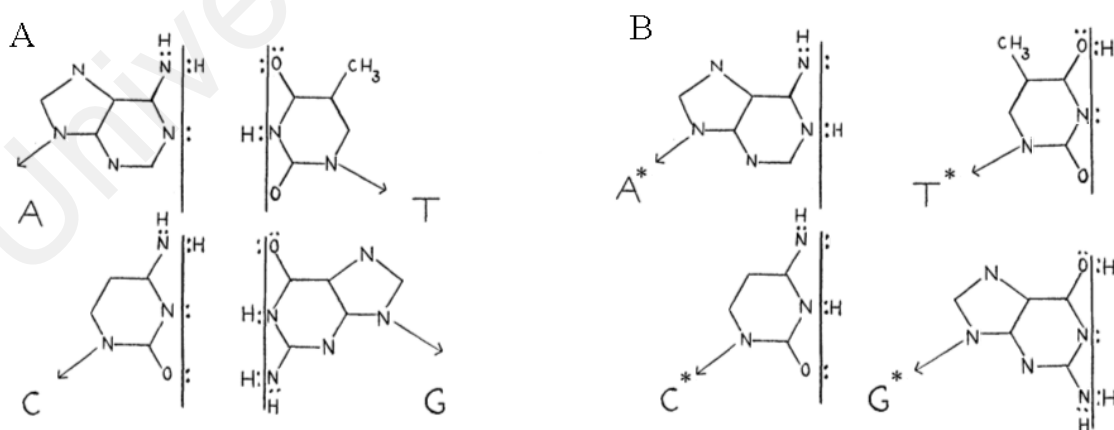


**Figure 1.2: A) The DNA bases where the adenine pairs with thymine and guanine pairs with cytosine in a normal state. B) The tautomerized states of the DNA bases where the protons went through an intramolecular proton tunnelling in which case, the base pairs are not complementary to one another like those in A.**

It was proposed that decoherence occurs upon the interaction of the quantum system with the environment and the wavefunction collapses into either one of the tautomerized and normal states which are equally stable (Brovarets et al., 2013; Brovarets, & Hovorun, 2015). The occurrence of the former state during the DNA replication leads to the production of the tautomeric base pairs and mutated DNA (McFadden & Al-Khalili, 1999; Al-Khalili & McFadden, 2014).

Another important biochemical reaction where quantum tunnelling can play a significant role is the process of proton transfer in enzymes (Matta, 2010). The role of an enzyme in general is to increase the chemical reactivity and the rate of reaction. The origin of this catalysis however, is still unclear (Warshel & Bora, 2016). It is generally believed that the enzymes catalyse the chemical reactions by proper positioning of the substrates in the active site in such a way that the reacting groups are in close proximity to one another in a pre-reaction state (Matta, 2010). Based on this understanding, many different hypotheses have been put forward to describe this catalytic process, among which is the widely studied but yet to be generally accepted dynamical effect proposal (Kohen et al., 1999; Klinman, 2014; Kohen, 2014).

### ***Is dynamical effect proposal valid?***

Dynamical effect proposal has been a subject of many experimental studies to explain the origin of enzymes' catalysis (Olsson et al., 2006). However, as argued by Warshel & Bora (2016), lack of consistency in these studies in terms of significance of dynamical effect on catalysis makes its legitimacy questionable. This lack of consistency arises from the fact that dynamical effect is not a direct observation, rather, it is concluded

from other experimental observations such as active site reorganization or induced fit mechanism, which themselves are still rather ambiguous.

Despite this inconsistency, Klinman and collaborators took one step further and related the enzymatic dynamical effects to tunnelling induced catalysis for the reaction of dehydrogenase catalysed ethanol oxidation in liver alcohol dehydrogenase (ADH) enzyme (Kohen et al., 1999). In this hypothesis, the dynamical motion of the enzyme is coupled with the motion of the transferring proton along the reaction path resulting in minimizing the donor-acceptor distance and enhancing the tunnelling effect. From this, they suggest another enzymatic catalytic role that is, thinning of the barrier width for some proton transfer reactions (Kohen & Klinman, 1998; Kohen et al., 1999, Basran et al., 2001; Ley et al., 2012; Klinman, 2014; Kohen, 2014).

It is worth mentioning that the illegitimacy of the dynamical effect proposal does not by any means dispute the tunnelling induced catalysis in enzymes since the latter can occur due to enzymatic effects other than dynamical effect. This observation opens the debate on whether or not the tunnelling phenomenon is dominant in some enzymatic reactions which involve hydrogen bond proton transfer mechanisms.

The importance of proton tunnelling in such reactions arises when the observed rate of reaction is significantly higher than what is expected from classical mechanics. The occurrence of tunnelling is usually predicted by the observation of a curvature on the Arrhenius plot (Figure 1.3 A) and/or large kinetic isotope effects (KIE) (Figure 1.3 B).

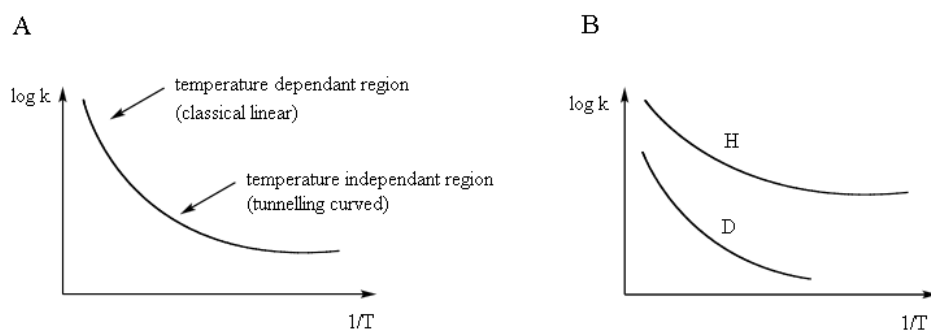


**Figure 1.3: The Arrhenius plot indicating the dependence of the rate of reaction on the temperature. A) Divergence from classical behaviour is observed at lower temperatures where the reaction is independent of the temperature. B) Large KIE where there is an apparent gap between the deuterium and hydrogen transfer reaction rates.**

Among the different types of enzymatic proton transfer reactions, some are associated with unexplained large rates. A well-known example is the process of peptide bond formation which is at the core of biology's most important and vital chemical reaction—the protein biosynthesis process (Massa et al., 2010). This process occurs in a large and complex enzyme called the ribosome<sup>1</sup> (Figure 1.4).

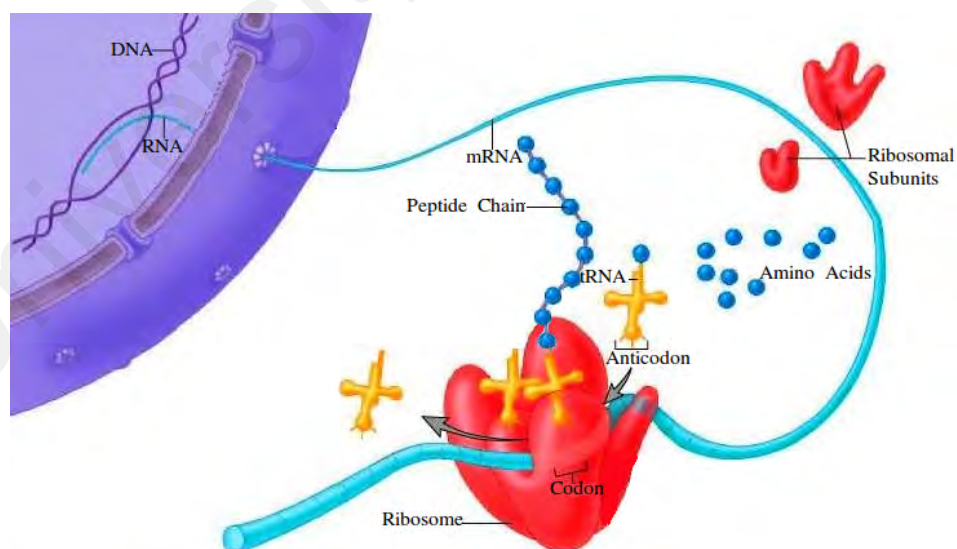


**Figure 1.4: The central dogma of biology: From the top left, the DNA genetic code in the nucleus unwinds → mRNA transcription → protein synthesis in the ribosome.**

<sup>1</sup> A large ribonucleoprotein enzyme that translates the genetic code from DNA into a sequence of amino acids which then folds into a 3D protein structure.

Although it is known that the proton transfer plays a significant role in this reaction; the detailed mechanism and catalytic role of the ribosome during this process is still unknown (Massa et al., 2010; Polikanov et al., 2014). Extensive crystallographic studies had been carried out for nearly two decades which culminated in the award of the 2009 Nobel Prize in Chemistry (Ramakrishnan, 2010; Steitz, 2010; Yonath, 2010). The complex structure of the ribosome as well as the high rate of reaction, however, makes it very difficult to observe the transition from the reactant to the product in a clear picture.

## 1.2 Challenges

A common way to study the mechanism of a chemical reaction is by predicting the transition structure of that reaction using KIE experiments. Several attempts have been carried out to predict the structure of the transition state during ribosomal peptide bond formation (Hiller et al., 2011; Rodnina et al., 2012). However, isotopic effect measurements on the ribosome would be quite difficult due to the large size of both the enzyme and the substrate (Seila et al., 2005). Therefore, simplified models, which do not precisely resemble the real system mechanism, must be used.

Besides the experimental work that had been carried out on the KIE, another way to obtain useful information on the mechanism of a chemical reaction is through the theoretical and computational study of its kinetics (Klippenstein et al., 2014). Theoretical methods which contribute to the understanding of the mechanism of biochemical reactions apply the laws of quantum mechanics to the motion of electrons and nuclei in atoms and molecules (Slater, 1951; Schwinger, 1962). The electronic structure calculations from these methods construct the electronically adiabatic potential energy surface (PES) from which the calculated gradient and curvature can provide

knowledge of the molecular geometry and reaction dynamics along the minimum energy path (MEP).

For certain reactions, knowing the relative stability of the stationary points is sufficient to determine the reaction mechanism without any further investigation (Meana & Fernández, 2010). From the information of the molecule on certain stationary points of the PES, one can calculate the kinetic parameters of the reaction such as the rate constants using the theory of activated complex, otherwise known as the transition state theory (TST) (Laidler, 1984; Steinfeld et al., 1999).

This theory was developed in 1935 by Henry Eyring (Eyring, 1935) and is now widely used in many studies to investigate the mechanism of complex chemical reactions (Truhlar et al., 1996; Åqvist et al., 2012; Xu et al., 2012-b; Klippenstein et al., 2014; Truhlar, 2015 and the references therein). One main challenge in computational chemistry calculations of enzymatic reactions is the size of the system. High accuracy demands high computational power and even the most powerful computers are not able to perform electronic structure calculations on an enzymatic reaction by taking the whole enzyme (in case of large enzymes) into account.

It is therefore very important to properly choose a small enough model system which enables one to employ a very high level of theory, yet large enough to take into consideration the effect of the enzyme on the chemical reaction. In the case of ribosome, this involves around 50 to 100 atoms which is significantly small with respect to the whole enzyme (i.e. around three hundred thousand atoms without the substrates which are themselves five to six thousand atoms).

A few computational and theoretical studies have been carried out on systems that include the active sites of the ribosome (Sanbonmatsu et al., 2005; Trobro & Åqvist, 2006; Sanbonmatsu, 2012; Šponer et al., 2014), however, those studies use Newtonian laws of motion which are not suitable for chemical reactions since these laws do not include electrons in their algorithm. Several other computational studies were carried out employing electronic structure methods that only focuses on the groups which are directly involved in the reaction without considering the surrounding catalytic groups of the ribosomal active site (Wallin & Åqvist, 2010; Wang et al., 2010, 2015; Hiller et al., 2011; Acosta et al., 2012; Xu et al., 2012-b; Byun & Kang, 2013; Świderek et al., 2015).

It is important to consider the effect of the active site groups since it is known that the ribosomal catalytic role in the process of peptide bond formation is chemical in nature (Seila, et al., 2005; Polikanov et al., 2014). Furthermore, none of the previous studies have included the possibility of proton tunnelling, whose effect is of vital importance since as long as there is proton transfer there is always the possibility of tunnelling.

Understanding how enzymes function to enhance the reaction rate is an important step towards inducing enzymatic efficiency into synthetic chemical reactions. One such reaction in particular is the esterification of boronic acids with diols which is also dominated by proton transfer process and might exhibit proton tunnelling. This reaction is important in non-enzymatic glucose monitoring applications and can contribute towards a more stable and accurate glucose sensor. Additional to the study of peptide bond formation (Monajemi et al., 2015), we have also studied the process of proton transfer in the reaction of boronic acid with diol (Monajemi et al., 2014).

### 1.3 Objectives

The main focus of this study is to calculate the tunnelling effect in two types of proton transfer reactions. The mechanisms of these reactions are unclear and need to be evaluated as thorough as possible. To achieve that, this work aspires to:

- 1- Propose rational reaction mechanisms for the proton transfer process that occurs during peptide bond formation using the available crystallographic structures of the active site of the ribosome.
- 2- Propose rational reaction mechanisms for boronic acid esterification reaction with diols.
- 3- Use computational quantum chemistry methods to calculate the critical points of the proposed reaction mechanisms on the PES.
- 4- Calculate the rates of reaction from the information achieved of the critical points for all the proposed reaction mechanisms using transition state theory.
- 5- Assess the tunnelling contribution on the rates of all the proposed reaction mechanisms by calculating their tunnelling correction factors using both numerical and analytical approaches.

We hope that this mechanistic investigation would eventually lead us to a fundamental understanding of the proton transfer mechanisms that occur in the peptide bond

formation process. This can lead us to inducing the tunnelling in non-enzymatic proton transfer reactions, i.e. the esterification of boronic acid in this study.

#### **1.4 Thesis**

This thesis contains five chapters. The next chapter reviews the work that had been carried out by various researchers on the theme studied in this work and gives a brief introduction to the different topics discussed in this thesis. In the third chapter, quantum mechanical methods used in our calculations are discussed and elaborated in detail. Chapter 4, which comprises the results and discussion of the work carried out in this research are divided into two sections. The first section discusses the detailed mechanistic studies of proton transfer during peptide bond formation and the second section discusses the details of the esterification reaction of boronic acid with diols. In each section we elaborate the reaction kinetics and mechanism from both classical mechanics as well as quantum mechanics viewpoints. The final chapter is focused on concluding remarks.

## CHAPTER 2

### PROTON TRANSFER REACTIONS-A REVIEW

The proton is a singly charged ion with no electron outside of its nucleus which makes it rather unique, due to its significantly smaller radius compared to the other charged ions like  $\text{He}^{2+}$  or  $\text{Li}^{3+}$  (Bell, 1973). This characteristic makes the proton transfer reaction quite efficient since it involves the movement of only a nucleus without any attached electron, hence, no electronic repulsive force throughout the transfer. Furthermore, the small size of protons causes low steric requirement during the transfer. Under certain conditions such as high temperature in gas phase or high energy particle bombardments, a hydrogen might transfer instead of proton. Nevertheless, it is rather easy to distinguish hydrogen transfer with proton transfer.

In the field of kinetics, the most important characteristic of a proton is its small mass. As opposed to the other nuclei, the motion of which can be described with sufficient accuracy by the laws of classical mechanics, proton may show deviation from classical behaviour. That is, proton transfer might occur through a phenomenon known as quantum tunnelling.

#### 2.1 Chemical Kinetics and Reaction Rate Theories

The theory of chemical kinetics began to emerge around the 1850s by extensive experimental studies as well as theoretical activities (Wright, 1999). It wasn't however until the early 1930s that this theory started to advance dramatically towards the technical improvements till this day (Klippenstein et al., 2014). Chemical kinetics is an old topic of physical chemistry which investigates the mechanisms of chemical

reactions and assigns the calculated reaction rate constants to a specific mechanism. Different methods calculating the reaction rate constants were developed for different types of chemical reactions. Methods such as the transition state theory (TST) (Glasstone et al., 1941), the Rice–Ramsperger–Kessel–Marcus theory (RRKM) (Marcus, 1952), and the Marcus theory (Marcus, 1993) were used to calculate the pressure independent thermal rate constants, the uni-molecular pressure dependant microcanonical rate constants, and the electron transfer rate constants respectively.

Theoretical models almost always rely on computational chemistry methods to be applicable to a certain chemical reaction. Thus, the study of theoretical chemical kinetics usually involves two main steps:

- 1- Calculation of the PES for the electronically adiabatic reaction mechanisms or calculation of the multiple PESs for the electronically non-adiabatic reaction mechanisms using computational chemistry tools (electronic treatment).
- 2- Calculation of the kinetics (nucleic treatment).

The electronic structure energy is calculated in the first step which provides the potential energy for the nuclei in the second step.

### **2.1.1 Calculation of the PES**

For a simple reaction where no bonds are being formed or broken with an exclusion of the electronically non-adiabatic process, a classical methods can be used to obtain the PES in step 1. For reactions that involve the breaking and forming of chemical bonds,

the PESs must be obtained from ab initio quantum chemistry methods which are based on the Schrödinger equation.

### 2.1.1.1 $H\Psi=E\Psi$

Chemical reactions involve both nuclear and electronic motions. Thus, for a many-body system, the wavefunction ( $\Psi$ ) would be a function of position of all the electrons ( $r_N$ ) as well as the nuclei ( $R_M$ ). The Hamiltonian operator from the time independent Schrödinger equation (SE) for N electrons and M nuclei:

$$H(r, R)\Psi(r, R) = E\Psi(r, R) \quad (2.1)$$

can be written as the sum of all kinetic and potential energies of the system:

$$\hat{H} = -\sum_{i=1}^N \frac{\hbar^2}{2m_e} \nabla_{r_i}^2 - \sum_{a=1}^M \frac{\hbar^2}{2M_a} \nabla_{R_a}^2 - \sum_{a=1}^M \sum_{i=1}^N \frac{Z_a e^2}{4\pi\epsilon_0 |R_a - r_i|} + \sum_{a=1}^M \sum_{b>a}^M \frac{Z_a Z_b e^2}{4\pi\epsilon_0 |R_a - R_b|} + \sum_{i=1}^N \sum_{j>i}^N \frac{e^2}{4\pi\epsilon_0 |r_i - r_j|} \quad (2.2)$$

From left to right the terms are: kinetic energy of the electrons, kinetic energy of the nuclei, potential energy from Coulombic electrons-nuclei attraction, potential energy from Coulombic nuclei-nuclei repulsion, and potential energy from Coulombic electron-electron repulsion. Solving the SE for any molecule with more than one electron is impossible and as a result, a few approximations are needed to be made.

The first approximation is the separation of the time scale of electronic and nuclear vibrational and rotational motions since the former moves in a different time scale due

to its relatively light weight. Thus, the nuclear kinetic energy term for the nuclei is neglected in the Hamiltonian and the SE is solved only for the motion of the electrons. The resulting Hamiltonian, the clamped nucleus Hamiltonian ( $H^0$ ) is then written in the form of:

$$H^0 = - \sum_{i=1}^N \frac{\hbar^2}{2m_e} \nabla_{r_i}^2 - \sum_{a=1}^M \sum_{i=1}^N \frac{Z_a e^2}{4\pi\epsilon_0 |R_a - r_i|} + \sum_{a=1}^M \sum_{b>a}^M \frac{Z_a Z_b e^2}{4\pi\epsilon_0 |R_a - R_b|} + \sum_{i=1}^N \sum_{j>i}^N \frac{e^2}{4\pi\epsilon_0 |r_i - r_j|} \quad (2.3)$$

This is the so-called Born-Oppenheimer (BO) approximation which gives rise to the concept of potential energy surface.

Another complexity in solving the SE is the last term of  $H^0$  which is still troublesome since it is pairwise and not additive (Equation 2.3). This gives rise to the second approximation, the mean field approximation in which the Coulomic electron-electron repulsion potential is approximated by one electron additive potential and the wavefunction can be presented as a product of functions (spin orbitals) of each electronic coordinate. This wavefunction must be presented in the form of a Slater-determinant to satisfy the antisymmetry requirement for any choice of orbitals (Slater, 1951).

Some of the wavefunctions can be written as a single Slater-determinant which is the basis of Hartree-Fock (HF) method (Knowles et al., 2000; Levine, 2009; Wilson, 2014). However, the way a single Slater-determinant expresses an electronic arrangement when a bond is being broken is invalid. Even if each electron in the frontier orbital is assigned to a different orbital using unrestricted methods, the slope in the PES (and not the

energy itself) becomes discontinuous since the electronic configuration at the frontier orbitals tend to be different at the minimum energy state compared to that when the bond is being broken. Thus, for cases when there are two electrons in the breaking bond, the wavefunction must be written in a form of multi-determinant which takes into consideration the electron correlation (Walter & Carter, 2001; Szalay et al., 2011).

Despite the ability to handle chemical reactions with high degree of accuracy (Robinson & Knowles, 2012-a, b), electron correlation methods such as configuration interaction (CI), multi-configurational self consistent field theory (MCSCF), many body perturbation theory (MBPT), and coupled cluster theory (CC), are very time consuming and can't handle large biological molecules (Walter & Carter, 2001; Varandas, 2012; Piecuch et al., 2015).

Meanwhile, Density Functional Theory (DFT) with computational cost compatible with HF methods, but the accuracy compatible with the post-HF methods is been widely used to handle larger molecules (Scott & Radom, 1996; Zhao & Truhlar, 2008-a, b; Goerigk & Grimme, 2011; Alecu et al., 2012; Klimes & Michaelides, 2012; Kohn & Sherrill, 2014).

Being able to handle large molecules with reasonable level of accuracy and low computational cost, this method has been immensely applied in variety of fields including solid state physics (Zangwill, 2013; Hasnip et al., 2014), computational material science (Jones, 2015), and computational biophysics and biochemistry (Åqvist et al., 2012; Jones, 2015; Samish et al., 2015).

### 2.1.1.2 Density Functional Theory

The fundamental underpinning of the DFT are the Hohenberg-Kohn theorems (Hohenberg & Kohn, 1964) which are as follows:

**Theorem 1.** Density as the basic variable: The external potential of an N-electron system is a unique functional of the electron density of that system.

**Theorem 2.** The Variational Principle: The density that minimizes the total energy of the overall functional is the exact electron density that corresponds to the full solution of the Schrödinger's equation.

From these two statements, Kohn and Sham came up with a set of equations which can describe the electron density in the form of single-electron wavefunctions (Kohn & Sham, 1965) (Equation 2.4):

$$\left[ -\frac{\hbar^2}{2m} \nabla^2 - \sum_A \frac{Z_A e^2}{|r - R_A|} + e^2 \int \frac{\rho(r')}{|r - r'|} dr' + \frac{\delta E_{xc}[\rho]}{\delta \rho(r)} \right] \psi_i = \varepsilon_i \psi_i \quad (2.4)$$

where the terms on the left are, in order, the electron kinetic energies, the nuclear attraction potential, the coulomb interaction of the electrons in orbital  $\psi$  with the other electrons in the molecule and the exchange-correlation potential (which is the heart of DFT) (Sholl & Steckel, 2011). An exact exchange-correlation functional has not yet been found despite the many attempts that are being carried out (Hohenberg & Kohn, 1964; Hohenberg et al., 1990; Becke 1993-a, b; Zhao et al., 2005; Zhao & Truhlar, 2006-a, b, 2008-a-c; Peverati & Truhlar, 2011-a, b, 2012-a-c).

Initially, DFT was vastly used in the field of solid state physics for transition metals with the least popularity in computational chemistry, specially the main group chemistry. The reason being the initial density functional known as the local density approximation (LDA) is written for the uniform electron gas and gives a very poor description of the inhomogeneous electron density (Cramer & Truhlar, 2009; Cohen et al., 2011; Pribram et al., 2014).

DFT started to gain popularity among chemists during 1980s with the introduction of the first derivative of the density in the form of generalized gradient approximation (GGA) (Langreth & Perdew, 1982; Perdew & Yue, 1986; Becke, 1988). The major leap however, was when Becke described a functional in which a fraction of Hartree Fock exact exchange was used, leading towards the development of B3LYP functional which made the DFT one of the most popular tools in computational chemistry (Lee et al., 1988; Becke, 1993-a). This functional has been extensively used in many areas chemistry, biochemistry, and even physics (Tirado & Jorgensen, 2008; Cohen et al., 2011; Burke, 2012; Becke, 2014; Pribram et al., 2014; Jones, 2015).

Despite the success and popularity of B3LYP, the challenge for developing a more accurate exchange-correlation functional is still on (Scuseria & Staroverov, 2005; Peverati & Truhlar, 2011-a,b 2012-a-c). Various density functionals are being developed with a better performance over the standard B3LYP functional (Cohen et al., 2011).

Besides the transition metal chemistry which can be well treated with local functionals, some chemical systems within the main group chemistry require better functionals than B3LYP to be more adequately described. Systems with medium range ( $\sim 2-5$  Å) interactions, such as biological systems interacting through dispersion forces are the

examples of those systems for which B3LYP may not provide a reasonable description (Zhao & Truhlar, 2008-a). Truhlar's M06 suit of functionals was developed to address such problems (Zhao & Truhlar, 2008-b). The M06-L has no HF exchange which is mainly used for transition metal chemical systems, while the M06, M06-2X and M06-HF have high percentage of HF exchange which are suitable for main group chemical systems and addressing problems such as calculation of the reaction barriers and London dispersion forces.

Within all these functionals, B3LYP and M06-2X can provide reasonable information on the PES which can be used to accurately measure the barrier heights in mechanistic studies of chemical and biochemical reactions (Bhat et al., 2004; Acosta et al., 2012; Xu et al., 2012-b; Byun & Kang, 2013; Świderek et al., 2013, 2015). Hence, these two methods are the methods of choice in this study. The accurate measurements of barrier heights of a chemical reaction can lead towards the accurate prediction of a reaction rate. The theory of chemical kinetics is a tool to calculate this rate.

### **2.1.2 Chemical kinetics**

In addition to the electronic structure calculations of the PES, the study of chemical kinetics in most cases involves the calculation of the dynamical properties of the system. The interface between these two provides the knowledge of the reaction mechanism for many unknown chemical and biochemical reactions. Methods such as direct dynamics (Chuang & Truhlar, 1998) or the transition state theory (Truhlar et al., 1996; Klippenstein et al., 2014) are the most popular and widely used methods for studying the dynamical properties of the complex systems. The former is computationally expensive and not feasible for large systems. The latter on the other

hand, can be used to predict the mechanism of complex reactions by associating the rate constant to a specific reaction mechanism. Thus, the emphasis in this thesis will be on the kinetics of a reaction rather than studying the real dynamical motion of the system.

The foundation of chemical kinetics was laid by Arrhenius when he first postulated that among all molecules in a chemical system, only those that gain a certain amount of energy would go through a chemical reaction. Based on this idea, the collision theory was proposed stating that the energy of activation in molecules is gained through collision of the molecules with one another. Despite the success of the collision theory in expressing the rate of most of the chemical reactions, it overestimates the rate of unimolecular reactions (Wright, 1999).

Besides collision theory, another theory was being explored which gained more popularity and interest. It was based on the idea that all the atoms in the reacting system go through a specific spatial arrangement and configuration at a critical point during the reaction. That critical point was called the transition structure and the theory was called the transition state theory (Evans & Polanyi, 1935; Eyring, 1935).

#### **2.1.2.1 Conventional Transition State Theory (CTST)**

The general form for calculating the reaction rate was first proposed by Svante Arrhenius in 1889 which is known as Arrhenius equation (Equation 2.5) (Arrhenius, 1889; Laidler & King, 1983; Laidler, 1984)

$$k = Ae^{\frac{-E_a}{RT}} \quad (2.5)$$

where  $R$  is the gas constant,  $A$  is the pre-exponential factor and  $E_a$  is the Arrhenius activation energy. There are a few different treatments to interpret the  $A$  and  $E_a$  (Laidler, 1984) that were brought together by Eyring (Eyring, 1935) and independently by Evans and Polanyi (Evans & Polanyi, 1935) in 1935 and formed what is now known as the conventional transition state theory (Steinfeld, 1999). This theory is formulated based on four basic assumptions which are as follows:

**Assumption 1:** All the trajectories that originate from the reactants, cross the dividing surface (a hypersurface on the saddle point, orthogonal to the reaction pathway) towards the formation of the products only once.

**Assumption 2:** The activated complexes that were the reactant molecules in immediate past are always in *quasi-equilibrium* with the reactants.

**Assumption 3:** The motion of the system along the reaction coordinate over the saddle point can be separated from the other degrees of the freedom of the activated complex and treated as an independent classical translational motion.

**Assumption 4:** CTST can give qualitatively good results for the chemical reactions with solely classical motions where the quantum effects are completely neglected.

The first two assumptions are the most fundamental CTST assumptions which are correlated with each other, i.e. for a system at *quasi-equilibrium*, all the activated complexes in the saddle point region which were the reactant species in the immediate past will form the product. From treating the equilibrium constant with the methods of

statistical mechanics in CTST (Steinfeld, 1999), the general form of the rate equation for a bimolecular reaction can be obtained:

$$k = \frac{k_B T}{h} \frac{q_{\ddagger}}{q_A q_B} e^{\frac{-E_0}{RT}} \quad (2.6)$$

where  $E_0$  is the molar energy change at  $T_0$  (Figure 2.1),  $q_A$  and  $q_B$  are the partition functions for reactants species and  $q_{\ddagger}$  is a special type of partition function for the activated complex which according to the third assumption has  $3N-7$  degrees of freedom over the saddle point, orthogonal to the reaction coordinate.

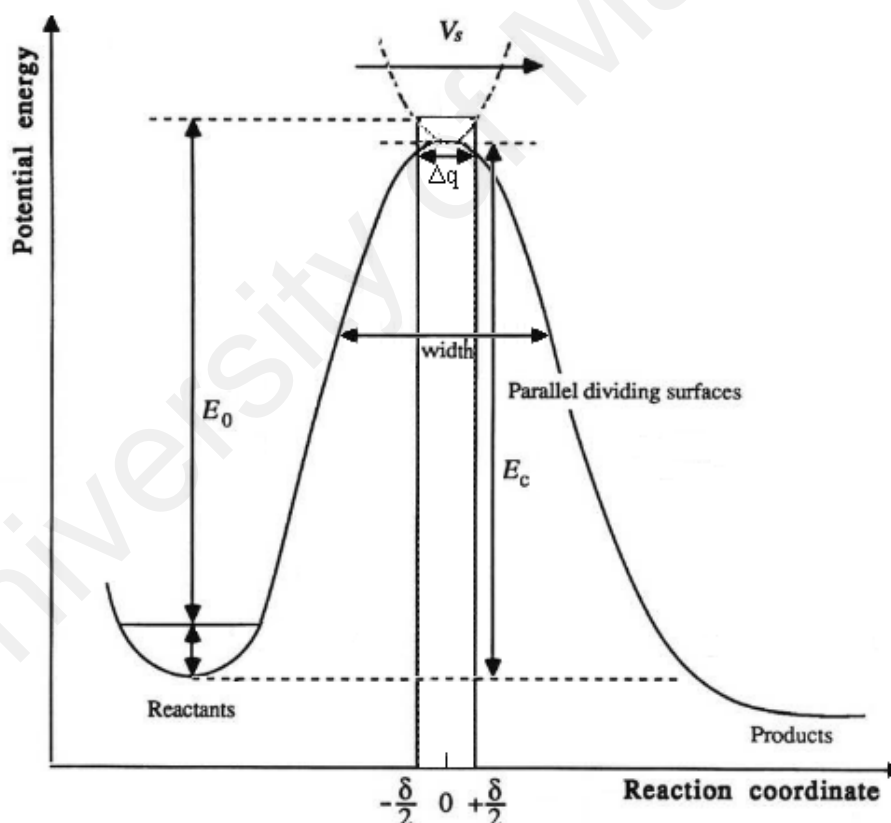


Figure 2.1: The reaction coordinate profile where the  $E_0$  indicates the zero point corrected energy of activation and  $E_c$  indicates the classical energy of activation (Steinfeld, 1999).

To include the missing degree of freedom to the activated complex, one must use the term  $q^\ddagger$  in the rate equation which according to derivation carried out by Wynne-Jones and Eyring (Wynne-Jones & Eyring, 1935) includes very loose vibrational motion and can be expressed as:

$$q^\ddagger = q_\ddagger \frac{k_B T}{h \nu} \quad (2.7)$$

It would be more convenient to reformulate the derived transition state rate equations in terms of thermodynamic quantities. By combining the Van't Hoff equation (Van't Hoff, 1884)

$$\Delta G^\ddagger = -RT \ln K^\ddagger \quad (2.8)$$

where

$$K^\ddagger = \frac{q_\ddagger}{q_A q_B} e^{\frac{-E_0}{RT}} \quad (2.9)$$

with Equation 2.6, the rate equation can be written in terms of the standard Gibbs energy of activation ( $\Delta G^\ddagger$ ) as expressed in Equation 2.10 (Laidler, 1977; Steinfeld, 1999).

$$k = \frac{k_B T}{h} e^{\frac{-\Delta G^\ddagger}{RT}} \quad (2.10)$$

This equation provides a reasonable upper bound to the actual reaction rate with very low deviation, provided that all four CTST assumptions are met (Laidler, 1984; Alsallaq & Zhou, 2007; Nguyen et al., 2010; Manthe, 2011; Klippenstein et al., 2014). However, there are some certain chemical reactions where the classical dynamics effect (recrossing) or quantum dynamics effect (tunnelling) are not negligible and the CTST assumptions would simply break down (Laidler, 1977; Steinfeld, 1999; Meana et al., 2010; Andersson et al., 2011; Alecu et al., 2012; Zhang & Dibble, 2011; Zhang et al., 2014; Zheng et al., 2014).

At high temperatures for example, the CTST overestimates the reaction rate due to the violation of *no recrossing* and *local equilibrium* assumptions whereas in lower temperatures, it significantly underestimates the reaction rate due to the violation of *separability* and *classical motion* assumptions. To overcome these breakdowns, corrections have been made to CTST which led towards the development of generalized transition state theory (GTST) and quantum mechanical effects in transition state theory (QTST) (Wigner, 1932; Shavitt, 1959; Keck, 1960; Miller, 1974, 1975-a, b; Garrett & Truhlar, 1979-a, b; Truhlar & Garrett, 1980, 1984; Miller et al., 1983; Truhlar et al., 1985, 1996; Voth et al., 1989; Hu et al., 1994; Thompson, 1999; Gao & Truhlar, 2002; Park et al., 2012).

#### **2.1.2.2 Generalized Transition State Theory (GTST)**

GTST is a version of TST where the transition state is not restricted to the saddle point and the location of the dividing surface is varied towards the minimization of the reaction rate (VTST) (Truhlar & Garrett, 1980; Truhlar, 1984; Truhlar et al., 1985). Figure 2.2 is a schematic view of the re-crossing problem in CTST (trajectories 2, 3, 5

and 6) which is corrected by locating an alternative dividing surface along the reaction path. This method provides a more accurate and “lowest” upper bound to the reaction rate for those classical reaction mechanisms with significant recrossing problem (Garrett & Truhlar 1979-b; Klippenstein et al., 2014; Masgrau & Truhlar, 2014).

The recrossing problem for reactions at high temperature has been extensively addressed by GTST with a reasonable amount of accuracy (Pu et al., 2006; Alecu et al., 2012; Xu et al., 2012-a). Furthermore, various enzymatic reactions have been studied in a wide temperature range, combining the VTST with multidimensional tunnelling corrections to treat the recrossing problem in higher temperatures as well as non-separability problem in lower temperatures respectively (Pu et al., 2006; Dybala et al., 2007; Fernández et al., 2007; Pollak, 2012; Klippenstein et al., 2014; Masgrau & Truhlar, 2014; Truhlar, 2015).

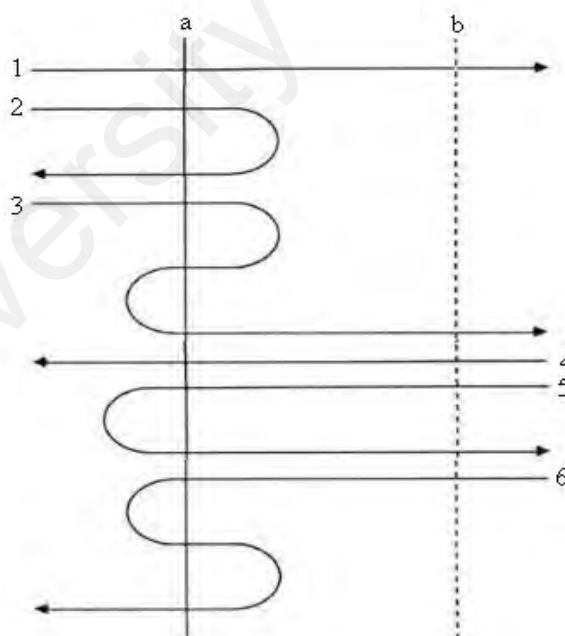


**Figure 2.2: The schematic view of the trajectories of crossing from the dividing surface over the saddle point (a) and an alternative dividing surface (b) (Laidler, 1984).**

One type of such chemical reaction is the proton transfer reaction which is very common in biological systems (Pu et al., 2006; Pollak, 2012; Masgrau & Truhlar, 2014). When a light atom like proton is transferred in a chemical reaction, certain quantum deviations such as quantum tunnelling appear, which is known to be the reason for high rate of some enzymatic reactions (Bothma et al., 2010; Zhang et al., 2014; Masgrau & Truhlar, 2014).

Quantum tunnelling cannot be studied using the CTST approach, nor can it be studied with the exact quantum treatment for the large complex systems (Laidler, 1977; Steinfeld, 1999). Therefore, several approximate methods are developed to treat the tunnelling phenomenon in chemical reactions (Wigner, 1932; Shavitt, 1959; Kuppermann & Truhlar 1971; Miller, 1974, 1975-a, b; Miller et al., 1983; Truhlar, 1984; Voth et al., 1989; Truhlar et al., 1996; Thompson, 1999; Gao & Truhlar, 2002; Pu et al., 2006; Park et al., 2012).

### **2.1.2.3 Quantum Transition State Theory (QTST)**

Quantum transition state theory cannot be represented with similar concepts as the CTST since the latter's assumptions will simply fail in the quantum mechanical framework (Small et al., 2006; Hele, 2014). Additional to the obvious contradiction of the fourth CTST assumption with quantum mechanical tunnelling path, one basic difficulty in generalizing the CTST to QTST is the non-locality of the transition structure within the saddle point region due to the large de Broglie wavelength associated with the motion along the reaction coordinate (Steinfeld, 1999). This delocalization of quantum mechanics which results in a curved  $\Delta q$  region over the saddle point (Figure 2.1) initiates a problem, that is, for the curved  $\Delta q$  region where the

system is not freely moving, the reaction coordinates cannot be treated as a classical translational motion. In other words, for the curved  $\Delta q$  region, the motion along the reaction coordinate is inseparable from the remaining degrees of freedom and as a result, the total partition function cannot be written in separated forms as it is done in the classical rate expression (Miller, 1976; Steinfeld, 1999). Thus, to achieve a working quantum mechanical rate equation which accounts for the quantum mechanical motions along the reaction path, corrections must be made to the classical rate equation.

There are various attempts to develop methods with tunnelling corrections which account for quantum delocalization through different approximations (Truhlar & Garret, 1984; Yamamoto & Miller, 2006; Fernández et al., 2007; Zhang et al., 2014; Zheng et al., 2014). Among them are several useful approaches that have been proposed to address the curvature problem in QTST (Marcus & Coltrin, 1977; Miller et al., 1980; Truhlar & Garrett, 1980; Gray et al., 1981; Miller, 1998; Mavri et al., 2016). However, their practicality varies depending on the type of the chemical reaction under study.

For instance, multidimensional tunnelling corrections such as small curvature tunnelling (SCT) or large curvature tunnelling (LCT) are usually carried out for the reactions with reaction path curvature (Pollak, 2012; Masgrau & Truhlar, 2014). Small curvature tunnelling (SCT) is a model developed by Truhlar's group (Kuppermann & Truhlar, 1971) for the reactions with small reaction path curvature in which the motion along the reaction coordinate is coupled with the vibrational modes transverse to it (Truhlar, 1984, 2015). This coupling shortens the tunnelling path by “cutting the corner” through the concave side of the reaction path. Zero-curvature tunnelling (ZCT) on the other hand, neglects this coupling and significantly underestimates the tunnelling effect for the

reactions with reaction path curvature (Kuppermann & Truhlar 1971; Dybala et al., 2007; Zhang & Dibble, 2011).

Similar to the SCT model, LCT model uses the corner-cutting tunnelling approach. However, instead of moving along the concave side of vibrational turning points on the MEP (as in the SCT approach), it uses a straight line to connect the reactant region to the product region. This straight line might pass through an area of the PES which is far from the MEP, though, it shortens the tunnelling path (Kuppermann & Truhlar 1971; Pu et al., 2006; Dybala et al., 2007).

There are some certain reactions that do not have curvature in their reaction path, among which are hydrogen bond (H-bond) proton transfer reactions. Hence for these reactions, neglecting the coupling between the reaction coordinate and the transverse modes would not affect the tunnelling rate significantly (Staib et al., 1995; Truhlar et al., 1996). Therefore, the ZCT or Eckart model would provide a reasonable tunnelling correction to the overall reaction rate in H-bond proton transfer reactions (Zhang & Dibble, 2011). This reaction is one of the simplest, immensely investigated chemical reaction which is involved in many important biological processes (Gregory et al., 1997; Ohmine & Saito, 1999; Horsewill et al., 2001; Bothma et al., 2010; Arabi & Matta, 2011; Vilčiauskas et al., 2012).

Due to the low mass of the proton, proton transfer reaction satisfies the key requirements for the quantum dynamical motion. In fact, there are many enzymes and mutants in biological systems have demonstrated a behaviour that cannot be explained with classical dynamical motions and the only explanation for their behaviour is the tunnelling of proton (Cha et al., 1989; Kohen & Klinman, 1998; Tautermann et al.,

2002; Basran et al., 2003; Olsson et al., 2004; Valley & Fitzpatrick, 2004; Masgrau, et al., 2006; Gil & Waluk, 2007; Stojković & Kohen, 2009; Horsewill, 2010; Bothma et al., 2010; Truhlar, 2010; Park et al., 2012). However, the fact that the biological systems are constantly interacting with their noisy and hot environment makes it highly possible that quantum mechanical effects get destroyed by decoherence (Bothma et al., 2010). At this point of ambiguity, there is only one clear question which we intend to address in this thesis, that is, do proton transfer processes in biological systems occur through tunnelling?

## **2.2 Proton transfer reactions**

Enzymes catalyse most biochemical reactions by many orders of magnitude compared to the uncatalysed reactions in solution. The general textbook explanation for enzyme catalysis was given by Linus Pauling in his proposal where the rate enhancement is achieved by proper substrate positioning in the enzyme's active site to induce preferential binding interaction between the enzyme and the substrates (Klinman & Kohen, 2013). This would lower the energy barrier height to reduce the required energy for the substrates to react and form the product.

Most enzymatic catalyses involve proton transfer reactions (Ball, 2004; Bothma et al., 2010; Horsewill, 2010). Due to its light mass, proton has a relatively large de-Broglie wavelength which would make it highly probable for its wavefunction in the reactant side to overlap that in the product side, resulting in proton tunnelling. This phenomenon is highly sensitive to the width and height of the reaction profile energy barrier. Proton tunnelling can occur well below the maximum of a tall energy barrier if it is sufficiently narrow and conversely, tunnelling can occur close to the peak if the barrier is broad.

It is argued that some enzymes induce proton tunnelling by thinning the energy barrier width in addition to lowering the energy barrier height (Kohen et al., 1999; Basran et al., 2001; Klinman, 2014; Kohen, 2014). This argument is based on the results of highly temperature-dependent kinetic isotope effect (KIE) studies which support the idea of vibrational hypothesis (Pudney et al., 2010; Hay et al., 2009 & 2010; Hay & Scrutton, 2012). This so-called vibrational gating is observed in some protein enzymes in which the barrier height and/or width is lowered by reduction of the proton donor-acceptor distance and coupling of the proton transfer with the molecular vibrations between the donor and acceptor atoms through some protein dynamical motions (Ley et al., 2012).

It is worth mentioning that this argument is not contradictory to the study carried out by Warshel and collaborators, suggesting that the origin of enzyme catalyses is mainly due to lowering the barrier height and not narrowing the barrier width (Mats et al., 2006; Braun et al., 2007; Warshel & Bora, 2016). Based on this model, the height of a non-enzymatic reaction barrier with a narrow top is significantly lowered by the enzyme without any significant effect on the width. It makes the classical over the barrier reaction more probable than tunnelling due to the thickness of barrier width in the catalysed reaction (Kamerlin et al., 2010).

This is exactly the case for the enzymes which reduce the barrier height to as low as 5 kcal/mol and even lower, where the classical over the barrier mechanism dominates the reaction rate and tunnelling becomes irrelevant at biological temperature. Therefore, despite the observed large tunnelling effects for these enzymatic reactions, these effects do not contribute to enzyme catalysis (Mavri et al., 2007; Warshel & Bora, 2016).

On the other hand, for enzymatic reactions with the activation barrier of more than 5 kcal/mol, tunnelling becomes relevant to the point where it dominates the overall reaction rate (Truhlar, 2010). Reactions in protein enzymes such as yeast alcohol dehydrogenase (YADH), amine oxidase (AO) or glucose oxidase (Gox) are among those enzymatic reactions with a large barrier height which are suggested to induce proton tunnelling through such protein vibrational motions (Cha et al., 1989; Kohen & Klinman, 1998; Benkovic & Schiffer, 2003; Schiffer & Benkovic, 2006; Pudney et al., 2010; Hay et al., 2009, 2011, 2012). In some enzymes, these vibrational motions in the active site result in negative activation entropy (Young & Post, 1996) which is known to be an indication for tunnelling (Whitman & Carpenter, 1982; Dix et al., 1993). Thermal fluctuations are also said to have a significant effect on increasing the probability of tunnelling (Cha et al., 1989; Bruno & Bialek, 1992; Rucker et al., 1992).

An important example of such enzymatic reaction for which a large negative activation entropy has been observed is the process of peptide bond formation during the synthesis of proteins in the ribosome (Sievers et al., 2004). Similar to many enzymes, the origin of catalytic power of the ribosome is still unknown and is being immensely investigated. This proton transfer reaction is biology's vital chemical process where the genetic code from the DNA is translated to the cell's most important molecules, proteins.

### **2.2.1 The Central Dogma of Biology**

The transcription of the genetic code from DNA (Deoxyribonucleic acid) to mRNA (messenger Ribonucleic acid) and consequently to the proteins is known as the central dogma of biology. The sequence of amino acids (which depends on the sequence of nucleotides in the DNA) gives the protein its three dimensional (3D) structure which is

vital for living cells to maintain life. Thus, the process of protein synthesis is required to occur with a high accuracy and efficiency (and it indeed does!), making it one of the most complex and important processes in all living organisms. In this process, a copy of the genetic code is transcribed from the DNA into a single strand mRNA molecule. The ribosome would then attach to the mRNA and reads the genetic code three nucleotides at a time to form a particular protein that this gene codes for. The protein is formed in the active site of the ribosome through a process called the peptide bond formation between the amino acids.

The ribosome is composed of a large and a small subunit (LRS and SRS respectively) that come together around the mRNA and move along the mRNA to read the genetic code. The amino acids are carried into the ribosome attached to a tRNA (transfer RNA) molecule that is specific for each amino acid (Figure 2.3).

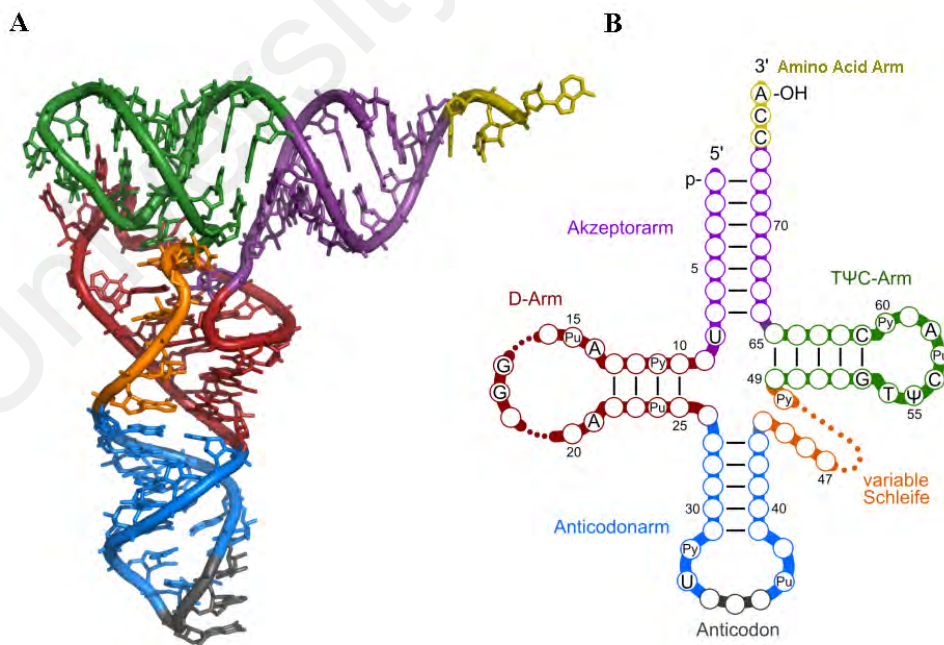


**Figure 2.3: The A) 3-D and B) 2-D structure of the tRNA molecule.**

The SRS positions the mRNA such that it can be read in groups of three nucleotides, known as codons. The LRS binds the amino acids together with peptide bond and form a growing protein chain. Each codon on the mRNA molecule matches to a corresponding anti-codon on the tRNA (Monajemi et al., 2012). As the mRNA is read through the ribosome, the mRNA codon is translated into the sequence of amino acids. There are three locations inside the ribosome (both at SRS and LRS) for the tRNA molecules, known as the A-site, P-site and the E-site, accommodating the aminoacyl-tRNA (aa-tRNA), peptidyl-tRNA and exiting de-acylated tRNA respectively.

The process of peptide bond formation occurs in cycles (Figure 2.4). At the beginning of each cycle, the P-site of the ribosome is occupied with the tRNA which is attached to the growing polypeptide chain, while the A- and E-sites are empty (Monajemi et al., 2011-a). The cycle begins with a random aa-tRNA entering the ribosome at the A-site and is tested for a codon-anticodon match (initial selection and kinetic proofreading). Upon the correct codon-anticodon match, the aa-tRNA is accommodated in the ribosomal A-site and brings the amino acid arm to the peptidyl transferase center (PTC) (accommodation). The growing polypeptide chain which is attached to the P-site tRNA is then transferred to the aa-tRNA in the A-site (peptidyl transfer).

Once the P-site tRNA is unloaded, it moves to the E-site of the LRS spontaneously with the A-site peptidyl-tRNA moving to the P-site of the LRS. Following this so-called *pre-translocational hybrid state* is the ratcheting movement of the ribosome along the mRNA strand which brings the P- and A- site anticodon loops of the tRNA to the E- and P-site of the SRS respectively, dragging the mRNA strand with them (Gagnon et al., 2014). This brings the next codon to the A-site of the SRS, followed by beginning of the next cycle (Voorhees & Ramakrishnan, 2013).

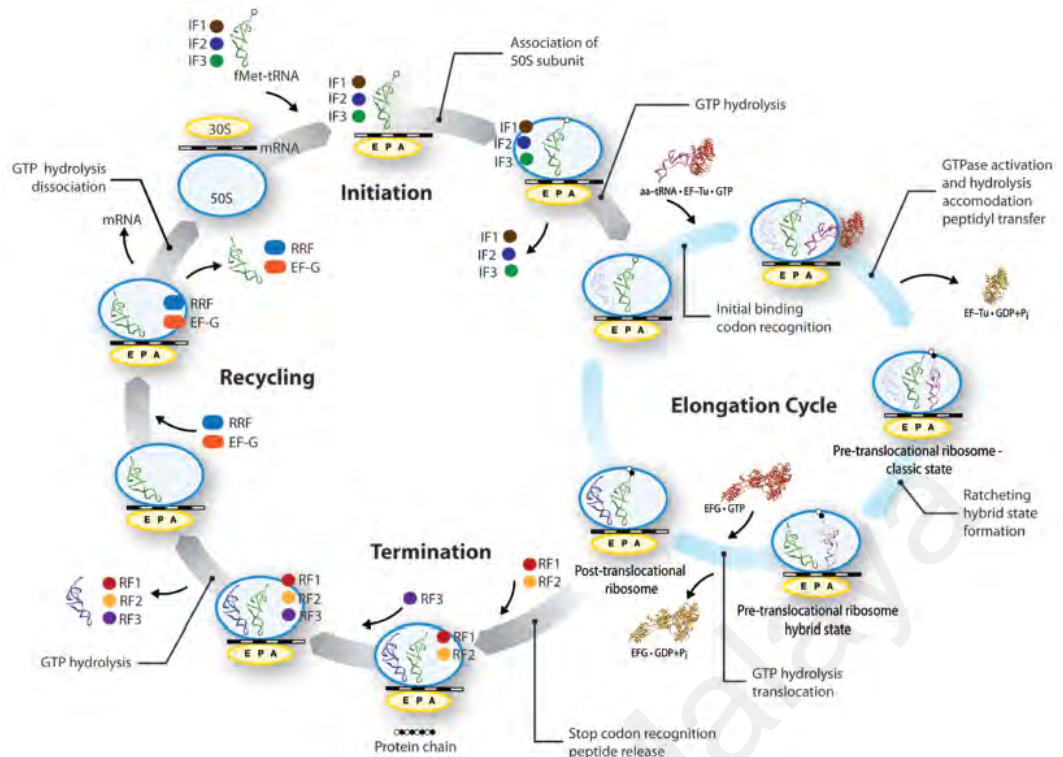


**Figure 2.4: The schematic view of the translation cycle: initiation step, elongation cycle, termination step, and recycling (Agirrezabala & Frank, 2010).**

These cycles continue one trinucleotide (codon) at a time until a stop codon is located at the A-site of the SRS, signalling for the termination of protein synthesis by bringing the release factor<sup>2</sup> to the A-site to hydrolyse the polypeptide chain (Trapp et al., 2014). The released polypeptide then folds up to a precise shape which is determined by the sequence of the amino acids. Thus, the central dogma of biology explains how the 4 letters of the DNA can turn into proteins and consequently life (Voorhees & Ramakrishnan, 2013).

Both bacterial and eukaryotic ribosomes contain approximately two thirds RNA and one third protein (Voorhees & Ramakrishnan, 2013) (Figure 2.5-A). However, there are several structural differences between these two types of ribosomes, taking the advantage of which has led towards the development of various antibiotic drugs.

<sup>2</sup> A protein that allows the termination of protein synthesis by reading the stop codon at the end of mRNA sense gene sequence.

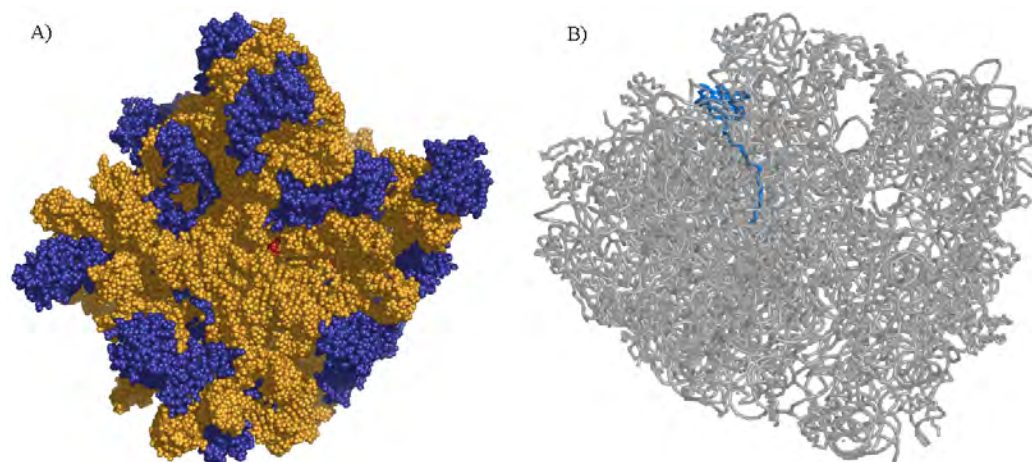


**Figure 2.5: A) The 50S ribosome (LRS) with proteins in blue, RNA in orange, and the active site in red. B) The protein L27 in blue and the rest of the 50S ribosome (LRS) in grey (PDB: 4W2H). It can be seen that the tail of this protein is extended to the active site which was thought to be directly involved in the reaction.**

Different antibiotics target different parts of the ribosome, e.g. the A-site to prevent the nascent aa-tRNA to enter the ribosome, the mRNA and SRS to misread the genetic code, or the PTC itself to prevent the peptidyl transfer (Lambert, 2012). The latter type is usually associated with serious complications and side effects. If a precise transition structure analogue<sup>3</sup> can be modelled, the protein synthesis inhibitor drugs can be used with less to no complications. To determine the transition state analogue, the exact reaction mechanism of peptide bond formation must be determined.

High resolution crystallographic structures of the ribosome have made a major contribution towards understanding the different stages of protein synthesis (Moore & Steitz, 2003; Ramakrishnan, 2008; Blaha et al., 2009; Moore, 2009; Schmeing & Ramakrishnan, 2009; Simonović & Steitz, 2009; Voorhees et al., 2009; Hiller et al., 2011). However, the high resolution structural data of the complete active site in complex with the whole ligands is still lacking (Polikanov et al., 2014). This makes it difficult to study the detailed mechanism of this process in terms of ribosomal catalysis.

<sup>3</sup> The transition structure analogue is a theoretical model for the transition state structure which is assumed to bind stronger to the enzyme's active site than the real substrate, hence, preventing the process of peptide bond formation to proceed.

The main challenge in understanding this mechanism started when the structure of 50S ribosome was obtained from *H. marismortui*, indicating that the ribosome is a ribozyme<sup>4</sup> (Ban et al., 2000; Nissen et al., 2000). The data supported an earlier study on peptide bond formation in “proteinless” ribosome and participation of the 23S-rRNA (ribosomal-RNA) residue on peptidyl transfer mechanism (Noller et al., 1992) (Figure 2.5-B). This was a breakthrough towards understanding the catalytic role of the ribosome; that is, the ribosomal proteins do not directly participate in chemistry of the reaction and the catalytic power of the ribosome is mainly from its RNA residues.

A different study was carried out in the same year on the chemical reactivity of a single adenosine residue from 23S-rRNA during peptidyl transfer, the A2451 (*E. coli* numbering is used throughout this thesis), suggesting that the mutation on the A2451 base is lethal *in vivo* (Figure 2.6) (Muth et al., 2000).

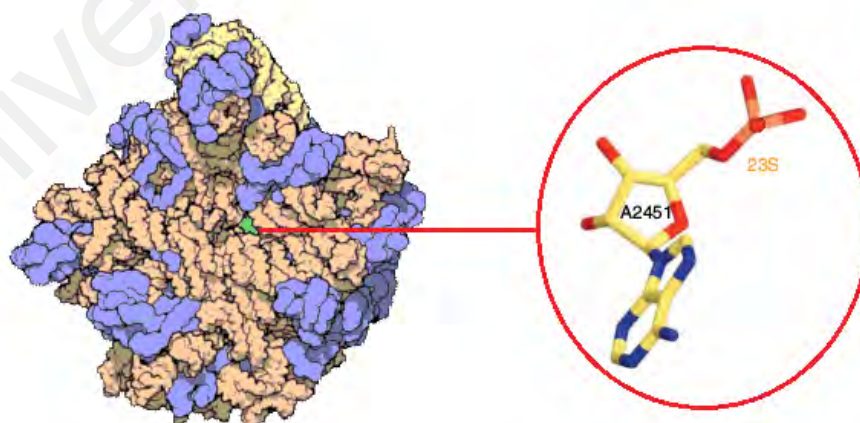


**Figure 2.6: The structure of the A2451 rRNA residue, located in the active centre (green) of the 50S ribosome with the 23S ribosomal RNA in orange, the 5S ribosomal RNA in yellow and the ribosomal proteins in blue.**

<sup>4</sup> Ribozyme is an enzyme in which the RNA structures are directly involved in catalysis rather than the protein structures.

There was another report in 2001 where the ribosomal A2451 residue is not a chemical catalyst and its role is to properly position the substrates in the proximity of one another to induce the nucleophilic attack of the A-site amino group (Polacek et al., 2001). A year after that, Steitz, Moore and collaborators achieved a higher resolution crystallographic structure of the 50S ribosome, indicating that the peptidyl transferase center (PTC) juxtaposes the A2451 residue of the 23S-rRNA in the active site to stabilize the transition structure by forming a hydrogen bond between the nitrogen of the adenosine residue (N3) and the amino group of the attacking nucleophile (Hansen et al., 2002) (Figure 2.7-a). The interaction of N3 from A2451 residue with  $\alpha$ -amine is also observed in the crystallographic structure of Ramakrishnan et al., in their 2009 study (Voorhees et al., 2009) (Figure 2.7-b).

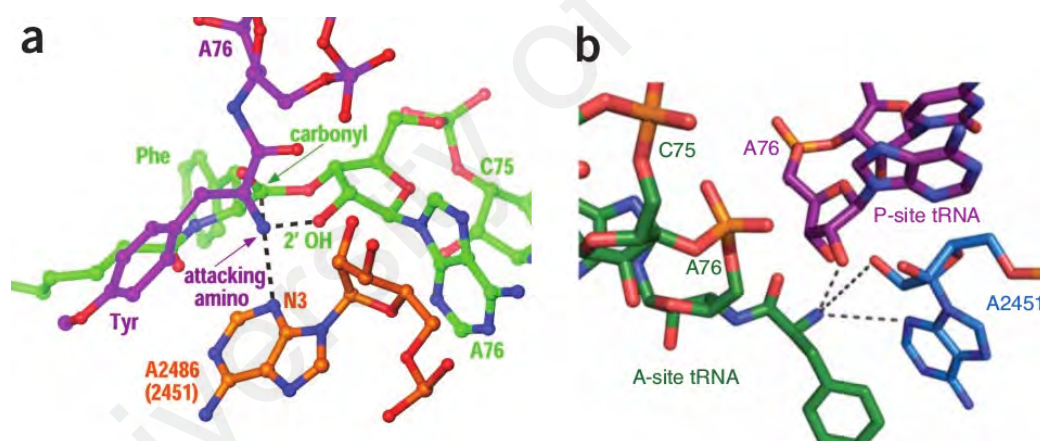


**Figure 2.7: The interaction of the N3 of A2451 with the attacking amine in a) (Hansen et al., 2002) and b) (Voorhees et al., 2009) crystallographic structures.**

In 2004, there was another major breakthrough in understanding the catalytic power of the ribosome by studying the temperature dependent rate of peptide bond formation between the P-site peptidyl-tRNA (transfer-RNA) and the A-site aminoacyl-tRNA analogous puromycin in comparison with the rate of uncatalysed peptide bond formation (Sievers et al., 2004).

A  $10^7$ -fold enhancement of the reaction rate in the ribosome compared to that in solution was observed where this rate enhancement was regarded to a very low entropy change in the ribosomal active site from reactant to the transition structure. Based on this, Sievers et al., suggested that the ribosomal catalytic role during the peptide bond formation is the alignment of the substrates in such a way that the rotational and translational entropy is reduced and as a result, activation enthalpy is increased (Monajemi et al., 2011-b).

On the other hand, the MD simulation carried out by Trobro and Åqvist indicated that the pre-organized reaction site which does not require a major reorganization throughout the reaction is the source of catalysis (Trobro & Åqvist, 2005). They have suggested that presence of highly ordered water molecules and forming a hydrogen bond network is the explanation for this unusual entropy effect in the active site. The latter explanation is further supported by the high resolution crystallographic structure data carried out by Steitz and collaborators studying the role of water molecules in the peptidyl transfer reaction with a rigid PTC throughout the catalysis (Schmeing et al., 2005-a, Polikanov et al., 2014).

They and a few earlier studies have also suggested that the P-site A76 2'-OH group has an effect on transition state stabilization, some signifying its critical role as proton shuttle (Dorner et al., 2003; Weinger et al., 2004; Erlacher et al., 2005; Brunelle et al., 2008). It was first suggested by Green and collaborators that the absence of this group would result in  $10^6$ -fold reduction in the rate of peptide bond formation (Weinger et al., 2004). Later in 2011, this premise was corrected by the same group which achieved only ~100-fold reduced rate prior to the 2'-OH functional group substitution (Zaher et al., 2011). It however raised back the question of whether it is mainly the P-site A76 2'-

OH which plays a significant role in catalysing the reaction, or other factors such as ribosomal bases and/or water molecules are (also) involved (Polikanov et al., 2014; Świderek et al., 2015; Wang et al., 2015).

Despite these important findings, the mechanistic principles of the ribosomal catalysis still remain a riddle. The different crystallographic characterization of the binding equilibrium and that of the catalytic mechanism causes the difficulty to solve this riddle. Due to the difficulty in identifying the mechanism from crystallographic data, complementary computational studies were also carried out.

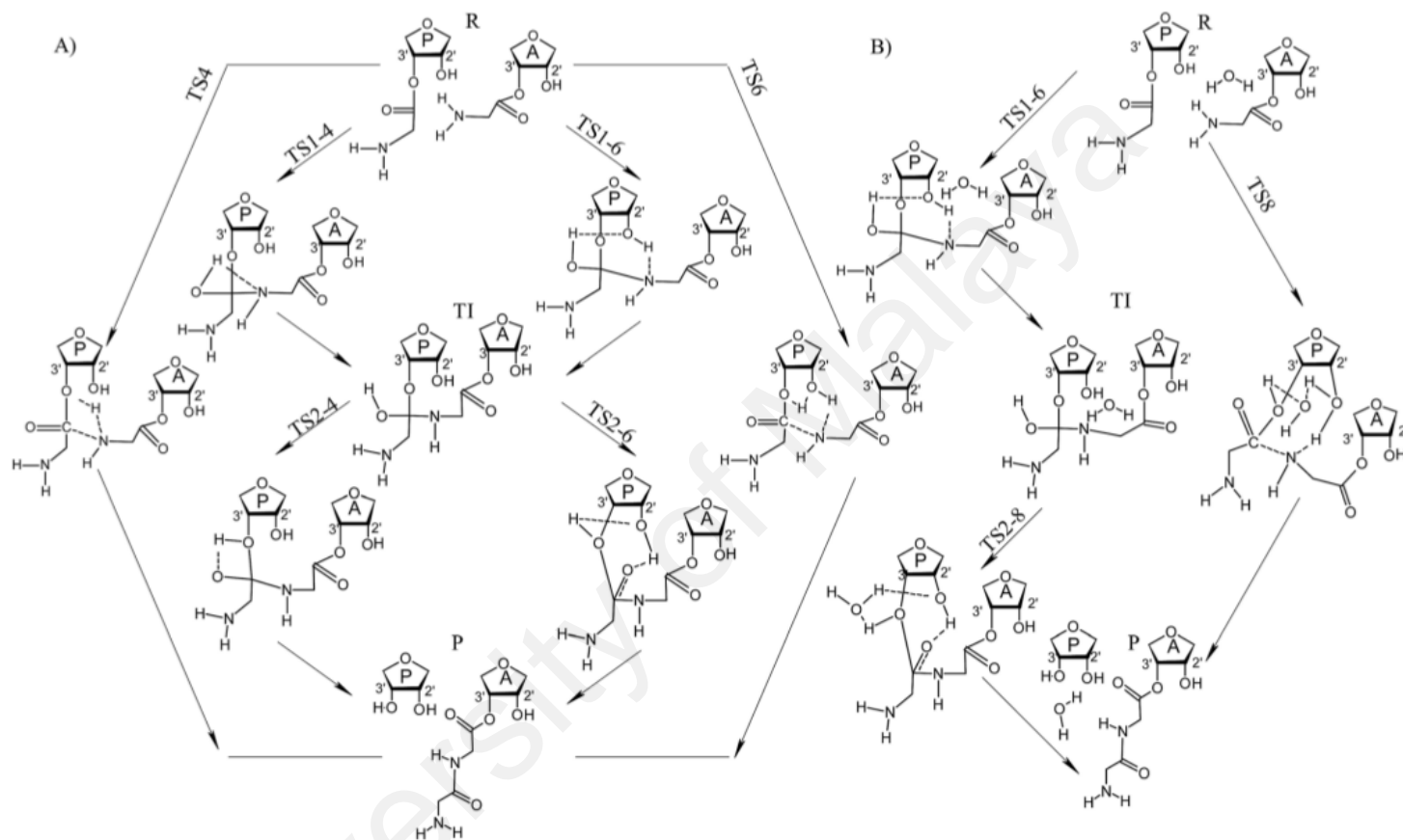
Different types of pre- and post-peptidyl transfer structures in the ribosomal active site are suggested by experimental crystallographic studies (Schmeing et al., 2005-a, b; Rhodes et al., 2006; Lang et al., 2008; Schmeing & Ramakrishnan, 2009; Simonović & Steitz, 2009; Voorhees et al., 2009; Zaher & Green, 2009; Zaher et al., 2011; Hiller, et al., 2011; Polikanov, et al., 2014). Based on those crystallographic structures, different reaction mechanisms have been proposed and further investigated in detail using computational quantum chemistry calculations (Trobro & Åqvist, 2005; Matta, 2010; Wallin & Åqvist, 2010; Wang et al., 2010; Acosta et al., 2012; Xu et al., 2012-b; Byun & Kang, 2013; Świderek, et al., 2013, 2015; Wang et al., 2015) which is also known as quantum crystallography (Matta, 2010). However, the limitation in computational calculations makes the study of macromolecule such as ribosome as a whole, impossible (Matta, 2010; Åqvist et al., 2012).

Based on the high resolution crystallographic data, considering the limitations in computational studies, a few mechanisms for the process of peptide bond formation have been proposed where only the atoms involved in the reaction were treated quantum

mechanically (Gindulyte et al., 2006; Rangelov et al., 2006; Massa et al., 2010; Wallin & Åqvist, 2010; Hiller et al., 2011) and further investigated (Wang et al., 2010; Acosta et al., 2012; Xu et al., 2012-b, Byun & Kang, 2013; Świderek et al., 2013).

In general, these mechanisms are divided into two main groups; concerted and stepwise. The proposed concerted mechanisms are 4, 6, and 8-membered mechanisms in terms of the number of atoms involved in the reaction. The stepwise mechanism occurs in two steps with forming a neutral tetrahedral intermediate (Scheme 2.1). The main challenge in the mechanistic study of peptide bond formation is to figure out the role played by the A76 2'-OH group since its activity was observed in many empirical studies (Dorner et al., 2003; Erlacher et al., 2005; Schmeing et al., 2005-a; Weinger et al., 2004; Brunelle et al., 2008; Polikanov, et al., 2014).

In the computational study carried out by Gindulyte and collaborators, the A76 2'-OH group was suggested to form a hydrogen bond with the oxygen atom of the A-site amino acid's carboxyl group (Gindulyte et al., 2006). It is however mentioned that this group does not directly participate in the reaction and its role is mainly to bring the reacting groups of the A-site and P-site amino acids in close proximity which would result in a 4-member transition structure (Matta, 2010). Åqvist's group proposed that the 2'-OH is directly involved in the reaction, forming a 6-membered transition structure; however, it does not constitute a catalytic effect (Trobro & Åqvist, 2005, 2006). Later in 2010, they proposed a mechanism in which a water molecule is also involved in the proton shuttle additional to the 2'-OH, forming an 8-membered transition structure. Their model was proposed based on an earlier high resolution crystallographic data carried out by Steitz group which confirmed the presence of water molecules in the active site (Schmeing et al., 2005-a, b).



**Scheme 2.1: Previously proposed concerted and stepwise mechanisms, indicated in valence and core of the scheme respectively. A) Both TS4 and TS6 correspond to the concerted 4-membered and 6-membered mechanisms. TS1-4 → TS2-4 corresponds to a 4-membered mechanism in both steps. TS1-4 → TS2-6 corresponds to a 4-membered mechanism in the first step and a 6-membered mechanism in the second step, and so on. B) TS8 corresponds to a concerted 8-membered mechanism, while TS1-6 → TS2-8 corresponds to a 6-membered one in the first step and an 8-membered one in the second step.**

The importance of the trapped water molecules for proper functioning of other ribozymes has also been previously reported (Rhodes et al., 2006). In the proposed 8-membered mechanism, a few water molecules are trapped in the active site of the ribosome and the 2'-OH donates its proton to the one which is at close proximity to the functional groups while accepting a proton from the attacking nucleophile. The water then donates its proton to the leaving 3'-O simultaneously.

According to their study, the rRNA bases do not directly participate in the chemical reaction; but they provide a suitable environment for those substrates (i.e. P-site A76 2'-OH and two trapped water molecules) that do (Wallin & Åqvist, 2010). This mechanism is also supported by a few other studies where the water molecules act as proton shuttle and stabilize the transition structure (Kuhlenkoetter et al., 2011; Xu et al., 2012 b; Świderek et al., 2013, 2015).

Another mechanism which is in a good agreement with some experimental observations is the stepwise mechanism where the reaction occurs through formation of an unstable carbon tetrahedral intermediate which results in forming two transition states (Rangelov et al., 2006; Wang et al., 2010, 2015; Acosta et al., 2012; Byun & Kang, 2013; Świderek et al., 2013), since the zwitterionic intermediates are not formed in the reaction in ribosome (Acosta et al., 2012). The neutral tetrahedral intermediate is formed when the P-site carbonyl oxygen is being protonated and the A-site  $\alpha$  amine is being deprotonated, resulting in a tetrahedral carbonyl carbon which is attached to the amino nitrogen from the A-site, and the 3'-O from the P-site while it is single bonded to its carbonyl oxygen.

The various possible origins of the transferred protons results in various proposed mechanisms, in most of which, formation of this intermediate is known to be rate determining (Rangelov et al., 2006; Wang et al., 2010, 2015; Byun & Kang, 2013), while in a few others it appears to occur quite fast relative to the second step, making the latter rate determining (Acosta et al., 2012; Świderek et al., 2013). Even though these studies share a similar tetrahedral intermediate structure, they go through different types of transition states in terms of number of protons “in flight”.

Except for the study carried out by Swiderek et al. (2013), and Rangelov et al. (2006) in which the amino proton is transferred directly to the P-site carbonyl oxygen without going through the 2'-OH of the P-site ribose (concerted 4-membered), the first step in all aforementioned studies is the same and involves a double proton transfer from attacking nucleophile to the 2'-OH and from the latter to the carbonyl oxygen (corresponding to a 6-membered transition structure) (Wang et al., 2010; Acosta et al., 2012; Byun & kang, 2013).

For some unknown reason, regardless of the confirmed direct participation of the P-site 2'-OH group during the reaction and its role in catalysing the reaction in the experiments (Dorner et al., 2003; Weinger et al., 2004; Schmeing et al., 2005-a; Wohlgemuth et al., 2006; Zaher et al., 2011), the proposed mechanisms in which the 2'-O is donating its proton to the leaving 3'-O where there is no stabilizing water in the active site occur relatively slow in computational studies. Finding out the reason can lead towards understanding the origin of the catalytic power of the ribosome. According to the experimental data in terms of presence of rRNA bases in the close proximity of the active site (Lang et al., 2008; Voorhees et al., 2009; Hiller et al., 2011; Polikanov, et al., 2014), the so-called A2451 base is of importance. The process of ester bond dissociation

upon the protonation of the P-site A76 3'-O and peptide bond formation upon deprotonation of the A-site attacking nucleophile are also well defined. What happens in between these two processes is still unanswered and the detailed mechanism of peptidyl transfer as well as the atoms and functional groups involved in this process are still a big dilemma (Matta, 2010; Polikanov et al., 2014).

Even though the presence of A2451 in the active site has been suggested in the experiments and also been used in a few computational studies (Erlacher et al., 2005; Lang et al., 2008; Acosta et al., 2012; Byun & Kang, 2013), the details of participation of this group have not been fully investigated. Furthermore, despite highlighting the importance of the P-site A76 2'-OH group in previous studies (Dorner et al., 2003; Weinger et al., 2004; Erlacher et al., 2005; Schmeing et al., 2005-a; Brunelle et al., 2008), its actual role during the process is still unclear. Finally, whether the process of peptidyl transfer is a stepwise mechanism (Hiller et al., 2011; Wang et al., 2010, 2015; Byun & Kang, 2013) or a concerted one (Wallin & Åqvist, 2010; Acosta et al., 2012; Xu et al., 2012-b; Świderek et al., 2013, 2015) is still on debate.

Several computational mechanistic studies have been carried out to investigate the catalytic power of the ribosome, yet, not all of them cover the three concerns mentioned above (Trobro & Åqvist, 2005; Wallin & Åqvist, 2010; Åqvist, et al., 2012; Acosta et al., 2012; Xu et al., 2012-b; Byun & Kang, 2013; Świderek, et al., 2013, 2015; Wang et al., 2015). There is also the possibility of tunnelling in the ribosomal enzymatic proton transfer reaction which has not been considered in any of the previous studies. It is known that the enzymes are being evolved to enhance the reaction rate. This enhancement does not necessarily mean lowering the activation energy since it is also

not the case for many enzymes (Klinman, 1989; Knapp & Klinman, 2002; Basran et al., 2003; Mincer & Schwartz, 2003; Pudney et al., 2006, 2010; Sen & Kohen, 2010).

The high reaction rate in some of the enzymes can be regarded to vibrationally assisted tunnelling which occurs in biologically relevant temperatures (Gil & Waluk, 2007; Truhlar, 2010). That is, the contracting effect of some of enzymes on the barrier width through a process known as *vibrational gating* facilitates the tunnelling at higher temperatures (Klinman, 1989; Ley et al., 2012), which can be the case for the ribosome.

In this study we show that the catalytic role of the ribosome is not solely due to lowering the barrier height, but it is also due to inducing the proton tunnelling by compressing the barrier width and shortening the donor-acceptor distance. At this point of understanding of how some enzymes induce proton tunnelling to catalyse the reaction, we may take one step back and ask whether the same effect can be done in non enzymatic reactions? To address this question, we examined the non-enzymatic proton transfer reaction of the formation of cyclic boronic ester in interaction of boronic acids with diols.

### **2.2.2 Boronic Acid as Glucose Sensor**

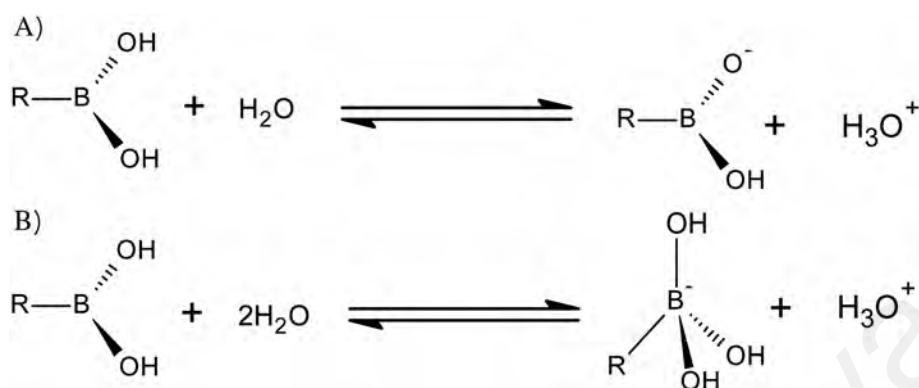
Boronic acids are well-known for their ability to complex with saccharides and form cyclic boronic esters or cyclic boronate ions (Toghill & Compton, 2010; Xu et al., 2010; Nishiyabu et al., 2011-a, b; Bull et al., 2012; Wu et al., 2013; Lacina et al., 2014; Zhai et al., 2015). Increasing the reactivity of boronic acids can lead towards the development of a highly responsive sensor for non-enzymatic glucose monitoring applications. Many studies have been carried out to investigate the reactivity of boronic acids towards diols

in different environmental effects (Martínez et al., 2013). Their reactive species in terms of symmetry around boron however, still remains an open question (Springsteen & Wang, 2002; Watanabe et al., 2013).

Being covalent-based receptors, boronic acid sensors are superior to the synthetic receptors which function via hydrogen bonding (Davis & Wareham, 1999). They rapidly and reversibly form cyclic boronic esters with diols through covalent bonds. Even though this characteristic was known for quite a long time in boric acids (Böeseken, 1949), it was first observed in phenylboronic acid in 1954 upon its addition to a solution of saturated mannitol which eventually led towards formation of cyclic boronic esters (Kuivila et al., 1954). This important finding was followed by several studies on the properties of boronic acids; of particular importance is the Lorand & Edwards' study in 1959 on the structure of benzenboronate ion (Lorand & Edwards, 1959).

It was well understood from the Raman spectrum that the structure of borate ion was similar to that of fluoborate due to the symmetry around boron. However, since boronic acids lack this symmetry, whether the conjugate basic form of boronic acid is trigonal (Scheme 2.2-a) or tetrahedral (Scheme 2.2-b) was still unknown (Edwards et al., 1955). The method Lorand & Edwards (1959) used in their study involved the measurement of the equilibrium constants for formation of complexes between benzenboronate ion and hydroxyl containing compounds. Comparing these constants with that of borate, they concluded that the conjugate basic form of boronic acid and the boronate ester is tetrahedral. This brought up an argument on the reactive form of boronic acid, whether it is trigonal or tetrahedral. It was suggested by Lorand & Edwards (1959) that boronate ion is reactive in alkaline medium since its complex formation lowers the pH. Several other studies have also suggested that the tetrahedral boronate ion is predominant since

most of the reactions occur in alkaline solutions where sensors are most operative (Ishihara et al., 1991; Pizer & Tihal, 1992, 1996; Shao et al., 2000; Bhat et al., 2004).



**Scheme 2.2: Two possible conjugates of a) trigonal, and b) tetrahedral boronate ion**

On the other hand, a few other arguments claim that trigonal boronic acid is the reactive species regardless of the pH of the medium (Kagawa et al., 1995; Ito et al., 2003; Matsumura et al., 2005). The latter group has argued that high reactivity of boronate ion in alkaline solution where it exists abundantly is only due to the low concentration of its conjugate acid and does not necessarily mean that the basic boronate ion itself is more reactive than its conjugate acid. Their study shows that “trigonal boronic acid is always a reactive species irrespective of the pH of the solution and the reactivity of its conjugate tetrahedral boronate ion is comparable with or less than that of the boronic acid” (Iwatsuki et al., 2007, 2012; Miyamoto et al., 2008; Watanabe et al., 2013).

They have also recently validated their conclusion by setting up the reaction systems using the sensors and ligands with different pKa values, without proton ambiguity and fully protonated ligand (Watanabe et al., 2013). They argue that even in alkaline solution, boronic acid is more reactive than its conjugate basic counterpart. Another factor influencing the reactivity of boronic acid is the type of R-group attached to boron. Majority of the studies are carried out using either phenylboronic acid (Pizer & Tihal,

1996; Springsteen & Wang, 2002) or boric acid (Ishihara et al., 1991; Shao et al., 2000; Kagawa et al., 1995; Ito et al., 2003). Their studies are mainly focused on various combinations of diols and the pH values to investigate the selectivity. We on the other hand, have focused on the R-group variety to investigate Boronic acid's reactivity.

One way to look at this problem is to study the rate of which boronic acid or boronate ion is reacting with diols. There are several limitations in experimental studies to figure out the accurate reaction mechanism and kinetic measurements because of the so called proton ambiguity; the transition structure cannot be clearly identified and the reaction of boronic acid in complexing diols can hardly be measured kinetically (Pizer & Tihal, 1992; Ito et al., 2002; Iwatsuki et al., 2012; Miyamoto et al., 2008). Therefore, we use computational quantum calculations and propose a number of alternative reaction pathways between boronic acid and 1,2-ethanediol to identify its most reactive form.

### **2.3 Summary**

In general, protons can act as a link between two atoms by either a hydrogen bond or a three-centre two-electron bond. The former occurs during proton transfer reactions when the transferring proton forms a hydrogen bonding intermediate between the other two atoms (Bell, 1973). These reactions occur abundantly in biochemical systems, specially in enzymes. The mechanistic studies of this type of proton transfer reaction requires careful and detailed investigation since there is always possibility of proton tunnelling. Specially the reactions associated with such a high rate that classical laws of motion are unable to provide an explanation for. This is when the theoretical and computational investigation is required to be carried out additional to the experimental analysis to further confirm the quantum mechanical effects on the reaction rate.

## CHAPTER 3

### METHODS OF CALCULATING THE REACTION RATE

The need for using computational and theoretical tools to investigate chemical reaction mechanisms arises from certain limitations in experimental studies. In the case of enzymatic reactions, these limitations are usually the relatively high reaction rates as well as the complexity of the enzyme structures. The ribosome, in which the process of peptide bond formation occurs, is among the most complex enzymes. The structural complexity of the ribosome and the high rate of protein synthesis ( $\sim 20/s$ ) make it rather difficult to understand the details of this process experimentally. This is where additional computational calculations using appropriate theoretical methods enable us to investigate the details of this mechanism. This type of investigation requires a full knowledge of the system's structure.

#### 3.1 *In Vitro* Crystallographic Structures

High resolution crystallographic structures of both eukaryotic and prokaryotic ribosomes are available in the Research Collaboratory for Structural Bioinformatics (RCSB) protein data bank ([www.rcsb.org](http://www.rcsb.org)). These structures may vary in terms of the attached aa-tRNA and/or mRNA substrates. Sometimes they use substrate analogue instead of the full tRNA molecule to simplify the structure. Nevertheless, it is vital to include both the A-site and the P-site substrates in the peptidyl transferase centre (PTC) of the ribosomal active site if one is focusing on the reaction mechanism of peptide bond formation. The snapshot of the PTC in the ribosome in interaction with the substrates during peptide bond formation however, differs in different studies. This can be due to the major reorganization of the enzymatic active site groups during the

process which makes the determination of the exact pre-peptidyl transfer structure as well as the determination of the exact transition structure and the reaction mechanism rather difficult.

The challenge in finding the exact transition structure which also involves the complementary and extensive computational studies on the active site of the ribosome is still ongoing. In almost all previous computational studies, a very small part of the active site (i.e. around 100 atoms) is being considered, even though the PTC is made of thousands of atoms. Since the search for an exact transition structure requires the study of a chemical reaction which involves breaking and formation of chemical bonds, accurate electronic structure methods are required to handle such systems. These types of reactions are quite demanding, especially for large enzymes which involve large numbers of atoms. As a result, a proper modelling of the enzymatic active site in such a way that it is small enough to be easily handled by electronic structure methods, yet large enough to consider the key elements of the enzymatic active site groups and mimic the whole enzyme to a certain level of accuracy is of particular importance.

### **3.1.1 Theozyme**

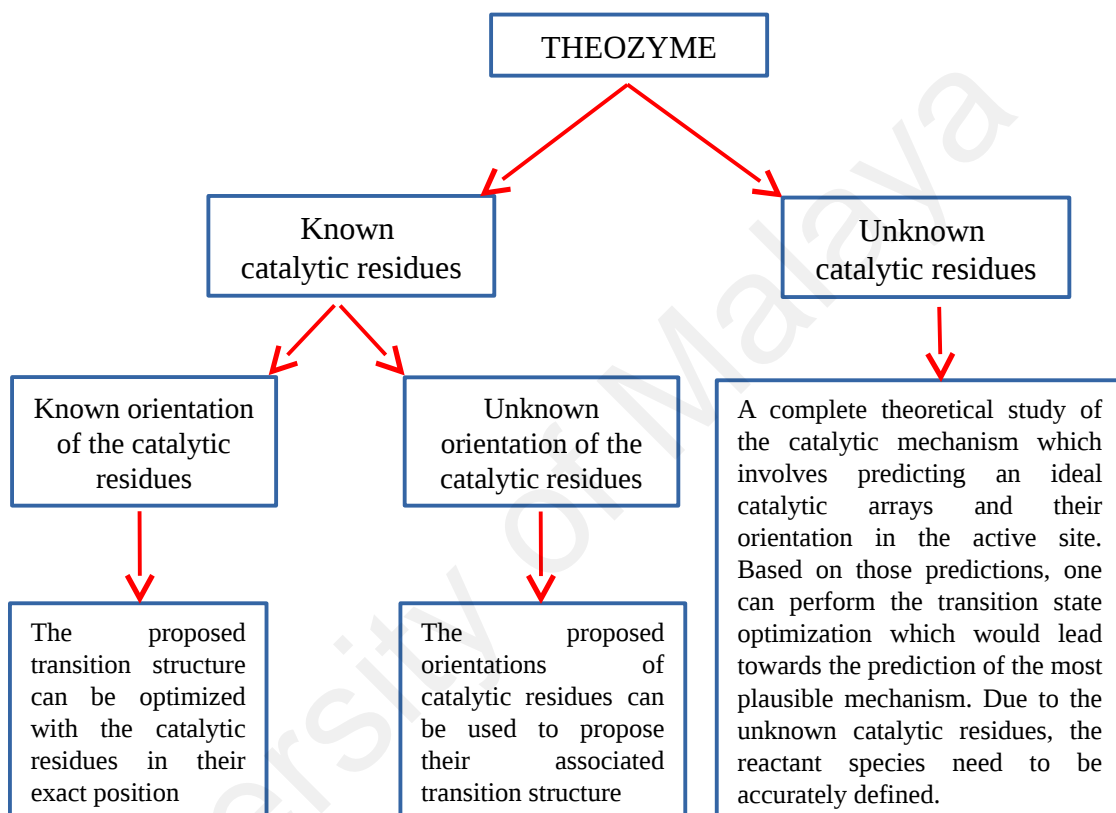
Recent advances in large scale molecular modelling methods made it possible to study the enzymatic reactions by simulating them as a whole or a large part of their active site, provided that the identity and orientation of the enzymatic catalytic arrays are well-known. For large, complex enzymes such as ribosome, neither the identity nor the orientation of the catalytic residues are well-defined and different crystallographic structures of the active site report different pre-peptidyl transfer structures with significantly different orientations of the active site groups. This results in various

possible reaction mechanisms and the large scale modelling would dramatically increase the computation time.

Based on the idea of *theozymes* or *compuzymes* from Tantillo and collaborators (Tantillo et al., 1998), we are able to determine the most appropriate arrangement of catalytic arrays in the active site during the peptidyl transfer reaction by modelling a smaller part of the active site. This will enable us to predict the structure of the pre-peptidyl transfer and as a result, an accurate transition structure. A theozyme is a theoretical model for studying biological catalyses. Tantillo et al., defines a theozyme as: “*An array of functional groups in a geometry predicted by theory to provide transition structure stabilization*”. This is an indication of a theoretically predicted geometry and arrangement of functional groups which can quantitatively validate the individual atomic contribution in transition structure stabilization, which is the role played by all enzymes. The  $10^7$ -fold enhancement in the rate of peptide bond formation in the ribosome compared to that in solution is a very good example of this role (Sievers et al., 2004). Figuring out the type of enzymatic functional groups and their role in ribosomal catalysis is the major goal of this study.

Scheme 3.1 illustrates the different possibilities for constructing a theozyme based on the available crystallographic structures. For known catalytic arrays and their orientation around the substrates, constructing the model system is rather straightforward and the possible reaction mechanisms can be narrowed down. However, the orientation of the catalytic arrays is not always well-defined. Hence, testing more possible reaction mechanisms are required to work out the most plausible one, which can then be used as the model system for large scale modelling of the enzymatic reaction. In the case of ribosomal catalysis, both the active site residues and their

orientation in the active sites are unknown. This puts the ribosome at the far right side of the diagram in Scheme 3.1. With the high resolution crystallographic structures and various computational and theoretical studies on this problem, we are slowly moving towards the left side of the diagram.



**Scheme 3.1: Different conditions of constructing a theozyyme according to the available information in the enzymes' crystallographic data.**

To construct an ideal theozyyme, one must rely on the high resolution crystallographic structure of the ribosomal active site and propose a transition structure based on the assumption that the structure is the true pre-peptidyl transfer structure. In this work we used three different crystallographic structures from three different studies (Schmeing et al., 2005-b; Lang at al., 2008; Voorhees et al., 2009, (PDB codes of 1VQ6, coordinated based on 1VQN and 4V5C respectively)). These three structures have one thing in

common, that is, the presence and interaction of the A2451 rRNA base in the active site. The orientation and type of interaction however varies significantly between them. Not knowing which one of these structures are closer to the transition structure (i.e. the exact pre-peptidyl transfer structure), we have proposed three different reaction mechanisms with three different orientations of A2451 around the substrates.

The *proposed* ribosomal active site groups would rearrange the orientation of the reacting groups during energy minimization which might result in a preferred complex of pre-peptidyl transfer structure. According to the definition of the theozyme, the catalytic array which has a more stabilizing effect on the transition structure could bring us closer to the actual enzymatic catalysis. In this work, molecular properties of these structures are calculated with electronic structure methods. The choice and use of these methods as well as the molecular simulation are elaborated in the next section.

### **3.2 *In Silico* Calculations of Reaction Mechanism**

All calculations were performed at the constant temperature of 298.15 K and pressure of 1 atmosphere using the Gaussian09 suite of programs (Frisch et al., 2010) on a 64X dual core Intel Itanium2 64-bit Symmetric Multi-Processing machine as well as an 11-node, 702 processor-core and 2.7 TB RAM Linux cluster.

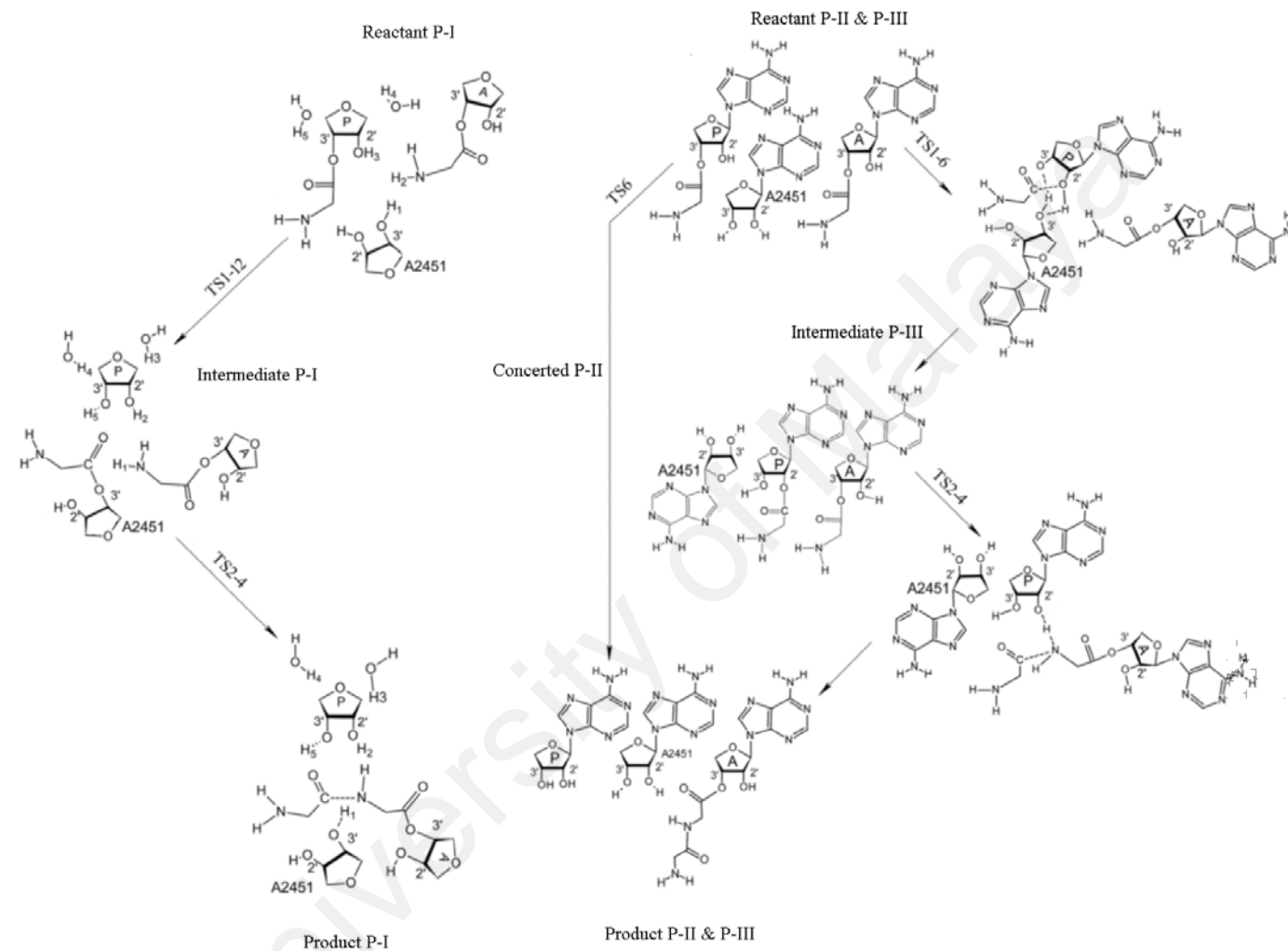
The temperatures are varied for the calculations related to the temperature dependant kinetic isotope effects from 53.15 K to 303.15 K. These conditions are applied to calculations involving both peptide bond formation and boronic acid esterification reactions.

### 3.2.1 Simulation of the Reaction Mechanism of Peptide Bond Formation

Overall, the reaction mechanisms of peptide bond formation calculated in this study are divided into two main groups: (i) those which follow the previously proposed mechanisms where the adenine bases are absent and only the sugar moieties of the A- and the P-site tRNAs have been taken into consideration (Chapter 2, Scheme 2.1), and (ii) three novel proposed reaction mechanisms. In two of the novel mechanisms, the participating groups in the reaction are defined by optimizing the active site in the presence of three adenosine bases (i.e. the A- and P-site A76 of the tRNAs as well as the A2451 of 23S rRNA). In the third mechanism, three ribose sugars represent the A-site tRNA, the P-site tRNA, and the A2451 rRNA base along with two water molecules in the active site (Scheme 3.2).

The left mechanism shows the originally proposed water catalysed peptide bond formation based on Steitz's crystallographic structure with a 12-membered proton transfer mechanism in step 1, with 5 protons in flight, and a 4-membered transition structure in the second step of the reaction. In this process, the 3' -OH group of the A2451 acts as a peptidyl shuttle to transfer the growing polypeptide chain from P-site leaving group to the A-site amino acid.

The TS-6 in the middle is based on the crystallographic structure of Ramakrishnan which indicates the concerted 6-membered mechanism with the N3 of A2451 interacting with the  $\alpha$ -amine. The TS1-6  $\rightarrow$  TS2-4 at the right indicates the stepwise mechanism which is proposed based on the crystallographic structure of Polacek and collaborators where there is no interaction between N3 of A2451 and the  $\alpha$ -amine.

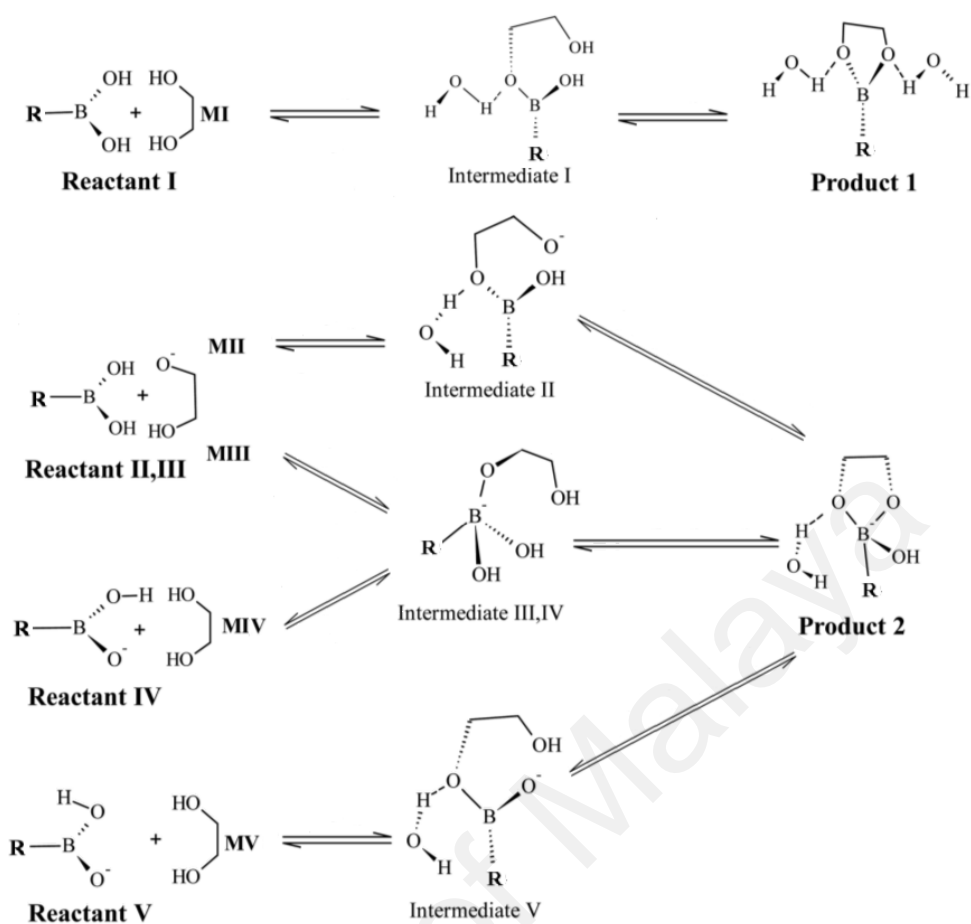


**Scheme 3.2: The three mechanisms proposed in this study. The reactant and products are taken from the pre- and post-peptidyl crystallographic structures of Steitz on the left (Schmeing et al., 2005-b), Ramakrishnan in the middle (Voorhees et al., 2009) and Polacek on the right (Lang et al., 2008).**

In this model, which is fully treated quantum mechanically, the phosphate backbones are substituted by hydrogen atoms which signify the boundary between our theozyme and the rest of the RNA molecule. The water catalysed reaction mechanism excludes the adenine bases since there is no key interaction between these bases and the active site in this proposed mechanism. The geometries of the reactants, intermediates and the products are optimized before the search for the transition structure. The energy of the reactant is taken as the energy of reactant complex, which is the energy of the reactant species interacting with hydrogen bonds. Even though the energy of the reactant complex might be lower than the energy of the reactant species (i.e. higher stability) which would result in a higher activation energy, it is more realistic to take the energy of the reactant complex since it is closer to forming the transition structure. The same goes for the optimization of the reactant species in boronic acid in reaction with diols.

### **3.2.2 Simulation of the Reaction Mechanism of Boronic Acid With Diol**

Five different mechanisms are proposed for this reaction where each one represents a different type of medium with a different effect on the reaction (Scheme 3.3). Mechanism I is a reaction between neutral diol and neutral boronic acid which is a strong lewis acid due to the empty  $p$  orbital on boron, deshielding its nucleus. The result of this is an interaction between boron in boronic acid and the electron lone pair on the oxygen of the incoming diol. However, it is not confirmed whether boronic acid is reactive in its trigonal form or tetrahedral form. A few studies calculated a higher reaction rate by 3-4 orders of magnitude for tetrahedral boronate ion compared to its trigonal boronic acid counterpart (Pizer & Tihal, 1992, 1996; Shao et al., 2000). It is however not wise to conclude that the tetrahedral boronate ion is the reactive species since it would be rather difficult to specify the rate determining step in experimental studies.



**Scheme 3.3: The five different proposed reaction mechanisms for the reaction of boronic acid with diol.**

The best way to examine the reactivity of tetrahedral boronate ion is to propose a reaction mechanism where the reaction between trigonal boronic acid and a diol would form a tetrahedral intermediate. For the formation of this intermediate, we need a trigonal boronic acid as starting material which is either a Brønsted basic sensor or a neutral boronic acid with a basic incoming ligand. The former occurs with the diol donating its proton to O<sup>-</sup> of trigonal boronic acid and forms a tetrahedral intermediate with boron (mechanisms IV&V). The latter occurs with the incoming ligand lacking an acidic proton where the negative oxygen would then react with the Lewis acidic boron (mechanisms II & III).

In all the stepwise mechanisms, the intermediate is treated as the product of the first transition structure calculation and the reactant of the second transition structure calculation. The only information needed to calculate the reaction rate for these mechanisms are the energies for the reactant complex and that of the transition structure. The difference between these two energies give the energy of activation which can be inserted into the Eyring-Polanyi equation (Equation 2.10 where  $k = \frac{k_B T}{h} e^{\frac{-\Delta G^\ddagger}{RT}}$ ) to calculate the rate of the reaction. The energies and other properties of the reactant structure and transition state complex are calculated using the electronic-structure method known as density functional theory (DFT) which will be briefly described in the next section.

### 3.2.3 Model chemistry

Two different model chemistries used in this study are:

- B3LYP/6-31+G(d,p) PCM for the esterification reaction of boronic acid with diols.
- M06-2X/6-31+G(d,p) SMD for the process of ribosomal peptide bond formation.

This section involves a brief theoretical background of the model chemistries mentioned above and the justification for using these specific methods in our research.

#### 3.2.3.1 The DFT Functionals

Around hundreds of density functionals in various categories have been introduced in the past four decades (Becke, 2014; Jones, 2015). The first generations of the functionals are the local functionals that are suited for solid-state physics. These

functionals lack the ability to handle van der Waals interactions such as London dispersion forces since the electronic energy density at each point in space only depends on the characteristics of the electronic density and kinetic energy at the neighbouring points. Introducing a high percentage of the HF (Hartree Fock) exchange to the exchange energy in hybrid GGA (Generalised Gradient Approximation) functionals overcomes this defect. Nevertheless, solid state physics systems containing transition metals favour lower percentage of the exact exchange. Thus, the hybrid GGA functionals are mainly developed and used for the main group thermochemistry, specially large biomolecules where the van der Waals forces play an important role.

The percentage of HF exchange varies in different hybrid GGA functionals, depending on the system and the type of application the functional is designed for. For example, functionals with full HF exchange are mainly suitable for isoelectronic systems and can treat long range charge transfer excited states. However, enforcing full HF exchange in a functional restricts the flexibility of the functional which does not provide the desired accuracy if used for complex systems (Zhao & Truhlar, 2008-b). Developing an ideal functional which covers all the systems and areas in physics and chemistry is impossible, at least in the near future. Therefore, the DFT functionals are being developed to be system specific. There are five areas which are the main focus of the functional developers:

TC → main group thermochemistry

NC → non-covalent interactions

BH → barrier heights

ES → electronic spectroscopy

TM → transition metal bonding

Most of the functionals usually cover one of these areas, but sometimes specific functionals are developed which can cover two or more of these areas. For instance, functionals which are designed for BH and NC should accurately predict the structure, energies and vibrational frequencies for transition states (BH) and for complexes which are having non-covalent interactions (NC). These functionals have been reported to perform well for specific thermochemical properties with medium range (  $\sim 2-5 \text{ \AA}$  ) interaction (Zhao & Truhlar, 2008-b). This is something that is usually performed by TC functionals for compounds which contain the main group elements. These insights are required for performing DFT calculation on a specific system to obtain the desired results with a high degree of accuracy. For the two different systems under study in this research, we have selected two main functionals: B3LYP and M062X.

### **B3LYP**

The three parameters in the exchange energy functional were first introduced in B3PW91 functional (Becke three parameter exchange functional and Perdew-Wang correlation functional) by Becke (1993-a, b). This led to the development of B3LYP functional (Equation 3.1) in which Perdew-Wang correlation functional (  $E_c^{PW91}$  ) (Perdew & Wang, 1992) is replaced by Lee-Yang-Parr correlation functional (  $E_c^{LYP}$  ) (Lee et al., 1988).

$$E_{xc}^{B3LYP} = (1-a) E_x^{LSDA} + a E_x^{HF} + b \Delta E_x^{B88} + (1-c) E_c^{VWN} + c E_c^{LYP} \quad (3.1)$$

The values 0.2, 0.72, and 0.81 were determined by fitting to experimental data for parameters a, b, and c, respectively. The second term is the exact exchange energy which is calculated using the HF orbitals and mixed with those obtained from Kohn-Sham orbitals (the first and third terms). The high efficiency of this functional in terms

of computer power as well as its ability to accurately predict geometries, binding energies and barrier heights made it the most popular functional in DFT to the point that the associated paper (Lee, et al., 1988) was cited more than 77000 times in 2018.

The B3LYP functional contains 20% exact exchange which provides enough accuracy for short range (  $\leq 2 \text{ \AA}$  ) and medium range (  $\sim 2-5 \text{ \AA}$  ) interactions and can be used for small molecules (Becke & Johnson, 2007; Zhao & Truhlar, 2008-a; Grimme et al., 2010; Torres & DiLabio, 2012). However, it is not well suited for the long range interactions (  $\geq 5 \text{ \AA}$  ) and might not provide reasonable results for the systems which are sensitive to the London dispersion forces such as large biomolecules (Zhao & Truhlar, 2008-a, b). This defect however, has been overcome by introducing higher percentage of the HF exchange to the  $E_{xc}$  and reducing the self interaction error.

### ***M06-2X***

The M06 family of exchange-correlation functionals (i.e. M06-L, M06, M06-HF and M06-2X) were developed by Truhlar and collaborators in 2006 (Zhao & Truhlar, 2006-a, b, 2008-a, b). These functionals cover a relatively wide area of research and can be used more efficiently in the topics which require to combine, for example, BH with TM. The M06-L functional for instance, is the least efficient functional of the M06 family for measuring barrier heights, which is sensible, being a local functional with no exact exchange. It is however the most accurate functional among the local functionals and can provide a relatively reasonable description of systems going through a chemical reaction. This can be specifically useful for demanding applications on large systems where only the local functionals are affordable.

The most efficient functional in treating the electron dispersion forces in this family which has been an improvement over the “standard” exchange correlation (XC) functionals is the M06-2X functional (Klimes & Michaelides, 2012). This functional has 54% HF exchange which is double the amount of that in the M06 functional (27%), hence the term 2X at the end (Zhao & Truhlar, 2008-b). It is however not necessarily the case where increasing the percentage of HF exchange in the exchange-correlation functional increases the accuracy and efficiency of that functional in the area of BH and TC. The M06-HF functional for example, with 100% HF exchange, is developed to cover the areas related to charge transfer and excited state which comes with the price of less ground-state accuracy. This functional is known as hybrid meta-GGA due to the hybrid exchange and meta-GGA exchange and correlation terms (Equation 3.2).

$$E_{XC}^{hyb} = \frac{X}{100} E_X^{HF} + \left(1 - \frac{X}{100}\right) E_X^{meta-GGA} + E_C^{meta-GGA} \quad (3.2)$$

X is the percentage of HF exchange energy in the hybrid functional which is deducted from the local meta-GGA exchange energy, as indicated in the first two terms. The last term is the correlation energy functional which is the same for all four M06 functionals (Zhao & Truhlar, 2008-b).

### ***Different functional for different systems***

In this study, we used the hybrid B3LYP functional to investigate the reaction mechanism of boronic acid in interaction with diols. Due to the relatively small size of the molecule, the non-covalent interactions are within small and medium range interactions and B3LYP would be highly efficient for this system in terms of both accuracy and time efficiency.

On the other hand, a larger molecule with high sensitivity towards the long range non-covalent interactions cannot be adequately treated with methods like B3LYP. This is the case where methods with long range corrections such as M06 family of functionals are to be used, even though they might appear to be more computationally expensive. This is the reason for selecting the M06-2X functional to investigate the process of peptide bond formation in the ribosome.

The M06 class of functionals have been known to be very successful in calculating the barrier heights and reaction free energies for large biomolecules and have been extensively used for peptide bond formation process in ribosome (Acosta et al., 2012; Byun & Kang, 2013; Świderek et al., 2015; Wang et al., 2015). The Minnesota group of density functionals, specifically the M06-2X, are further tested and validated using the double  $\zeta$  basis set, 6-31++G(d,p), which is also used in this study (Ditchfield et al., 1971; Zhao & Truhlar, 2008-b). A proper choice of basis set is another important part of the electronic structure calculations which is described briefly in the next section.

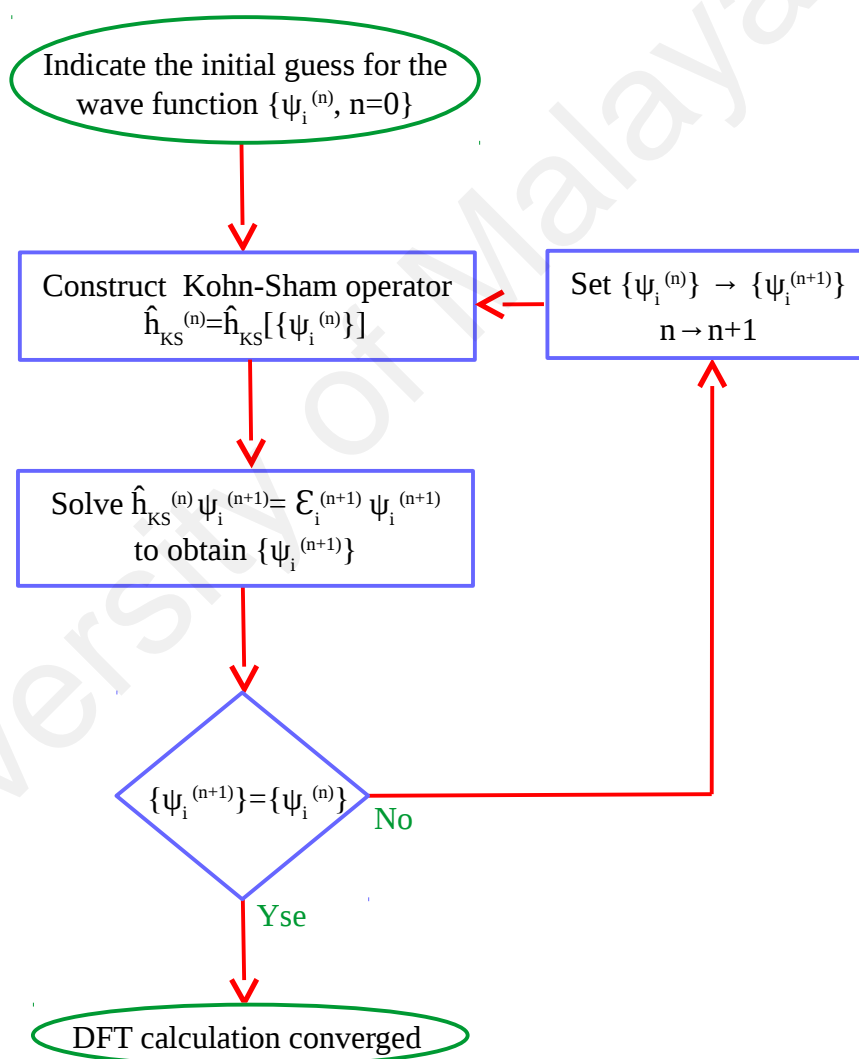
### 3.2.3.2 Basis Sets

Using the same analogy to the Roothaan-Hall method for solving the Hartree-Fock equation (Hall, 1951; Roothaan, 1951), the Kohn-Sham equation (Equation 2.4) can also be transformed into a matrix form of

$$F^{KS}C = SC\varepsilon \quad (3.3)$$

where  $\varepsilon$  is a square diagonal matrix of the orbital energies with its elements as the one electron orbital energies  $\varepsilon_i$  of Kohn-Sham orbital  $\psi_i$ ,  $C$  is the square matrix of the

molecular orbital expansion coefficient, and  $F^{KS}$  and  $S$  are the Kohn-Sham and overlap matrices respectively (Levine, 2009; Jensen, 2013). To form the Kohn-Sham matrix, the molecular orbital coefficients must be known. Since Equation 3.3 is to determine the molecular orbital coefficients for forming the elements of the Kohn-Sham matrix, an initial guess is required for these coefficients. This results in the Kohn-Sham self consistent field (SCF) procedure (Scheme 3.4).



**Scheme 3.4: The self consistent field procedure in Kohn-Sham density functional theory geometry optimization.**

The initial guess is a linear combination of a set of atomic orbital wavefunctions i.e. the basis functions or basis sets. The basis sets used in computational chemistry calculations are divided into two main groups. One group includes the projected augmented wave and plane wave pseudo-potentials, and the other group includes Slater-type orbitals (STOs) and Gaussian-type orbitals (GTOs). The basis functions in the former group are de-localized and they are the most suitable for atomic and solid-state physics (Cramer & Truhlar, 2009), while those in the latter are localized on the atomic nuclei, hence more suited for main group chemistry and biochemical structures. The STOs can be written as:

$$\psi_{STO}(x, y, z) = x^l y^m z^n e^{-\xi r} \quad (3.4)$$

where the  $x, y, z$  are the local Cartesian coordinates  $l, m, n$  describe the angular momentum of the orbital and  $\xi$  in the exponent characterizes the radial size from the atomic nuclei. The STOs show a rather accurate cusp behaviour near the nuclei (Figure 3.1), however, there is no analytical solution and the coulomb and exchange integrals can only be solved numerically which would make it practically impossible to be used in complex systems.

The GTOs on the other hand, overcome this problem by providing analytical evaluation of the coulomb and exchange integrals. They can be written as

$$\psi_{GTO}(x, y, z) = x^l y^m z^n e^{-\xi r^2} \quad (3.5)$$

where the quantum numbers  $l, m, n$  characterize the angular shape and direction of the orbital and  $\xi$  in the exponent characterizes the radial size. However, they are not as

accurate as STOs since they (1) decay too fast at larger  $r$  and (2) poorly represent the cusp condition near the nucleus as they are flat topped at  $r \sim 0$  (Figure 3.1).

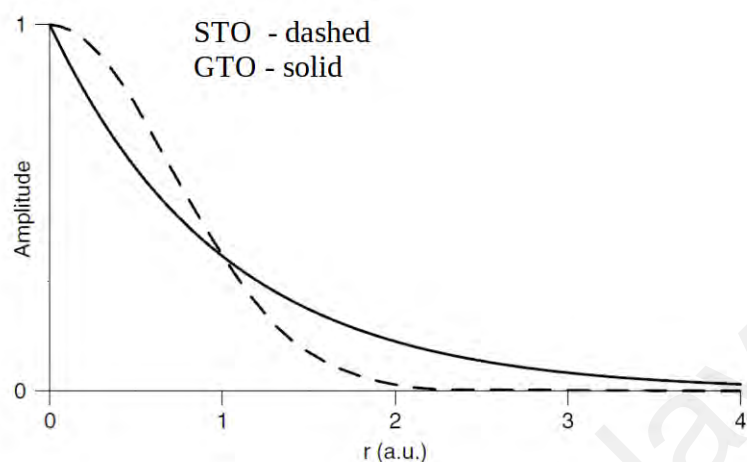


**Figure 3.1: The radial characteristic of the STOs and GTOs, indicating a correct cusp behaviour near the nuclei for the STOs and a wrong cusp behaviour for the GTOs.**

A fixed linear combination of a set of primitive GTOs or PGTOs ( $\psi_{PGTO}$  in Equation 3.6) can create a soft avoidance in proximity of the nuclei which more or less mimics the sharp cusp of the STOs. This combination which is not treated as linear combination of atomic orbital parameters in the basis function, is written as:

$$\psi_{CGTO} = \sum_i a_i \psi_{PGTO} \quad (3.6)$$

where  $\psi_{CGTO}$  is called contracted GTO (CGTO). The molecular orbital  $\psi_i$  is then created by the linear combination of  $\psi_{CGTO}$  (Equation 3.7).

$$\psi_i = \sum_r c_{ri} \psi_{CGTO} \quad (3.7)$$

The basis set contraction however does not create a real cusp since every PGTO has a zero slope at  $r \sim 0$ , so any combination would also have a zero slope. Nevertheless, obtaining an accurate cusp behaviour for the core orbitals is specifically important for the cases where there are some unpaired electron density near the nucleus. In most cases, especially when treating chemical reactions, the valence region is of more importance and needs to be treated more appropriately and forming the CGTOs for the core orbitals would be sufficient. To have a better description of the valence orbitals, Pople introduced the split valence basis sets in which the number of CGTOs for the valence orbitals are doubled (double  $\xi$ ) or tripled (triple  $\xi$ ), while the core orbitals are treated with minimal basis (Pople, 1999; Pietro et al., 1982). These types of basis sets are of particular importance in our study since a great deal of chemical reactions and reactivity is involved.

To give extra angular momentum to the atom's valence orbital space, the d function can be added to the atoms C, N, and O and the p function can be added to the atom H. These added functions are called polarization functions which give extra angular flexibility to the formation of molecular orbitals in the valence orbitals (Rassolov et al., 2001). They also add angular correlation to describe the electrons' movement and are therefore necessary for calculations which involve bond breaking-forming.

The polarization functions are similar in size to the valence orbitals, but different in shape. The radial freedom to the valence orbital space can be added to the basis set using diffuse functions. These functions account for the wavefunction which is distant from the nucleus, hence, are necessary for carrying out calculations on anionic systems as well as for the systems with long range interactions.

Among the extensively used family of basis sets for organic compounds are people's split valence 6-31++G(d,p) and 6-311++G(d,p) basis sets. In both notations, the core atomic orbital is expanded by 6 contracted Gaussians whereas the valence atomic orbitals are expanded by a contraction of 3 and 1 Gaussians in the former (double  $\xi$ ) and 3 and 1 and 1 Gaussians in the latter (triple  $\xi$ ). These basis functions further describe the set of d-functions added to the heavy atoms and a set of p-functions added to hydrogen atoms (indicated as "d, p"). The diffuse function is displayed as (+) which covers the portion of atomic orbitals distant from the nuclei. The second + adds the diffuse function to the hydrogen atom in addition to the heavy atoms. The third part of the model chemistry is the choice of the medium in which the reaction takes place. Since biochemical reactions mainly occur in water solution, water medium is used in this study. The next section elaborates on the type of solvent models used.

### 3.2.3.3 Medium

To feasibly calculate the solvent effects on solvent mediated chemical reactions, it is necessary to use an implicit solvent model rather than individual solvent molecules. The calculations in this study are carried out using two different water solvent models, i.e. the integral equation formalism for the polarizable continuum model (IEFPCM) and the Solvation Model based on Density (SMD).

The former is more suitable for the hybrid DFT methods such as B3LYP, hence, it is used in the boronic acid study (Tomasi et al., 1999, Tomasi et al., 2005). The latter is suitable for the Minnesota functionals which is used for the peptide bond formation study (Marenich et al., 2009).

The polarizable continuum model (PCM) in general involves the solute which is described quantum mechanically and the solvent which is a continuum model, interacting with the solute with a permittivity of  $\epsilon$ . The solvent in this model is a set of overlapping spheres centred on the nuclei of the solute forming a molecular cavity around it. One of the key issues in all implicit solvation models is the boundary between the solvent and solute's cavity. The shape and size of the cavity differs in different versions of the continuum models. In the IEFPCM model, the cavity is defined as a series of overlapping spheres which are characterized by the van der Waals radii of the nuclei. The advantage of this model is in providing a complete answer to the free energy of solvation which is defined as

$$G_{\text{solvation}} = G_{\text{electrostatic}} + G_{\text{dispersion-repulsion}} + G_{\text{cavitation}} \quad (3.8)$$

It however fails to provide a complete description of the cavitation dispersion repulsive energy (Tomasi et al., 2005). The SMD model on the other hand, defines the cavity by enclosing a superposition of nuclear-centered spheres with intrinsic Coulomb radii, the values of which depend only on the atomic numbers of the atoms. The solvation free energy in this model which is expressed as

$$\Delta G_S^\circ = G_{\text{CDS}} + \Delta G_{\text{EP}} \quad (3.9)$$

is divided into two main components (Marenich et al., 2009). One is  $G_{\text{CDS}}$  which denotes the free energy change related to solvent cavitation, dispersion energy, and the local solvent structure, which are short range interactions between the solute and the solvent. The other is  $\Delta G_{\text{EP}}$  which involves the contribution of the electronic and polarization components of the free energy to the total free energy, which is obtained by

solving the non-homogeneous Poisson equation (NPE) for electrostatics in terms of the integral equation formalism polarizable continuum model (IEF-PCM) through self consistent reaction field calculation (for the details please refer to Marenich et al., 2009).

Unlike the previously developed SM8 model by the same group (Marenich et al., 2007) in which the solute molecules are represented as partial atomic charges in a cavity using the GB (Generalized Born) approximation (Still et al., 1990), the SMD model is based on the continuous charge density of the solute. The SMD model does not rely on the accurate calculation of partial atomic charges, and this makes such model applicable in a wider range of electronic structure methods compared to SM8. A few recent studies have also mentioned the aptness of this solvation model with the M06-2X level of theory and reported rather reliable free energies of activation for the ribosomal peptide bond formation (Acosta et al., 2012; Byun & Kang, 2013).

#### **3.2.4 Response theory: Gradients, Hessians and Reaction Paths**

Additional to calculating the wavefunction and energy of a molecule, it is also important to calculate the response of the energy to certain perturbations. In the study of chemical reactions, the perturbation is to search for transition structures on the potential energy surface (PES). This involves the study of the derivative of the energy with respect to vibrational distortions of a chemical bond, or in other words, the study of how the energy evolves as a function of molecular deformation on the PES. The energy path towards the saddle point can describe the details of the reaction coordinate and the energy on the saddle point can describe the kinetics of the chemical reaction. Since we are dealing with the bare proton transfer where the motion of the proton is not coupled

with that of the electron, the electronically adiabatic formulation is used to calculate these energies. The general way to search for a saddle point on the PES (Figure 3.2) is to search for a point where all the gradient components are zero (optimum points) and the Hessian eigenvalues are positive along the  $3N-7$  degrees of freedom<sup>5</sup> and negative along one degree of freedom.

The energy change along the Hessian eigenmodes can be expressed as

$$\delta E = \sum_a \left\{ g_a \delta V_a + \frac{1}{2} \lambda_a (\delta V_a)^2 \right\} \quad (3.10)$$

where  $V_\alpha$  is the Hessian eigenmode,  $g_\alpha$  is the gradient parameter and  $\lambda_\alpha$  is the Hessian eigenvalue. This is a linear combination of the two separate terms, the linear term ( $g_\alpha \delta V_\alpha$ ) plus the quadratic term ( $\lambda_\alpha / 2 (\delta V_\alpha)^2$ ) along each separate eigenmode direction.

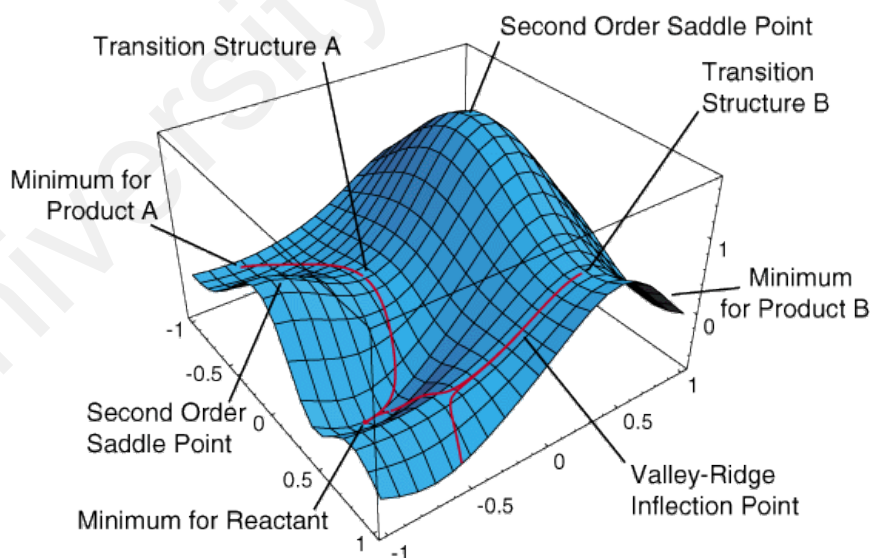


**Figure 3.2: The three dimensional PES of the energy change with respect to displacement along two directions.**

<sup>5</sup> A non-linear molecule with  $N$  atoms has  $3N-6$  vibrational degrees of freedom. Based on the no separability assumption in the transition state theory, the transition structure is assumed to have one degree of freedom along the reaction coordinate and  $3N-7$  degrees of freedom along all other directions.

On the stationary points, minima, maxima and saddle points, the derivative of the energy with respect to the displacement is zero, giving:

$$\delta V_a = -g_a / \lambda_a \quad . \quad (3.11)$$

The  $\lambda_\alpha$  in the denominator indicates that each step on the PES along the reaction path is taken with different magnitude, that is, for larger values of  $\lambda_\alpha$  (large curvature), the next step must be shorter to avoid sudden change in energy. The displacements taken in searching for the minimum are along the modes with positive Hessian eigenvalue and opposite the modes with negative Hessian eigenvalues. In searching for the saddle point, these displacements are taken along all the modes, whether or not the Hessian eigenvalues are positive, that is, for points moving towards minima with positive  $\lambda_\alpha$  as well as those moving towards maxima with negative  $\lambda_\alpha$ . This would result in the displacement steps to remain on the so-called “stream bed” until a point is reached where there is a negative Hessian eigenvalue along one direction and positive Hessian eigenvalues along all other directions, i.e. the saddle point (Figure 3.2). This method is known as the local eigenvector following which requires a reasonable initial guess for the transition structure (Schlegel, 1982). In the cases where finding the initial guess is difficult or impossible, one can use the global method such as Quadratic Synchronous Transit (QST) which interpolates between the reactant and the product.

In searching for the saddle point, it is very important to start up with an initial guess which is a geometry near the saddle point region. It is however important to avoid falling into a false saddle point. For example, the reaction of boronic acid with diols in this study involves the transfer of a proton from diol to the OH of the boron. This results in the OH to break its bond with boron and form a water molecule (Scheme 3.3-MI).

Knowing that boronic acid has a very low barrier to the hydrogen bond complex formation with the diol, one cannot simply take a low energy step towards the negative curvature as it might result in finding a transition structure to the hydrogen bond formation rather than the esterification reaction. Hence, in this case and many other cases, the reactant and product geometries are required as an input to insure the accuracy of the transition structure. Therefore we used a method known as Synchronous Transit Quasi-Newton (STQN) which requires the structures of the reactant and product as input to generate the initial guess for the first order saddle point by moving along the parabola that connects the reactant and the product (QST method) (Peng & Schlegel, 1993; Peng, et al, 1996). It then uses the local eigenvector following method to complete the search. Despite this, there is still a risk of falling into a different reaction path and finding a transition structure which is not related to the desired chemical reaction. This is when the reaction path test becomes of importance.

The reaction path test can be carried out once the transition structure has been found. This is followed by evaluation of harmonic vibrational frequencies which are given by:

$$\omega_a = (\lambda_a)^{(1/2)} \quad (3.12)$$

using the eigenvalues of the mass weighted Hessians,  $\lambda_\alpha$ . These eigenvalues are all positive on the saddle point, except for one which is negative. The dynamical motion along the eigenvector of negative  $\lambda_\alpha$  would lead towards the reaction path. This is the so-called intrinsic reaction coordinate (IRC) calculation which confirms that the transition structure is associated with the reactant and product one has started with.

The importance of finding the transition structure for a chemical reaction arises from the necessity of calculating the rate at which the reaction is taking place. For this purpose, one must accurately know the energy of activation,  $E_a$  which is the difference between the free energy of the reactant and that of the transition structure. There are various theoretical methods to calculate the rate of a chemical reaction, one of which is the theory of activated complex or the transition state theory (TST). This is the theory used in this study and will be elaborated in the next section.

### 3.3 Calculating the Reaction Rates

Once the detailed description of the transformation from the reactant to the products has been established, the rate of this transformation can be calculated using the transition state theory. One of the most important contributions to TST is the van't Hoff's equation (Equation 2.8) which links the reaction rates to thermodynamics. The velocity of a reaction (rate) can be written as

$$v = \text{constant} \times e^{-\Delta G^\ddagger/RT} \quad (3.13)$$

where the  $\Delta G^\ddagger$  is the change in Gibbs free energy from the reactant to the activated species and the constant is a multiplying factor. Kohnstamm et al. (Laidler, 1977) later split  $\Delta G^\ddagger$  into entropy and enthalpy terms:

$$v = \text{constant} \times e^{\Delta S^\ddagger/R} e^{-\Delta H^\ddagger/RT} \quad (3.14)$$

They were however unable to interpret the multiplying factor which was later interpreted in TST.

### 3.3.1 Conventional Transition State Theory (CTST)

The CTST postulates that there is a quasi-equilibrium between the reactants and the transition state. Suppose we have a system at equilibrium:



where A and B are the reactant species and C and D are the product species. In CTST, the main focus is on the saddle point of the PES where there is a transformation (Figures 2.1 & 3.3).

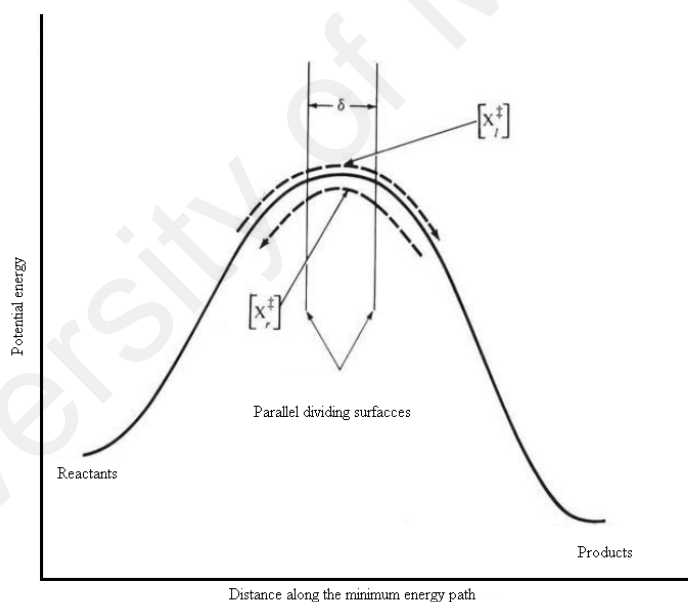


**Figure 3.3: Minimum energy path profile (Laidler, 1984).**

This transformation occurs through an imaginary surface on the PES with the reactants at the left and the products at the right, arbitrarily. Since there is no physical transition structure anywhere at the saddle point, we assume a second dividing surface parallel to the first one with an infinitesimally small distance of  $\delta$  through which the activated

complexes would pass. With this assumption, we can measure the flux of the activated complexes from reactants to the products. We can then write:

$$[X_f^\ddagger] + [X_r^\ddagger] = [X^\ddagger] = K_c^\ddagger [A][B] \quad (3.16)$$

where the  $K_c^\ddagger$  is the equilibrium constant, the  $[X^\ddagger]$  is the total concentration of the activated complexes and  $[X_f^\ddagger]$  and  $[X_r^\ddagger]$  are the concentration of the activated complexes entering the  $\delta$  region for both the forward (f) and the reverse (r) reaction mechanisms respectively.

To satisfy the *no-recrossing* assumption (first TST assumption in Chapter 2, Section 2.1.2.1) in a system at equilibrium, we can get rid of the product species and arrive at Equation 3.17:

$$[X_f^\ddagger] = \frac{1}{2} K_c^\ddagger [A][B] \quad (3.17)$$

where all  $[X_f^\ddagger]$  species must form the product. Provided that the first TST assumption is satisfied, the other way round must also be true:

$$[X_r^\ddagger] = \frac{1}{2} K_c^\ddagger [C][D] . \quad (3.18)$$

From the first two TST assumptions and by applying the methods of statistical mechanics to the equilibrium constant  $K_c^\ddagger$ , we can get an expression for the rate at which the activated complexes  $[X_f^\ddagger]$  that were the reactants in the *immediate past* are forming the products (Laidler, 1984). This expression can be seen in Equation 2.6

(Chapter 2) where the term  $q_{\ddagger}$  indicates the partition function for the activated complex and follows the third TST assumption. That is, the actual motion over the saddle point is omitted and is represented as a classical translational motion.

It was first suggested by Wynn-Jones and Eyring (1935) to treat this motion as a very loose vibration. Instead of  $3N-6$  degrees of freedom (for a non-linear complex) we then would have one weak vibration along the reaction coordinate which in the limit of  $\nu \rightarrow 0$  can be expressed by Equation 3.19 (for which the vibrational partition function is expressed by Equation 3.20), and  $3N-7$  degrees of freedom along all directions orthogonal to the weak vibration which is expressed as  $q_{\ddagger}$  in Equation 2.7 (Chapter 2).

$$\lim_{\nu \rightarrow 0} \frac{1}{1 - e^{-h\nu/k_B T}} = \frac{k_B T}{h \nu} \quad (3.19)$$

$$q_{\nu} = \frac{1}{1 - e^{-h\nu/k_B T}} \quad (3.20)$$

Replacing  $q_{\ddagger}$  with  $q_{\ddagger} \frac{k_B T}{h \nu}$  in Equation 3.21

$$\frac{[X^{\ddagger}]}{[A][B]} = \frac{q_{\ddagger}}{q_A q_B} e^{-E_0/RT} \quad (3.21)$$

which is the partition function expression of Equation 3.16, would then result in;

$$\nu [X^{\ddagger}] = [A][B] \frac{k_B T}{h} \frac{q_{\ddagger}}{q_A q_B} e^{-E_0/RT} \quad (3.22)$$

where the  $\nu$  is the frequency of the conversion of the activated complexes into their product along the reaction coordinate. Hence, the term at the left side of the equation is the rate of reaction where

$$k[A][B] \equiv [A][B] \frac{k_B T}{h} \frac{q_{\ddagger}}{q_A q_B} e^{-E_0/RT} \quad (3.23)$$

which results in the CTST formula (Equation 2.6 in Chapter 2).

Another derivation which was suggested by Eyring (Eyring, 1935) and independently by Evans and Polanyi (Evans & Polanyi 1935) expresses the motion along the saddle point as a separate translational motion

$$q_t = \frac{(2\pi m_{\ddagger} k_B T)^{1/2}}{h} \delta \quad (3.24)$$

from which the partition function for the activated complex can be written as

$$q_{\ddagger} = \frac{(2\pi m_{\ddagger} k_B T)^{1/2} \delta}{h} q_{\ddagger}^{\cdot} \quad (3.25)$$

This derivation would result in the same rate expression as Equation 2.6 (for the detailed derivation please refer to Laidler, 1977). The second derivation might appear somewhat different from the first one, but both result in the same reaction rate expression.

Despite its success in providing a reasonable upper bound to the reaction rate which is close to the experimental values, CTST suffers from a few errors (Laidler, 1984). This method uses normal expressions for partition functions which are only reliable under the conditions where all the four CTST assumptions are met. For instance, the vibrational partition function (Equation 3.20) is based on the assumption that the vibrations are harmonic, which is not the condition at higher temperatures. Furthermore, the summations in translational (Equation 3.24) and rotational (Equation 3.26) partition functions are replaced by integrations which would make them invalid for systems where energy levels have large gaps between them, i.e. reactions at lower temperatures.

$$q_r = \frac{8\pi^2 \sqrt{8\pi^3 I_A I_B I_C} \sqrt[3]{k_B T}}{\sigma h^3} \quad (3.26)$$

Except for systems in normal conditions at room temperature, CTST overestimates the reaction rate at higher temperatures, and underestimates the reaction rate at lower temperatures and requires some corrections to provide reliable results. The remedy for the former with multi-crossing problem is variational transition state theory (VTST) which is not within the scope of this study (for more information please refer to Chapter 2 Section 2.1.2.2 and the references therein). The remedy for the latter is using the tunnelling correction to the reaction rate (Masgrau & Truhlar, 2014; Truhlar, 2015).

The reactions occurring at extremely low temperatures go through quantum tunnelling since they do not have the energy to overcome the energy barrier. As it has been mentioned in Chapter 2, additional to the low temperatures, quantum tunnelling can also occur at biological temperatures. Proton transfer reactions are the most significant reactions which occur abundantly in biological systems and might go through quantum tunnelling. Both reactions in this study involve the proton transfer mechanism which

could go through quantum tunnelling. Therefore, it is necessary to include the tunnelling phenomenon to the reaction and account for the tunnelling correction in the reaction rate.

### 3.3.2 Tunnelling Corrected Reaction Rate

It is theoretically impractical to develop a quantum mechanical transition state theory (QTST) with identical expression to the classical TST (Small et al., 2006, Hele 2014). The problem is that a quantum mechanical phenomenon contradicts the CTST assumptions. For example, considering the Heisenberg uncertainty principle ( $\Delta p \Delta q \geq \hbar$ ) for the reaction coordinate, if we replace  $\Delta p$  with  $h/\lambda$ , then we have  $\Delta q > \lambda/2\pi$  which would make the transition state delocalized along the reaction coordinate. This would cause a problem, that is, for a large de-Broglie wavelength, the potential on the  $\Delta q$  region is not flat and the system's motion along the reaction coordinate cannot be treated as a classical translational motion (Figure 2.1).

A large curvature on the  $\Delta q$  region along the reaction coordinate would also make it impossible to separate its degrees of freedom from that of the rest of the molecule. Thus, the rate expression in Equation 2.6 can no longer be separated to  $k_B T/h$  for the reaction coordinate and  $q_{\ddagger}$  partition function for the rest of the degrees of freedom. This is in contradiction with the third CTST assumption.

It is however possible to account for quantum effects in the reaction rate to a certain degree of approximation by considering the separability assumption. That can be achieved by making some corrections to the classical rate expression (Equation 2.6) where the vibrational motions are expressed by quantum mechanical partition function

(Equation 3.20). For this partition function, the quantum mechanical energy barrier (i.e. the difference between the zero-point energies of the transition state and the reactants) must be taken into account (Figure 2.1).

On the other hand, the translational and most of the rotational motions can be treated by classical partition functions. The only problem is that the tunnelling correction is not valid at very low temperatures when the characteristic rotational temperature ( $\theta_R$ ) is significantly smaller than  $T$  (Shavitt, 1959). However, this wouldn't be a real issue here since the system under study is at biological temperature.

In the classical framework, for an incident particle with the energy  $E$  reaching a barrier (arbitrarily from left to right) with potential of  $V(x)$ , if  $E < V(x)$  the particle begins to move in the opposite direction ( $x \rightarrow -\infty$ ) after reaching the energy barrier and this is known as reflection. However, if  $E > V(x)$  the particle remains in its original direction and continues moving towards that direction ( $x \rightarrow \infty$ ). In the quantum mechanical scheme on the other hand, for  $E > V(x)$  there is a probability of reflection (antitunnelling) and for  $E < V(x)$ , there is a probability of transmission (tunnelling). Both these phenomena are forbidden in classical framework. The degree of reflection (for  $E > V(x)$ ) from, and the degree of transmission (for  $E < V(x)$ ) to, the potential barrier, can be calculated for any type of barrier from the Schrödinger equation;

$$\frac{\partial^2 \Psi}{\partial x^2} + \frac{8\pi^2 m}{h^2} [E - V(x)] \Psi = 0 \quad (3.27)$$

where  $m$  is the mass of incident particle and  $E$  is the energy of the system.

Solving this equation in the limit of  $x \rightarrow \infty$  where the incident particle passes over the barrier gives:

$$\psi \approx A e^{ik_2 x} \quad ; k_2 = \frac{\sqrt{2m(E-V_0)}}{\hbar} \quad (3.28)$$

where  $A$  is a constant and  $V_0$  is the endothermicity (Figure 3.4).

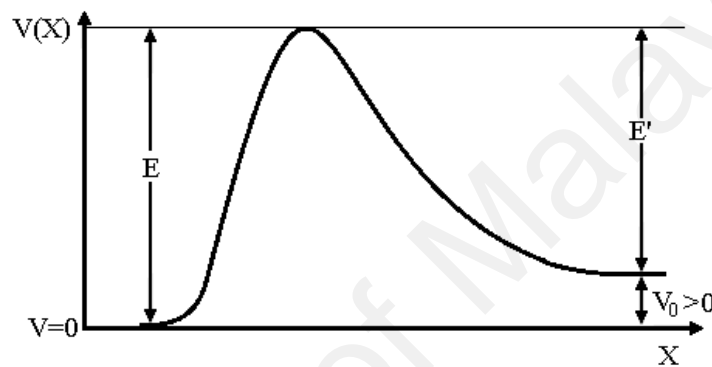


**Figure 3.4: The endothermic potential barrier.**

Calculating the asymptotic expression for  $x \rightarrow -\infty$  on the other hand, gives:

$$\psi \approx e^{ik_1 x} + B e^{-ik_1 x} \quad ; k_1 = \frac{\sqrt{2mE}}{\hbar} \quad (3.29)$$

which is a linear combination of the incident wave (assuming unit amplitude) and reflected wave with the reflection constant of  $B$  (Landau & Lifshitz, 1958). The transmission coefficient can then be defined as the ratio of the current density of the transmitted wave ( $k_2 |A|^2$ ) to that of the incident wave ( $k_1$ );

$$T(E) = \frac{k_2}{k_1} |A|^2 \quad (3.30)$$

The reflection coefficient is then defined as the ratio of the current density of the reflected wave ( $k_1|B|^2$ ) to that of the incident wave ( $k_1$ );

$$R(E) = |B|^2 \quad (3.31)$$

which would result in unity if summed with the transmission coefficient ( $T+R=1$ ). For  $E < V_0$ ,  $k_2$  becomes purely imaginary and the wavefunction would decay exponentially in the classically forbidden region of the potential barrier (tunnelling). For  $E > V_0$ ,  $k_2$  becomes real and the system has enough energy to pass over the barrier (classical). In this case, if there is no transmission, the incident wave is reflected (antitunnelling).

The transmission coefficient describes the permeability of the potential barrier towards the incident particle which depends on the exact shape of the barrier. Solving the permeability function for most potential barrier shapes requires complex numerical integration over all energies.

There is one simple barrier shape for which the exact expression for  $T(E)$  has been calculated, i.e. the Eckart barrier. Eckart has exactly derived the permeability function for the asymmetric potential barrier (Eckart, 1930). The symmetric form of the Eckart potential barrier can be expressed as:

$$V(x) = E_0 \operatorname{sech}^2(\pi x/\ell) \quad (3.32)$$

where  $\ell$  is the characteristic length of the barrier and  $E_0$  is the zero-point corrected energy (Figure 3.5) (Shavitt, 1959; Atkins & Friedman, 2005).

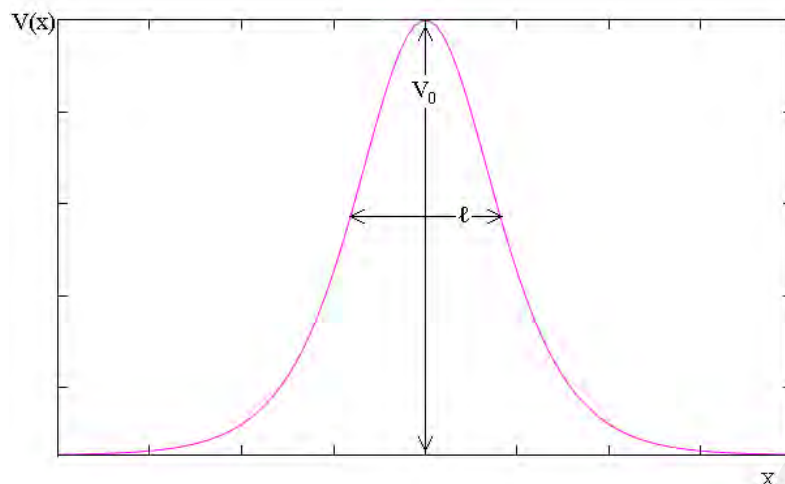


**Figure 3.5: The symmetric Eckart potential barrier.**

The permeability function  $T(E)$  for this barrier can then be written in the form of:

$$T(E) = \frac{\cosh\left(\frac{4\pi\ell}{h}\sqrt{2mE}\right) - 1}{\cosh\left(\frac{4\pi\ell}{h}\sqrt{2mE}\right) + \cosh\left(\frac{2\pi\ell}{h}\sqrt{8mE_0 - \frac{h^2}{4\ell^2}}\right)} \quad (3.33)$$

where  $h$  is the Planck's constant and  $E$  is the energy of the system. Accounting for classical separable approximation<sup>6</sup> allows to simplify the potential barrier into one dimensional. The permeability function would then be plugged in the integration over the Boltzmann distribution to yield the tunnelling correction factor ( $\Gamma$ );

$$\Gamma(T) = e^{\beta E_0} \int_0^{\infty} \beta e^{-\beta E} T(E) dE \quad ; \quad \beta = \frac{1}{k_B T} \quad (3.34)$$

where  $E_0$  is the zero-point corrected barrier height and  $E$  is the energy of the transferring particle varied over the potential barrier.

<sup>6</sup> According to the third CTST assumption (Chapter 2, Section 2.1.2.1), the vibrational degrees of freedom is assumed to be separable at the saddle point to one along the reaction coordinate and 3N-7 along all other directions.

The tunnelling correction factor in this study is calculated numerically using a code written in Fortran programming language. The double exponential integral formula is used for the integration. The library program for this formula is taken from the Mathematical Software Packages of Takuya OOURA in the Research Institute for Mathematical Sciences (<http://www.kurims.kyoto-u.ac.jp/~ooura/intde.html>). The program used is the integrator of  $f(x)$  function over a finite limit which requires simplification of the integral in Equation 3.34.

It is shown in Figure 3.6 that the transmission  $T(E)$  is strongly dependent on  $E$ . For the values of  $0 < E < E_0$ ,  $T(E) \approx 0$  and as  $E \rightarrow E_0$ ,  $T(E) \rightarrow 1$ . With these boundary conditions, by splitting the integrand into two intervals, we arrive at Equation 3.35;

$$\Gamma(T) = \beta e^{\beta E_0} \left[ \int_0^{U_{\ell im}} e^{-\beta E} T(E) dE + \int_{U_{\ell im}}^{\infty} e^{-\beta E} T(E) dE \right] \quad (3.35)$$

where  $U_{\ell im}$  is an arbitrary cut off value for the potential energy, indicated in Figure 3.6.

For energies greater than  $U_{\ell im}$ ,  $T(E)$  is 1. Therefore, we will have:

$$\Gamma(T) = \beta e^{\beta E_0} \left[ \int_0^{U_{\ell im}} e^{-\beta E} T(E) dE + \frac{1}{\beta} e^{-\beta U_{\ell im}} \right] \quad (3.36)$$

which would leave a double exponential formula for the integration of the energies lower than  $U_{\ell im}$ . The important variables in  $T(E)$  are the imaginary vibrational frequency ( $\nu$ ) of the activated complex and the mass of the transferring particle ( $m$ ). Comparing the second derivative of the Eckert potential with the force constant expression indicates

that the barrier width ( $\ell$  in Equation 3.37) is inversely correlated to the vibrational frequency:

$$\begin{aligned} \ell &= \sqrt{\frac{E_0}{2m} \frac{1}{|\nu|}} \\ &= \sqrt{\frac{E_0}{2m} \frac{1}{c|\sigma|}} \end{aligned} \quad (3.37)$$

where  $c$  is the speed of light and  $\sigma$  is the imaginary wave number, taken from the Gaussian09 output.

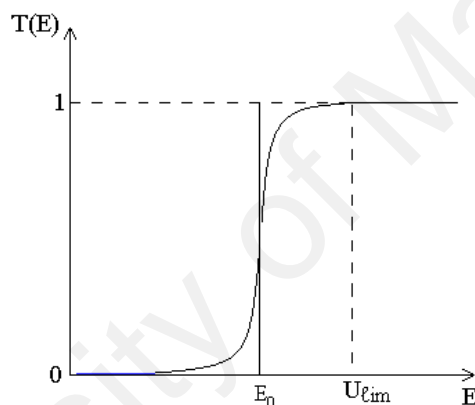


**Figure 3.6: Transmission coefficient vs. the energy where:**  $\begin{cases} \text{if } E > U_{\ell im} \rightarrow T(E) \approx 1 \\ \text{if } E \leq U_{\ell im} \rightarrow 0 < T(E) < 1 \end{cases}$

For thinner barrier widths and lower barrier heights, less energy is required to induce tunnelling of a particle. Wigner (1932) came up with an analytical formulation of the tunnelling correction factor for these types of barriers:

$$\Gamma = 1 - \frac{1}{24} (\beta \nu_u)^2 \quad (3.38)$$

where  $\nu_u$  is the imaginary frequency of the activated complex over the saddle point.

A more precise and satisfactory treatment for elevated temperatures was derived by Shavitt (1959):

$$\Gamma = 1 - \frac{1}{24} (\beta v_u)^2 \left(1 + \frac{RT}{E_c}\right) \quad (3.39)$$

where  $E_c$  is the classical activation energy without the zero point energy level corrections. While being applicable for any form and shape of potential energy curve, the Wigner and Shavitt equations are mainly valid when there is only a small degree of tunnelling and cannot be applied to the reactions with large deviations from classical behaviour. Therefore, the values of  $\Gamma$  are obtained from both the analytical approaches of Wigner and Shavitt using Equations 3.38 and 3.39 respectively, and the exact numerical approach based on Eckart potential using Equations 3.34. This is carried out to make a simple comparison between these two different approaches.

The  $\Gamma$  component is a multiplicative factor which is a quantum correction to the classical over the barrier reaction rate. This results in the overall rate of reaction which is obtained from:

$$k_{\text{quantum}} = \Gamma \times k_{\text{classical}} \quad (3.40)$$

This model of proton tunnelling is called the *standard view* which involves the non-tunnelling classical over the barrier component ( $k_{\text{classical}}$ ) and the tunnelling through the barrier component ( $\Gamma$ ) (Kiefer & Hynes, 2010). The results of the calculated classical as well as quantum mechanical reaction rates for the two main chemical reactions (i.e. boronic acid and peptide bond formation) will be discussed in the next chapter.

## CHAPTER 4

### RESULTS AND DISCUSSION

This chapter presents the results and discussion of two separate parts. The first part concerns the process of peptide bond formation in ribosome and the second part discusses the esterification reaction of boronic acid with diols. Being dominated by proton transfer processes, both of these reactions might account for tunnelling phenomenon. Hence, the tunnelling contribution to the reaction has also been studied to investigate the possibility of tunnelling. The goal is to observe whether or not tunnelling plays a key role in the enzymatic reaction of peptide bond formation. The mechanism which the enzyme use to induce tunnelling can then be applied on non-enzymatic proton transfer reactions, which in this study is the reaction of boronic acid with diols.

#### **4.1 The important role of P-site A-76 2'-OH as a peptidyl shuttle**

The process of peptide bond formation in ribosome by itself is a simple chemical reaction, but the unidentified details of it points to the complexity of the biochemical processes leading to it. A proper model of the active site core of the enzyme is required for this chemical reaction to be investigated with electronic structure methods. This model must be large enough to cover the portion of the active site which accounts for all the necessary interactions between the enzyme and the substrates, yet, small enough to be feasible and calculable using demanding electronic structure methods. In this section, we elaborate on the calculations which are carried out based on the active site crystallographic structures from experimental studies. Some of these mechanisms have been proposed and rigorously investigated by other computational research groups, but no agreement has yet been reached on whether or not they are the actual mechanisms of

ribosomal peptide bond formation. What they lack is the so-called ribosomal base, the A2451 which might directly participate in the reaction. Its presence has been observed in close proximity of the active site in the experimentally obtained crystallographic structures. Its position and key interaction with the substrates though, is different among these structures.

Deciding on which one of these structures lead to the formation of peptide bond requires further computational studies. Hence, we have selected three different crystallographic structures with three different types of key-interactions between the A2451 ribosomal base and the substrates. The difference in key interactions between these structures leads us to propose different reaction mechanisms in this study which requires further computational calculations. These three mechanisms are novel and they have not been proposed in any of the previous computational studies.

#### **4.1.1 Calculations based on old mechanisms**

The most theoretically studied mechanisms are the concerted (4-, 6-, and 8-membered) and the stepwise mechanisms (Scheme 2.1). The numbers correspond to the number of atoms involved directly in the reaction. The concerted 4-membered mechanism for example, corresponds to a direct protonation of the 3'-O by nucleophilic nitrogen from the A-site amino acid (Scheme 2.1-A, TS4). This reaction only involves the N→H→O→C atoms. The concerted 6-membered reaction mechanism employs, in addition, the P-site 2'-OH to transfer the proton from the attacking nucleophile to the P-site 3'-O which adds up two more atoms directly involved in the reaction (Scheme 2.1-A, TS6). The 8-membered reaction mechanism is similar to the 6-membered one, with addition of a water molecule acting as a proton shuttle between the leaving 3'-O and its

neighbouring 2'-O while the latter receives its proton from the attacking nucleophile (Scheme 2.1-B, TS8). Some studies proposed a mechanism where the deprotonation of the attacking nucleophile and protonation of the 3'-O occur in two different steps, forming a carbon tetrahedral intermediate in between (Scheme 2.1-A & B). There is a slight disagreement among different studies on the steps of the reaction.

Some studies favour the concerted mechanism (Wallin & Åqvist, 2010; Kuhlenkoetter et al., 2011; Xu et al., 2012-b; Świderek et al., 2013, 2015), while some other studies favour the stepwise mechanism (Rangelov et al., 2006; Acosta et al., 2012; Wang et al., 2010, 2015; Byun & Kang, 2013), simply by comparing the resulting reaction rate to that of experiment. Table 4.1 illustrates the activation free energies and reaction rates of these mechanisms which have been calculated in this study and compared with those calculated and reported in previous studies.

Despite the mechanistic differences between concerted TS-4 and TS-6, the reaction rates are almost similar between these two mechanisms in each study (Table 4.1). The energy barrier for the TS-6 is even higher than that of the TS-4 in the study of Acosta et al.. Except for a few studies, the TS-6 is more favourable and can be attributed to the stabilizing effect of the water molecules in their active site model (Świderek et al., 2013; Xu et al., 2012). However, these are exceptions which are not of particular significance in comparison to other mechanisms. In particular, without stabilizing water molecules, TS-6 is the least favourable mechanism which can be due to the different orientation of the active site enzymatic residues around the reacting groups. This could cause a delay in the proton transfer mechanism and hence, lower rate of reaction. Presence of water molecules could facilitate the reaction by forming hydrogen bonds with the proton donating and accepting groups.

**Table 4.1: The calculated activation free energies and the reaction rates for old mechanisms calculated in this study and other studies. The rate in the SW reaction corresponds to the rate determining step.**

Mechanism	Study	Method	Medium	$\Delta G^\ddagger$	$k$ (s <sup>-1</sup> )	
TS-4	a	M06-2X/6-31++G**	Vacuum	44.47	0.2×10 <sup>-19</sup>	
		M06-2X/6-31++G** (SMD)	Implicit water	38.84	0.3×10 <sup>-15</sup>	
	b	M06-2X/6-31+G(d,p)	Explicit water	24.30	1.4×10 <sup>-5</sup>	
	c	M06-2X/6-311+G(d,p) (SMD)	Implicit water	30.11	0.8×10 <sup>-10</sup>	
	d	B3LYP/6-31+G(d,p)	Vacuum	43.60	1.0×10 <sup>-19</sup>	
e	B3LYP/6-31+G(d,p)	Vacuum	35.50	0.9×10 <sup>-13</sup>		
TS-6	a	M06-2X/6-31++G**	Vacuum	45.41	0.4×10 <sup>-20</sup>	
		M06-2X/6-31++G** (SMD)	Implicit water	38.92	2.7×10 <sup>-16</sup>	
	b	M06-2X/6-31+G(d,p)	Explicit water	24.20	1.7×10 <sup>-5</sup>	
	c	M06-2X/6-311+G(d,p) (SMD)	Implicit water	33.30	3.6×10 <sup>-12</sup>	
	d	B3LYP/6-31+G(d,p)	Vacuum	44.30	3.0×10 <sup>-20</sup>	
	f	B2PLYP-D/6-311++G(d,p) (SMD)/M06-2X/6-31G*	Implicit water	31.32	1.0×10 <sup>-10</sup>	
	g	B3LYP/6-31G*/MM	Explicit water	29.00	0.5×10 <sup>-8</sup>	
h	B3LYP/6-311G**	Vacuum	34.8	2.9×10 <sup>-13</sup>		
TS-8	a	M06-2X/6-31++G**	Vacuum	35.01	0.2×10 <sup>-12</sup>	
		M06-2X/6-31++G** (SMD)	Implicit water	30.41	0.5×10 <sup>-9</sup>	
	b	M06-2X/6-31+G(d,p)	Explicit water	26.80	2.1×10 <sup>-7</sup>	
	c	M06-2X/6-311+G(d,p) (SMD)	Implicit water	24.57	0.9×10 <sup>-5</sup>	
	f	B2PLYP-D/6-311++G(d,p) (SMD)/M06-2X/6-31G*	Implicit water	30.40	4.9×10 <sup>-10</sup>	
	g	B3LYP/6-31G*/MM	Explicit water	19.00	1.1×10 <sup>-1</sup>	
h	B3LYP/6-311G**	Vacuum	22.3	4.3×10 <sup>-4</sup>		
SW	a	M06-2X/6-31++G**	Vacuum	TS1-6	9.5	0.2×10 <sup>-6</sup>
				TS2-4	26.78	
	a	M06-2X/6-31++G** (SMD)	Implicit water	TS1-6	13.8	1.3×10 <sup>-4</sup>
				TS2-4	23.01	
	b	M06-2X/6-31+G(d,p)	Explicit water	TS1-4	33.40	0.9×10 <sup>-21</sup>
				TS2-4	46.40	
	d	B3LYP/6-31+G(d,p)	Vacuum	TS1-6	24.01	2.4×10 <sup>-5</sup>
				TS2-4	13.10	
	f	B2PLYP-D/6-311++G(d,p) (SMD)/M06-2X/6-31G*	Implicit water	TS1-6	20.84	0.5×10 <sup>-2</sup>
				TS2-6	13.34	
	c	M06-2X/6-311+G(d,p) (SMD)	Implicit water	TS1-6	16.02	1.1×10 <sup>-4</sup>
				TS2-4	23.09	
TS1-6				16.02	0.6×10 <sup>-5</sup>	
TS2-6				24.77		
TS1-6				7.60	0.6×10 <sup>2</sup>	
TS2-8				13.86		

a) this study;  
e) Gindulyte et al., 2006;

b) Świderek et al., 2013;  
f) Byun & Kang, 2013;

c) Acosta et al., 2012;  
g) Xu et al., 2012-b;

d) Wang et al., 2010;  
h) Wallin & Åqvist, 2010

In the study carried out by Xu and collaborators (2012-b) for instance, the presence of five water molecules is proposed in the active site which forms a hydrogen bond network and stabilizes the transition structure. One of the water molecules is a proton shuttle, assisting the 2'-OH in transferring its proton to the leaving 3'O in the 8-membered mechanism, whereas no water molecule is involved in the chemical reaction of the 6-membered mechanism (Xu et al., 2012). This results in about  $10^7$ -fold rate enhancement in the former mechanism. In general, the relatively higher reaction rate of the 6-membered mechanisms in the two aforementioned studies is due to the stabilizing effect of the water molecules rather than the effect of the P-site 2'-OH group as a proton shuttle. This is in agreement with the suggested catalytic model of Acosta et al., where there is no substrate assisted catalysis and the process occurs through ribosomal catalysis and two water molecules only (Acosta et al., 2012).

The stabilizing effect of the water molecule in transition state can be further observed in the stepwise mechanism of Acosta et al. (Table 4.1) where the rate in the first step of TS1-6  $\rightarrow$  TS2-8 is  $10^6$ -fold higher than the rates in the first steps of the TS1-6  $\rightarrow$  TS2-4 and TS1-6  $\rightarrow$  TS2-6 mechanisms (Scheme 2.1). Even though the water molecule is not directly participating in the rate determining step of TS1-6  $\rightarrow$  TS2-8, its presence has a stabilizing effect which enhances the overall reaction rate.

This can be further proven by observing the concerted 8-membered mechanism that they proposed where the water molecule is directly involved in the reaction, but the rate of this mechanism is  $10^6$ -fold lower than the TS1-6  $\rightarrow$  TS2-8. The same goes to our study where the rate of the concerted 8-membered mechanism is  $10^7$ -fold lower than that of the stepwise mechanism, despite of the absence of a water molecule in the stepwise mechanism.

The reason for this goes back to the peptidyl transfer where the growing polypeptide chain forms a peptide bond with the attacking nucleophile. This process is slightly delayed in the concerted 8-membered mechanism due to the delay in the nucleophile's deprotonation as well as the P-site 3'-O's protonation. On the other hand in the stepwise mechanism, the nucleophile's deprotonation and the P-site 3'-O's protonation occur in two different steps; the former occurs in the first step with the formation of the peptide bond and the latter occurs during the second step with the dissociation of the growing polypeptide chain from P-site tRNA. Due to the faster dissociation of the tetrahedral carbon from the P-site 3'-O during the rate determining step, the reaction rate is enhanced in the SW mechanism. This indicates the importance of the protonation of the P-site 3'-O in determining the overall rate.

From these observations it can be concluded that the participation of a water molecule in the reaction is not the main reason for the rate enhancement of the peptide bond formation since its proton shuttling role can be better played by the ribosomal active site groups. It is in fact its stabilizing effect through forming hydrogen bond with the substrates that causes this rate enhancement. This stabilizing effect can also be achieved through any hydroxyl containing group such as ribosomal rRNA bases. To have a better understanding of the stabilizing effect of the hydrogen bonds in the active site, a thorough examination of the transition structure for all the old mechanisms has been carried out. The transition state coordinates for these mechanisms are illustrated in Table 4.2. A rather late ester bond dissociation and peptide bond formation is observed in all concerted mechanisms compared to the stepwise mechanism. This is consistent with the calculated reaction rates. The same goes for all the aforementioned computational studies, regardless of the model chemistry they have used.

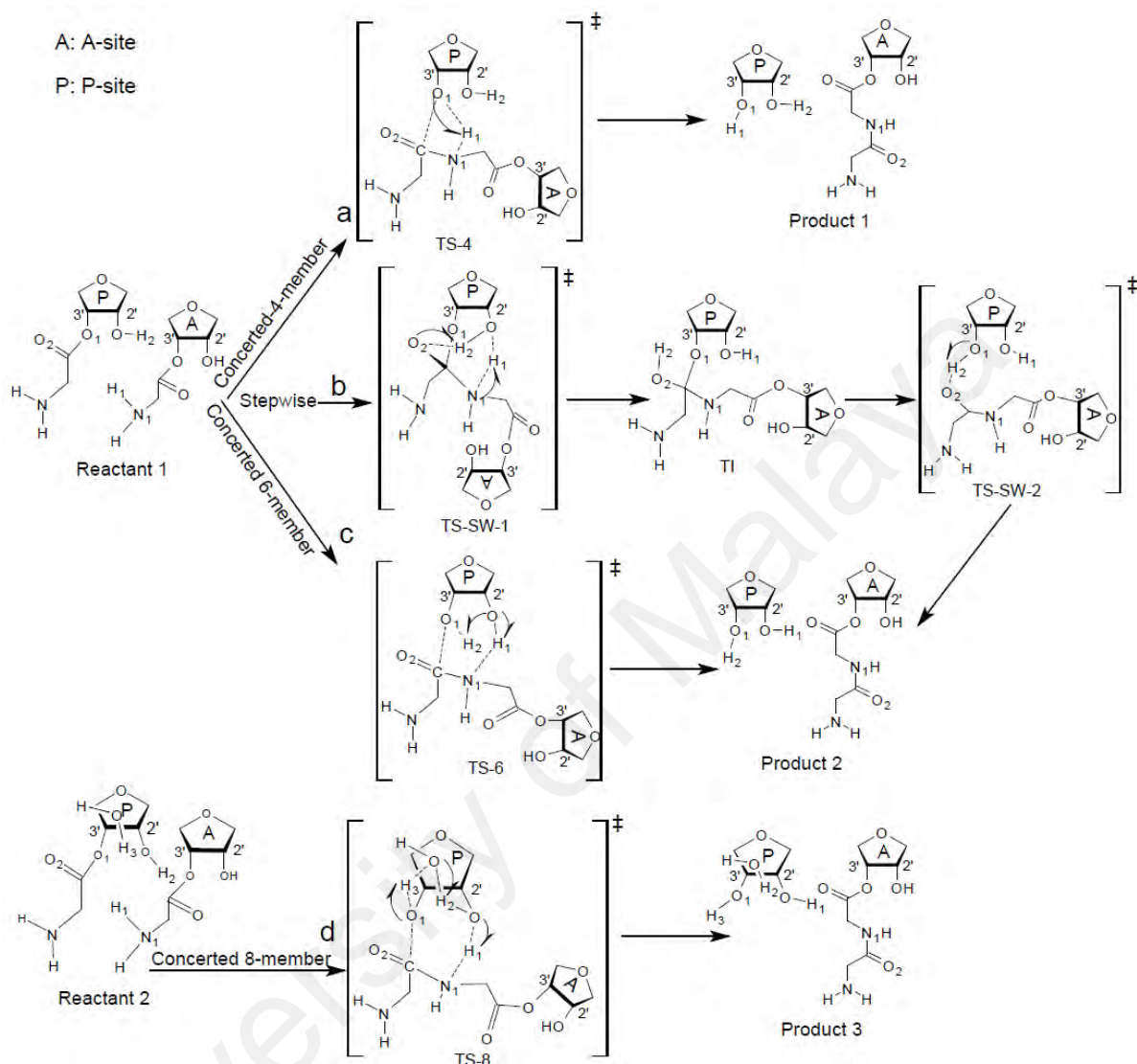
The only exception is the study carried out by Świderek et al., (2013) which favours the concerted 4- and 6-membered mechanisms which is due to the formation of Zwitterionic species immediately before the formation of the transition structure in their study. It results in faster protonation of the P-site 3'-O in the 4-membered mechanism and P-site 2'-O in the 6-membered and 8-membered mechanisms compared to protonation of the 3'-O in the stepwise mechanism. The reason would be the occurrence of the latter through the carbonyl oxygen, but the occurrence of the first three structures through the highly reactive positive nitrogen. It is however mentioned by Acosta et al., (2012) that the formation of zwitterionic species is not observed in the ribosome. The 2-D view of the transition structures of the aforementioned mechanisms carried out in this study are presented in Scheme 4.1. Additional to the differences mentioned above, there are also some similarities of these structures with the previous studies.

The experimental observations highly support the role of the P-site 2'-OH in accelerating the process of peptide bond formation. The computational results on the other hand, mainly agree with the rate reduction for mechanisms where the 2'-OH group protonates the leaving 3'-O. This is rather surprising and requires further thinking. This is where we have gone further to be able to answer the remaining dilemma of previously proposed mechanisms.

The main shortcoming of the old mechanisms is the small active site model system where mostly the A2451 ribosomal base is not present. We overcome this shortcoming by expanding the active site so that the effect of more active site groups are taken into account. Three novel reaction mechanisms are proposed in this study which are based on three different experimental studies. These mechanisms are thoroughly investigated in the next section.

**Table 4.2: The different transition state coordinates for previously proposed 4-member, 6-member, 8-member and stepwise mechanisms of peptide bond formation in this study.**

Mechanism	Medium	Bond name	Bond type	Distance (Å)	
4-member	Vacuum	N <sub>amino</sub> -C <sub>carbonyl</sub>	Forming	1.53	
		C <sub>carbonyl</sub> -3'O	Breaking	2.14	
		3'O-H <sub>amino</sub>	Forming	1.33	
	Implicit water SMD	N <sub>amino</sub> -H <sub>amino</sub>	Breaking	1.18	
		N <sub>amino</sub> -C <sub>carbonyl</sub>	Forming	1.50	
		C <sub>carbonyl</sub> -3'O	Breaking	2.17	
		3'O-H <sub>amino</sub>	Forming	1.57	
6-member	Vacuum	N <sub>amino</sub> -H <sub>amino</sub>	Breaking	1.08	
		N <sub>amino</sub> -C <sub>carbonyl</sub>	Forming	1.51	
		C <sub>carbonyl</sub> -3'O	Breaking	2.12	
		3'O-2'H	Forming	1.50	
		2'H-2'O	Breaking	1.04	
	Implicit water SMD	2'O-H <sub>amino</sub>	Forming	1.58	
		N <sub>amino</sub> -H <sub>amino</sub>	Breaking	1.07	
8-member	Vacuum	N <sub>amino</sub> -C <sub>carbonyl</sub>	Forming	1.50	
		C <sub>carbonyl</sub> -3'O	Breaking	2.23	
		3'O-2'H	Forming	1.63	
		2'H-2'O	Breaking	1.00	
		2'O-H <sub>amino</sub>	Forming	2.38	
		N <sub>amino</sub> -H <sub>amino</sub>	Breaking	1.02	
		SW	Vacuum	N <sub>amino</sub> -C <sub>carbonyl</sub>	Forming
C <sub>carbonyl</sub> -3'O	Breaking			2.10	
3'O-H <sub>wat</sub>	Forming			1.08	
H <sub>wat</sub> -O <sub>wat</sub>	Breaking			1.38	
O <sub>wat</sub> -2'H	Forming			1.51	
2'H-2'O	Breaking			1.03	
Implicit water SMD	2'O-H <sub>amino</sub>		Forming	1.52	
	N <sub>amino</sub> -H <sub>amino</sub>		Breaking	1.10	
	N <sub>amino</sub> -C <sub>carbonyl</sub>		Forming	1.52	
	C <sub>carbonyl</sub> -3'O		Breaking	2.12	
	3'O-H <sub>wat</sub>		Forming	1.13	
	H <sub>wat</sub> -O <sub>wat</sub>		Breaking	1.28	
	O <sub>wat</sub> -2'H		Forming	1.48	
SW	Vacuum	2'H-2'O	Breaking	1.03	
		2'O-H <sub>amino</sub>	Forming	1.50	
		N <sub>amino</sub> -H <sub>amino</sub>	Breaking	1.10	
		Step 1			
		N <sub>amino</sub> -C <sub>carbonyl</sub>	Forming	1.58	
	Implicit water SMD	H <sub>amino</sub> -2'O	Forming	1.49	
		N <sub>amino</sub> -H <sub>amino</sub>	Breaking	1.11	
		O <sub>carbonyl</sub> -2'H	Forming	1.17	
		2'O-2'H	Breaking	1.26	
		Step 2			
SW	Implicit water SMD	2'H-3'O	Forming	1.35	
		3'O-C <sub>carbonyl</sub>	Breaking	1.99	
		O <sub>carbonyl</sub> -2'H	Breaking	1.11	
		Step 1			
		N <sub>amino</sub> -C <sub>carbonyl</sub>	Forming	1.56	
SW	Implicit water SMD	H <sub>amino</sub> -2'O	Forming	1.59	
		N <sub>amino</sub> -H <sub>amino</sub>	Breaking	1.09	
		O <sub>carbonyl</sub> -2'H	Forming	1.09	
		2'O-2'H	Breaking	1.37	
		Step 2			
SW	Implicit water SMD	2'H-3'O	Forming	1.44	
		3'O-C <sub>carbonyl</sub>	Breaking	2.05	
		O <sub>carbonyl</sub> -2'H	Breaking	1.06	



**Scheme 4.1: The most well-known mechanisms for the formation of peptide bond:**  
**a) The concerted TS-4 mechanism, b) The stepwise mechanism with formation of a tetrahedral carbonyl carbon as a central atom binding to both the attacking nucleophile ( $N_1$ ) and the leaving  $3'O$  ( $O_1$ ), c) The concerted 6-member mechanism with the A76 2'-OH as a proton shuttle between ( $N_1$ ) and ( $O_1$ ), d) An 8-member mechanism with three protons *in flight*: the  $H_1$  from  $N_1$ , the  $H_2$  from 2'-O and the  $H_3$  from water.**

#### 4.1.2 Three novel mechanisms proposed in this study

The interactions in the initial geometries are determined by the crystallographic structures of the previous studies (Schmeing et al., 2005; Lang et al., 2008; Voorhees & Ramakrishnan, 2009). These studies highlight the importance of water molecules as well as the A2451 of the 23S-rRNA ribosomal base in the catalysis. Even though these studies do not agree well in some key interactions of the functional groups with substrates in the pre-peptidyl and post-peptidyl transfer structures, one cannot simply conclude the inaccuracy (or accuracy) of any of these structures since they might have been observed in different time frames during the peptidyl transfer mechanism.

The suggested *entropy trap* as the catalytic role of the ribosome (Sievers et al., 2004) could result in a major conformational change in the active site during substrate stabilization in a very short period of time. Any of these crystallographic snapshots could have been taken in different time frames before the peptidyl transfer mechanism. Our goal in this study is to figure out which one of these structures is the actual reactant structure with proper substrate-enzyme key interaction which would stabilize the transition structure. For convenience, we named the proposed mechanisms which are initiated from the crystallographic structure of Steitz, Ramakrishnan and Polacek, P-I, P-II, and P-III respectively.

##### 4.1.2.1 P-I mechanism

The crystallographic structure of Steitz and collaborators suggests that the  $\alpha$ -amino group of the A-site is within the hydrogen bond distance of the rRNA which is activated to donate its proton to the P-site A76 2'-OH group. They have also observed a water

molecule in the active site and suggested its role as a stabilizer of the oxyanion by acting as a hole during the carbon tetrahedral intermediate formation. The presence of two water molecules in the active site was suggested by Åqvist and collaborators, one of which would participate directly in the reaction while the other stabilizes the transition structure (Wallin & Åqvist, 2010).

Taking these observations into consideration, we optimized the structures of pre- and post-peptidyl transfer with the presence of two water molecules in the active site. The initial structures for optimization are taken from the crystallographic structure of Steitz (PDB code of 1VQ6). During the optimization, these active site residues would affect the orientation of the water molecules. This effect is such that the water molecules are positioned adjacent to one another between the 2' and 3'-OH of the P-site A76. After the optimization, the 3'-OH group of the A2451 ribose interacts strongly with the  $\alpha$ -amine.

The rest of the nucleobase in this model is not taken into consideration since no interaction between this group and the reacting groups have been observed throughout the reaction in the structure of Steitz. The elimination of A2451 nucleobase (excluding the sugar moiety) would then have no significant effect on the rate of peptide bond formation and it is only the 3'-OH of A2451 which is of particular importance in the mechanism (Acosta et al., 2012).

During the transition state optimization, formation of a rather stable intermediate structure was observed, suggesting a stepwise mechanism (Scheme 3.2) which is not similar to the proposed mechanism of Steitz et al. (Schmeing et al., 2005). The only thing common between these two reactions is the interaction of the A2451 3'-OH with the attacking nucleophile. This interaction stimulates the nucleophile to donate its

proton to the P-site A76 2'-O, resulting in the protons to be transferred as follows: from A2451 3'-O →  $\alpha$ -amine → P-site A76 2'-OH → water1 → water2 → P-site A76 3'-O. The growing polypeptide chain is then transferred from the P-site A76 3'-O to the A2451 3'-O which has just lost its proton to the  $\alpha$ -amine. This step involves the main proton transfer which results in a 12-membered transition structure with five protons *in flight* (Scheme 3.2, TS1-12).

In the structure of the intermediate, the growing polypeptide chain is in a closer proximity to the attacking nucleophile which would make the peptidyl transfer easier to occur. The second step occurs quite fast through a 4-membered transition structure where the growing polypeptide chain is transferred from the A2451 3'-O to the  $\alpha$ -amine with a simultaneous transfer of proton from the latter to the former group. In this proposed mechanism, the 3'-O of the A2451 acts as a peptidyl shuttle between the P-site A76 3'-O and the attacking nucleophile (Scheme 3.2, TS2-4).

As reported by Steitz (Schmeing et al., 2005), Acosta et al., (2012) and Xu et al. (2012-b), the presence of two water molecules in the active site and participation of the A2451 in the mechanism have an improvement on the reaction rate.

Based on these reports, a higher reaction rate of this proposed mechanism is expected relative to the old mechanisms. In our model, despite the abundance of OH groups as both proton shuttle and stabilizing agents, there is not much improvement in the reaction rate of this mechanism where the rate determining step (the first step) goes through 38.35 kcal/mol energy barrier (Figure 4.1).

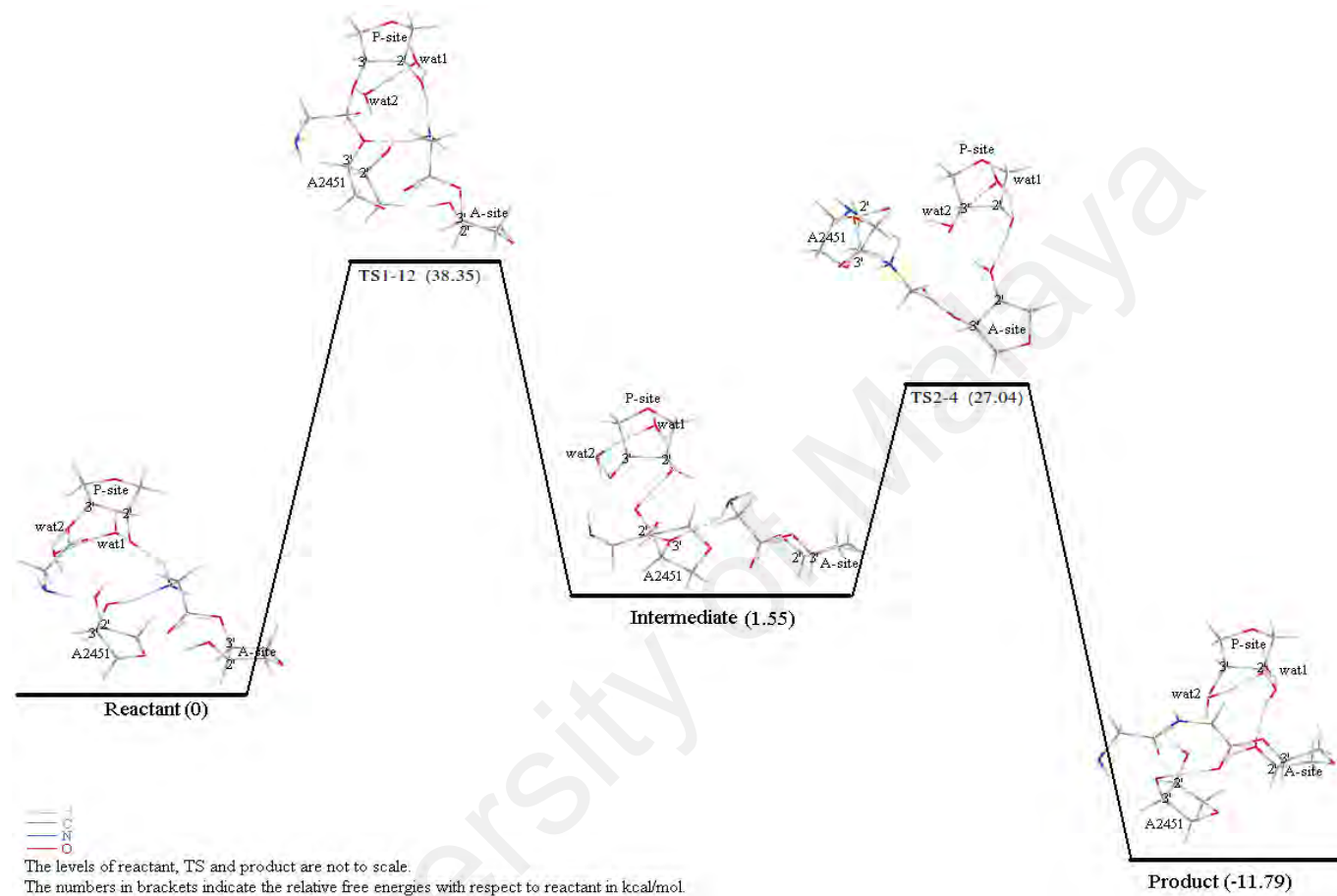


**Figure 4.1: The transition state coordinates of the stepwise mechanism based on Steitz crystallographic structure (Schmeing et al., 2005) with direct participation of two water molecules and the A2451 ribose in the active site (The schematic view of this mechanism can be observed in Scheme 3.2). Some key interactions of the pre- and post- peptidyl transfer structures are different from the original structure of Steitz after optimization.**

The main difference between this mechanism and that of the other studies is that both water molecules are directly involved in the proton shuttle mechanism whereas in the previous studies, only one water molecule directly participated in the reaction. Polikanov et al. (2014) for instance suggested a mechanism which goes through the formation of a tetrahedral intermediate. The universally conserved rRNA bases, A2602 and U2584, would then coordinate a water molecule to neutralize the zwitterion, while the second water molecule acts as a proton shuttle between the P-site 2'-O and 3'-O. The attacking nitrogen would then donate its proton to the P-site 2'-O and accepts the growing polypeptide chain.

Another example is the study of Acosta et al., where the second water molecule stabilizes the reactant complex through hydrogen bonding interaction with the active site with 6.2 kcal/mol decrease in the energy barrier (Acosta et al., 2012). Correspondingly, Xu et al., (2012-b) proposed the participation of only one water molecule in the reaction as proton shuttle despite having several water molecules in the active site (Xu et al., 2012-b).

These observations suggest the importance of the OH groups (whether they are of water molecules or the ribose groups) in stabilizing the transition structure rather than participating directly in the reaction. More importantly, the surprisingly low reaction rate observed in this study (i.e. around  $10^{-15}$ /sec) suggests that ribosomal catalysis is not limited to participation of several proton shuttling groups in the active site. Other factors may be involved which still remain to be investigated. Therefore, it is necessary to investigate other crystallographic structures with different orientation of the active site group. This would assist us to better understand the role of substrate positioning by enzymatic active site in catalysis.

#### 4.1.2.2 P-II mechanism

The snapshots of both pre- and post-peptidyl transfer structures with the PDB ID of 4V5C from the study of Ramakrishnan and collaborators (2009) were used for modelling another reaction mechanism. The structures are in the states where both the A-site and P-site tRNAs are located in the intact (70S) ribosome. There is a hydrogen bond interaction between both the N3 and 2'-OH of the A2451 with the A-site  $\alpha$ -amine. After the optimization, the A2451 2'-OH changes its orientation and interacts with the P-site A-76 2'-OH, while the A2451-N3 remains in interaction with the  $\alpha$ -amine. The sequential rearrangement of the catalytic arrays could clearly represent the reaction core's reorganization to form a shape suitable for the transition structure.

The optimized structure of the reactant and product in this case clearly suggest a mechanism with the A2451 2'-OH as a proton shuttle between the P-site 2'-OH and its neighbouring 3'-O. This role is played by a water molecule in the 8-membered mechanism. Subsequently the P-site 2'-OH can be protonated by the attacking nucleophile which would result in an 8-membered transition structure as well.

The difference between the A2451 and a water molecule is the latter's flexibility in the region which is not observed in the former since the A2451 is interacting with the N3 of the P-site A76 through its 3'-H. Additional to the reactant structure, this interaction is also observed in the product structure (Figure 4.2.) which suggests its rigidity throughout the mechanism. This rigidity further limits this group from getting closer to the P-site 3'-O (not less than 2.8Å), resulting in an absolutely not satisfactory transition state optimization in our simulation.

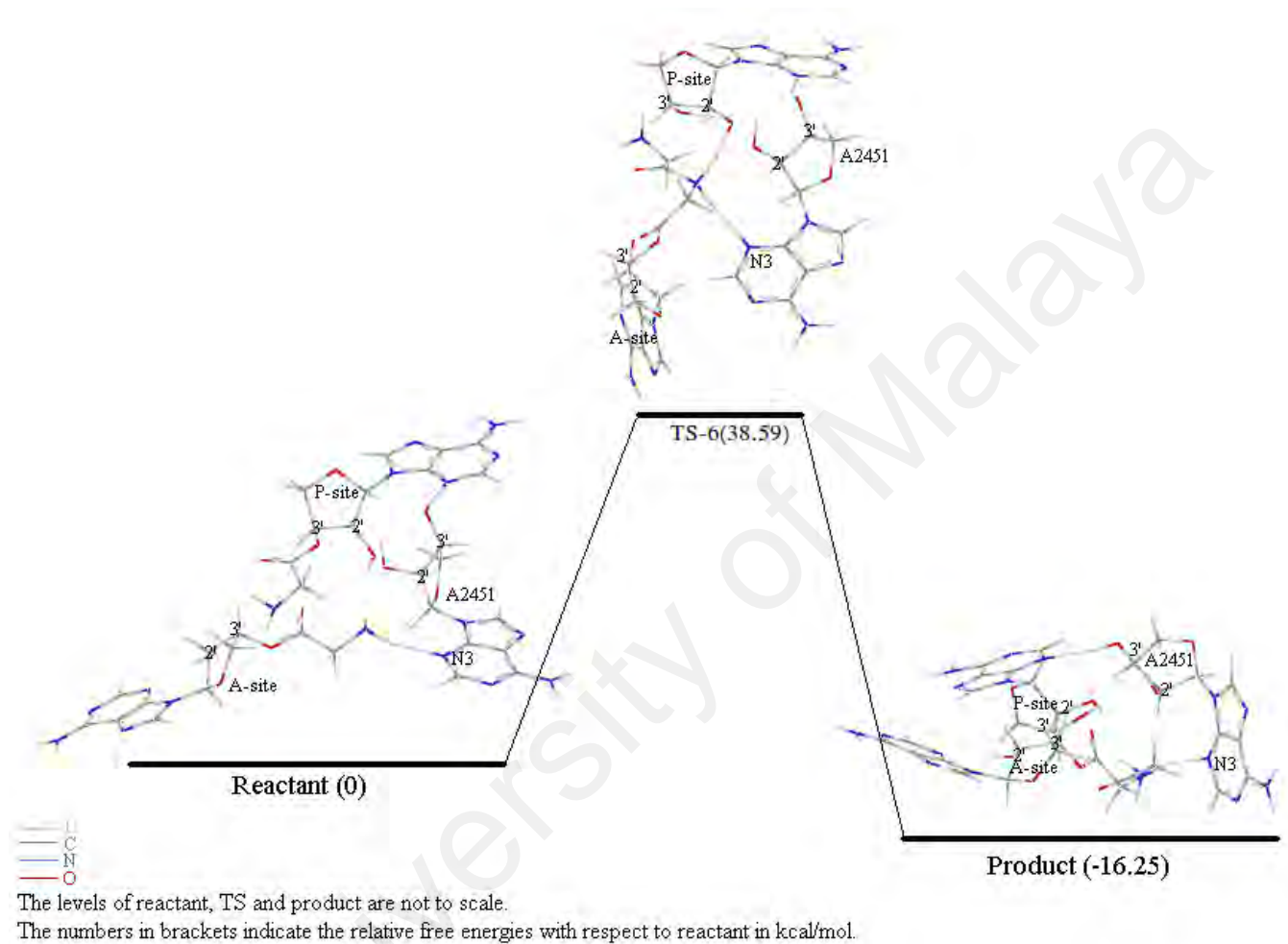


**Figure 4.2: The transition state coordinates based on the crystallographic structure of Ramakrishnan and collaborators (Voorhees et al., 2009) for the 6-membered transition structure. (The schematic view of this mechanism can be observed in Scheme 3.2., TS6).**

The most plausible and probable mechanism starting from this optimized structure would be a 6-membered mechanism where the A2451 does not directly participate in the reaction.

The role of A2451 in this mechanism is stabilizing the TS-6 by hydrogen bonding interaction with both the A-site attacking nucleophile and the P-site A76 2'-O through its N3 and 2'-O respectively. The TS-6 in this mechanism is almost similar to that of the old 6-membered mechanism in terms of the participating atoms in the reaction.

There is however a significant increase in the reaction rate of this mechanism which is a clear indication of the stabilizing effect of the A2451 on TS-6 (Figure 4.2). Adding the A2451 as well as the adenine bases of the A- and P-site A76 tRNAs results in a  $10^4$ -fold enhancement in the reaction rate of our proposed 6-membered mechanism compared to that of old 6-membered mechanism carried out in this study (Table 4.1).

This rate enhancement is a result of the A2451 residue acting as an anchor (i.e. the A2451-N3 interacting with  $\alpha$ -amine and A2451-3'-O interacting with the P-site A76-N3), holding the reactive complexes in their proper position for peptidyl transfer mechanism. This 6-membered mechanism advocates the importance of the A2451 in catalysis. It however does not highlight the main catalytic power of the ribosome since the reaction rate is still relatively low, hence, the position of the catalytic array might not be apt for formation of a stabilized transition structure.

To get another perspective from the position of the catalytic arrays in the active site, we have explored a different crystallographic structure of the ribosomal active site.

#### 4.1.2.3 P-III mechanism

In the crystallographic structure of Polacek and collaborators, the location of the A2451, i.e. between the A-site  $\alpha$ -amine and the P-site A76 2'-OH group suggests two types of interactions. Interaction 1 where there is a hydrogen bond interaction between the 2'-O of A2451 and hydrogen of the  $\alpha$ -amine and interaction 2 where there is a hydrogen bond interaction between the 2'-H of A2451 and the P-site A76 2'-O.

Since there is a large distance between these active groups, these two interactions are less likely to occur simultaneously. The occurrence of the former (interaction 1) in the transition structure suggests that the A-site  $\alpha$ -amine is a proton donor to the A2451 2'-OH group. It would however result in a reduced nucleophilicity of the  $\alpha$ -amine that might eventually affect the rate of peptidyl transfer. The occurrence of the latter (interaction 2) indicates the significance of the A2451 2'-OH group on hampering the spontaneous transesterification between the P-site C-3'-OH group and its adjacent C-2'-OH group. This suggests that the P-site A76 2'-OH group acts as a proton shuttle, deprotonating the attacking nucleophile directly with no proper participation of the A2451 base in the chemical reaction.

After the optimization of the active site, we observed that the A2451 3'-OH group is positioned between the P-site 2'-OH and 3'-O while the A2451 2'-H is hydrogen bonded with the N3 of the P-site adenine base. This results in the A2451 3'-O...2'-H (P-site A76) interaction instead of the A2451 2'-H...2'-O (P-site A76) interaction which is observed in the crystallographic structure of Polacek et al. (2008). The result is the relocation of the A2451 3'-H in a proton shuttling position towards the P-site 3'-O (Figure 4.3, Reactant), while the lone pair of the P-site A76 2'-O would be free to

interact with the hydrogen of the attacking nucleophile. The formation of this reactant complex from the crystallographic structure of Polacek as starting point requires a major reorganization in the active site group, which if correct, supports the idea of Sievers et al., where the ribosomal catalytic power is due to an entropy trap (Sievers et al., 2004).

As suggested by Polacek and collaborators, the A2451 2'-O hampers the spontaneous transesterification between the P-site 3'-O and 2'-O. The type of interaction which would cause the trans-esterification, is observed in Section 4.1.2.2 as well; the A2451 2'-O group interacts with the P-site 2'-H (A2451 2'-O...H (2') A76) and this can be the case at any point within the reaction before the actual pre-peptidyl transfer structure is formed.

Proceeding towards the reaction in the forward direction, we observe that instead of A2451 2'-OH group (A2451 2'-H...O (2') A76), its neighbouring 3'-OH group (A2451 3'-O...H (2') A76) is interacting with the P-site 2'-OH group. The change from H in the former to O in the latter in terms of hydrogen bonding interaction induces the A2451 to act as proton shuttle between the P-site 3'-O and 2'-O and results in facilitation of the transesterification reaction.

This transfer occurs through protonation of the P-site A76 3'-O and deprotonation of the neighbouring 2'-O with direct participation of the A2451 3'-O as proton donor and acceptor respectively. The fast esterification of the 2'-O prevents it from being protonated by the attacking nucleophile, but it remains in hydrogen bonding distance with it (Table 4.3).

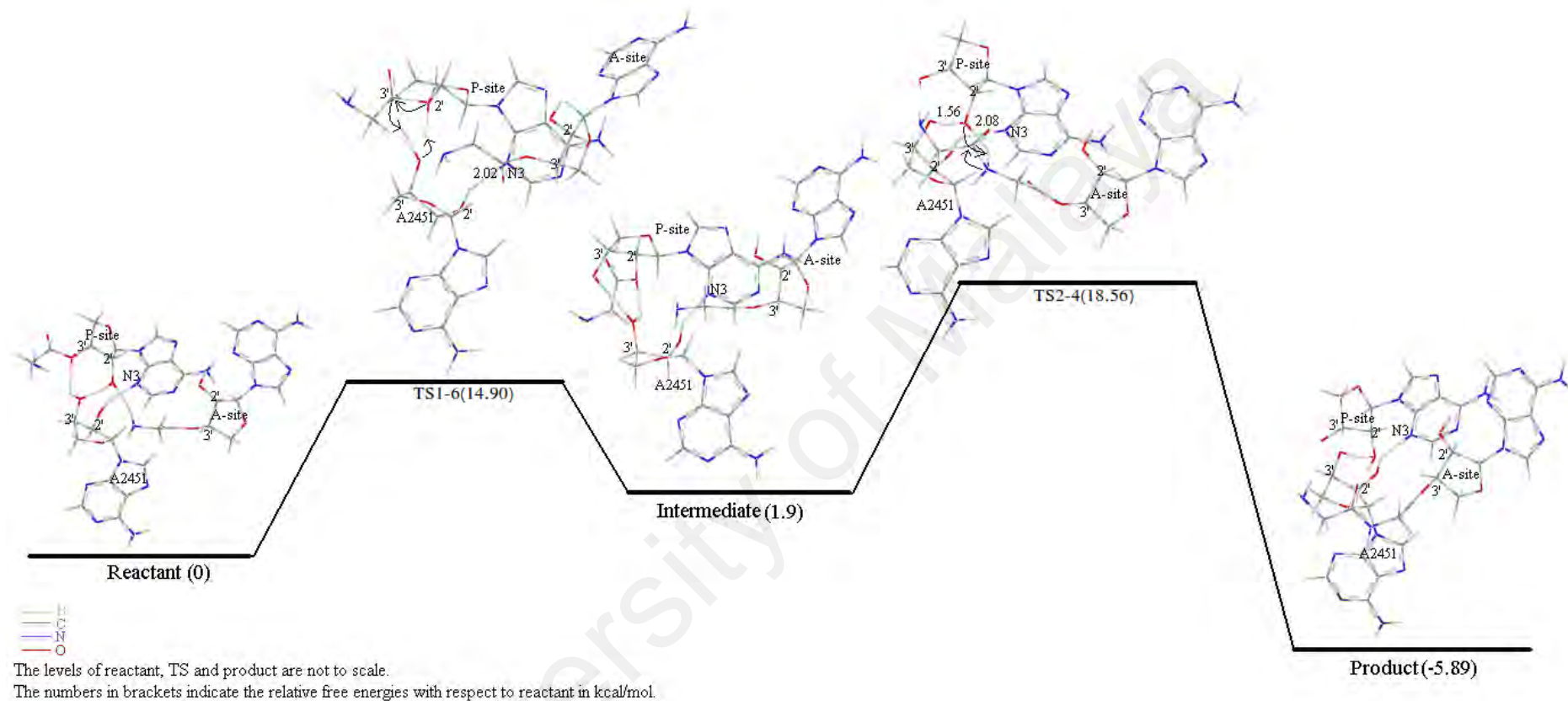


**Figure 4.3: The transition state coordinate for a stepwise mechanism proposed in our study based on the crystallographic structure of Polacek and collaborators (Lang et al., 2008). (The schematic view of this mechanism can be observed in Scheme 3.2. TS1-6 → TS2-4).**

**Table 4.3: The free energies of activation and reaction rates for the three novel proposed reaction mechanisms.**

Mechanism	Method	Step	$\Delta G^\ddagger$ kcal/mol	$k$ (s <sup>-1</sup> )
P-I	M06-2X/6-31++G**	TS1-12	38.35	$0.7 \times 10^{-15}$
		TS2-4	27.04	$1.4 \times 10^{-7}$
P-II	M06-2X/6-31++G**	TS-6	38.59	$0.4 \times 10^{-15}$
P-III	M06-2X/6-31++G**	TS1-6	14.90	$1.1 \times 10^2$
		TS2-4	18.56	$2.3 \times 10^{-1}$

With the polypeptide closer to the attacking nucleophile, the process of peptide bond formation occurs through a 4-membered reaction mechanism. In this step, the A2451 3'-OH group facilitates the peptidyl transfer from P-site A76 2'-O to the  $\alpha$ -amine by hydrogen bonding with the 2'-O with the very same proton it has received from it in the first step of the reaction. Throughout all these steps, the A2451 2'-H remains within the hydrogen bonding distance with the P-site N3 to hold the active site groups in close proximity to one another for a better transition state stabilization. The second step is the rate determining step since the reaction rate is  $10^3$ -fold lower than that in the first step. It is however only  $10^2$ -fold lower than the observed rate in the experiments (i.e. 20/s).

#### 4.1.3 Ribosomal catalytic role

Proton transfer activity during peptide bond formation in the ribosome has been immensely investigated in previous experimental and computational studies to answer whether this mechanism is catalysed by ribosomal bases (ribosomal catalysis), by the P-site A76 2'-OH group (substrate assisted catalysis) or by the water molecules in the active site (ribosome as water trap).

Upon mutation of the P-site A76 2'-OH group, a 100-fold reduction in the reaction rate was observed (Zaher & Green, 2011), which however small, can be the indication of this group's activity during peptidyl transfer reaction. The observed high activation energy barrier for the proposed 6-membered mechanism in this study and previous studies indicate that this activity is not due to the proton shuttling. Even for the mechanism P-II in this study (Section 4.1.2.2) where the interaction of A2451 2'-H with the P-site 2'-O is expected to stabilize the transition structure, the reaction rate is rather low. The abundance of OH groups in the active site also does not reduce the activation barrier as it can be observed in our stepwise mechanism P-I in Section 4.1.2.1 where the reaction rate of the TS1-12 → TS2-4 is similar to the 6-membered mechanism P-II in Section 4.1.2.2.

In all these mechanisms, the A-site attacking amine gets deprotonated and attaches to the growing polypeptide chain and the P-site A76 3'-O releases the polypeptide chain. Due to the large distance between the P-site A76 3'-O and the A-site attacking nucleophile, various means have been proposed as proton shuttling groups to transfer the proton of the  $\alpha$ -amine to the leaving 3'-O. However, not much attention has been paid to the problem of polypeptidyl transfer which is equally distant from the attacking nucleophile.

This issue has been addressed in the P-III mechanism (Section 4.1.2.3) and we can clearly observe a rather plausible stepwise reaction mechanism where the A2451 3'-O is actively present in both steps. Instead of its role as the so-called proton shuttling group, the P-site A76-2'O in this reaction acts as a *peptidyl shuttle* which in fact transfers the growing polypeptide chain to the A-side aminoacyl-tRNA.

This effect can be rationalized as the enzymatic catalytic effect of the ribosome to increase the rate of peptide bond formation by a proper substrate positioning. Since the barrier height contributes to the reaction rate exponentially (Equation 2.10), its value is considered to be more important in the TST formulation compared to all the pre-exponential terms put together. However, the regulation in biological systems dictates that even the slightest change in an enzymatic reaction rate which is affected by smaller factors than the barrier height can have a colossal effect on the biological outcome. Accordingly, effects on the pre-exponential terms such as recrossing or quantum tunnelling can be critical to the proper understanding of an enzymatic reaction. This is where exploring quantum tunnelling in the reaction becomes necessary, especially when the transfer of such a light atom like the proton is dominant in the rate determining step.

#### **4.1.4 Tunnelling effect in proton transfer reaction during peptide bond formation**

Enzymes are known to catalyse chemical reactions by lowering the energy barrier through some conformational changes and induced fit mechanisms. The question is that do enzymes induce tunnelling as a way of catalysis as well? Some studies show that for enzymatic proton transfer reactions with energy barrier of  $\sim 5$  kcal/mol and higher, tunnelling becomes dominant (Truhlar, 2010). Since the barrier height in most of the enzymatic proton transfer reactions is around 10-20 kcal/mol, it would be surprising if there is no tunnelling contribution to enzymatic catalyses. It can be associated to the thermal fluctuations in protein enzymes which induce tunnelling by thinning the barrier width as well as lowering the barrier height. Gil and Waluk (2007) called this scheme the vibrational gating, which indicates that vibrational fluctuation facilitate tunnelling, where tunnelling depends on donor-acceptor distance (Ley et al., 2012).

It was first discovered by Klinman and collaborators that at temperatures of 30°C and above, tunnelling contribution can be measured for the reaction of dehydrogenase catalysed ethanol oxidation in liver alcohol dehydrogenase enzyme, whereas at temperatures of 5°C and below, no tunnelling contribution can be measured. This can be explained based on the assumption that the enzymes demonstrate low frequency vibrational modes which in some cases have a constructive contracting effect on the barrier width. Since at biological temperatures, higher quantum states of the more rigid vibrational modes are usually not populated, large enzymatic molecules involve low frequency modes which can be populated at those states. However, there is a limit to how low the frequency levels would be.

#### ***Reaction rate at room temperature***

In the case of proton transfer reactions as argued by Bothma et al., (2010), the environmental frictions on the proton is quite weak. Therefore, the quantum effects on the reaction rate is not affected by environmental vibrations at biological temperatures with frequencies less than 1000 cm<sup>-1</sup>. These low frequencies have a low impact on the tunnelling correction factor  $\Gamma$  with least effect on the overall reaction rate.

The effect of low vibrations on the value of  $\Gamma$  can be seen in Table 4.4 for the calculated values of tunnelling correction for all the mechanisms of peptide bond formation from previous section. Among all these mechanisms, the most classically favourable mechanism is P-III because of its lowest barrier height, followed by SW and TS-8. However, the highest tunnelling correction factor due to imaginary frequencies higher than 1000 cm<sup>-1</sup> which implies narrow barrier widths (Equation 3.37) is only observed in three of these mechanisms.

**Table 4.4: The tunnelling correction factor ( $\Gamma$ ), width parameter ( $\ell$ ) and tunnelling rate for all proposed mechanisms of peptide bond formation in room temperature.**

Mechanism	$\Delta G^\ddagger$ (kcal/mol)	$k$ classical (s <sup>-1</sup> )	$E_o$ (kcal/mol)	$\ell$ (Å)	$\sigma$ (cm <sup>-1</sup> )	$\Gamma$			$k_{Q-tunnel}$ (s <sup>-1</sup> )		
						(Wigner)	(Shavitt)	(Numerical)	(Wigner)	(Shavitt)	(Numerical)
TS-4	44.47	$2 \times 10^{-20}$	41.79	2.766	1123	2.23	2.25	5.53	$4.4 \times 10^{-20}$	$4.5 \times 10^{-20}$	$1.1 \times 10^{-19}$
TS-6	45.41	$4.0 \times 10^{-20}$	46.71	14.18	231	1.05	1.05	1.00	$4.2 \times 10^{-20}$	$4.2 \times 10^{-20}$	$4.0 \times 10^{-20}$
TS-8	35.01	$2.0 \times 10^{-13}$	34.76	15.43	183	1.03	1.03	1.00	$2.0 \times 10^{-13}$	$2.0 \times 10^{-13}$	$2.0 \times 10^{-13}$
SW	9.51	$1.9 \times 10^6$	16.13	1.733	977	1.93	1.96	3.03	$1.9 \times 10^6$	$1.9 \times 10^6$	$3.0 \times 10^6$
	26.78	$4.4 \times 10^{-7}$	22.18	2.032	1114	2.20	2.23	4.94	$4.4 \times 10^{-7}$	$4.4 \times 10^{-7}$	$9.8 \times 10^{-7}$
P-I	38.35	$7.0 \times 10^{-16}$	35.24	13.75	207	1.04	1.04	1.04	$7.2 \times 10^{-16}$	$7.3 \times 10^{-16}$	$7.3 \times 10^{-16}$
	27.04	$1.4 \times 10^{-7}$	29.50	18.99	137	1.02	1.02	1.00	$1.4 \times 10^{-7}$	$1.4 \times 10^{-7}$	$1.4 \times 10^{-7}$
P-II	38.59	$4.0 \times 10^{-16}$	34.57	10.85	260	1.07	1.07	1.07	$4.2 \times 10^{-16}$	$4.2 \times 10^{-16}$	$4.2 \times 10^{-16}$
P-III	14.90	$1.2 \times 10^2$	12.857	91.51	188	1.03	1.04	1.04	$1.2 \times 10^2$	$1.2 \times 10^2$	$1.2 \times 10^2$
	18.56	$2.3 \times 10^{-1}$	20.60	1.801	1212	2.43	2.47	6.67	$5.5 \times 10^{-1}$	$5.6 \times 10^{-1}$	1.5

These mechanisms are TS-4, SW and P-III where the P-III is the only mechanism with highest  $\Gamma$  and lowest barrier height in addition to the narrow barrier width. This significantly enhances the rate of reaction in P-III mechanism (1.5/s) which is in a good agreement with the experimentally estimated rate of  $2.0 \times 10^1 \text{ s}^{-1}$  (20/s) (Table 4.4).

The P-III mechanism involves the so-called A2451 ribosomal active site group. This raises the question of whether or not this base plays any role in promoting tunnelling in the same way as protein enzymes do. One way to answer this question is to analyse the temperature dependant kinetics of this reaction and compare it with those of TS-4 and SW mechanisms which are purely substrate assisted mechanisms with no ribosomal catalysis.

#### ***Temperature dependent reaction rate***

An important aspect of chemical kinetics involves the Arrhenius law where the logarithm of the reaction rate is experimentally linear to the inverse of the temperature and the slope gives activation energy except for the very low temperatures. The empirical expression for this linear relationship can be illustrated from Equation 4.1 by plotting the logarithm of the reaction rate versus the inverse of the temperature.

$$\ln(k) = \ln(A) - \frac{E_a}{R} \frac{1}{T} \quad (4.1)$$

The intercept of this line with the y axis of  $\ln(k)$  corresponds to the logarithm of pre-exponential factor A ( $\ln(A)$ ). Deviation from linear to exponential descent as the temperature goes down is an indication of tunnelling. This deviation changes the Y intercept ( $\ln(A)$ ) of the tangent line at a particular temperature. For lighter particles, this

deviation is quite significant whereas for the heavier particles, less deviation is observed and the plot is inclined towards the linear classical behaviour.

The theoretical expression would however be quite different from Equation 4.1. Based on Equation 3.40 which calculates the overall quantum mechanical reaction rate, the theoretical rate expression can be written as

$$\ln k(T) = \ln \Gamma(T) + \ln \frac{k_B T}{h} - \frac{\Delta G^\ddagger}{R} \frac{1}{T} \quad (4.2)$$

The slope for this plot can be calculated from:

$$\frac{d}{d(\tau)} \ln k\left(\frac{1}{\tau}\right) = \frac{d}{d(\tau)} \ln \Gamma\left(\frac{1}{\tau}\right) + \frac{d}{d(\tau)} \ln \frac{k_B}{h\tau} - \frac{d}{d(\tau)} \frac{\Delta G^\ddagger}{R} \tau \quad (4.3)$$

and the intercept at a particular temperature of  $T_0$  can be calculated from:

$$Y = \left( \ln \Gamma\left(\frac{1}{\tau}\right) + \ln \frac{k_B}{h\tau} - \frac{\Delta G^\ddagger}{R} \tau \right) \Big|_{\tau=\tau_0} - \left[ \left( \frac{d}{d(\tau)} \ln \Gamma\left(\frac{1}{\tau}\right) - \frac{1}{\tau_0} - \frac{\Delta G^\ddagger}{R} \right) \times \tau \right] \Big|_{\tau=\tau_0} \quad (4.4)$$

where

$$\tau = \frac{1}{T} \quad \text{and} \quad \tau_0 = \frac{1}{T_0} \quad .$$

Figure 4.4 illustrates the Arrhenius plot of the reaction rate versus the inverse temperature. The three colours correspond to the three mechanisms in Table 4.4 with the

highest value for  $\Gamma$  i.e. TS-4, SW and P-III mechanisms. These plots are varied over a vast temperature range from 53.15 K to 308.15 K. The lower temperatures do not correspond to the biological temperatures, but they are used to view the overall tunnelling behaviour of these mechanisms. By looking at a larger picture, it is easier to compare the plots for classical, analytical and numerical approaches.

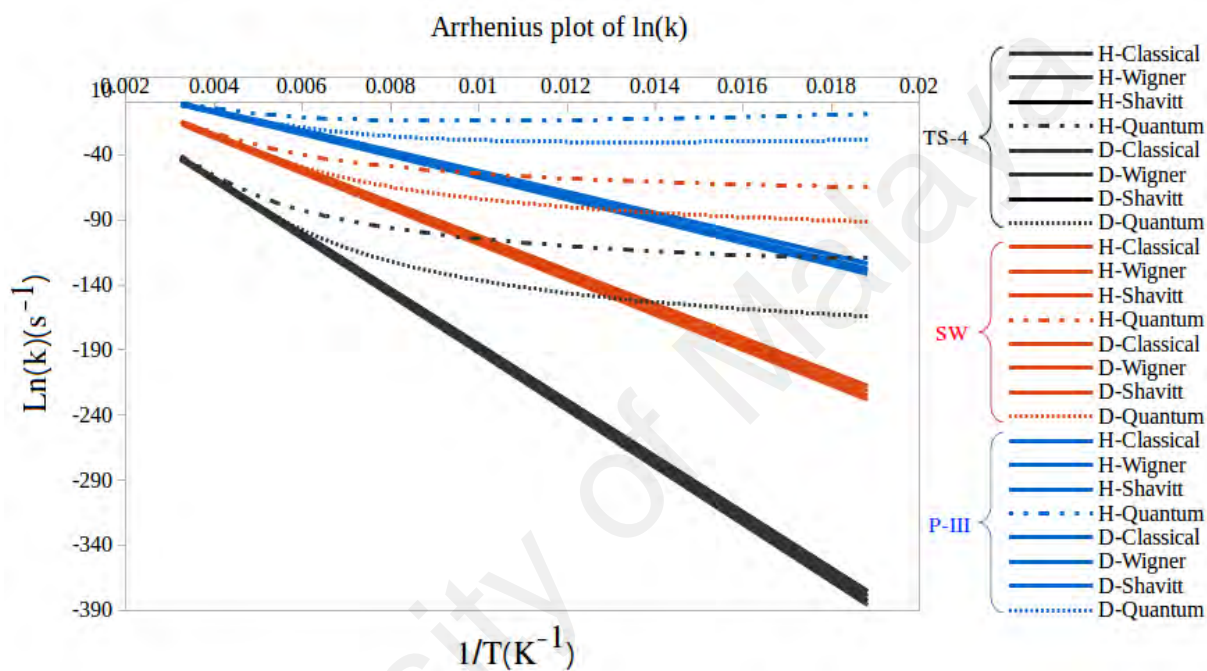


**Figure 4.4: The Arrhenius plot of the reaction rate of TS4, SW(TS2-4) and P-III mechanism from 53.15 K to 308.15 K. H stands for hydrogen and D stands for deuterium.**

The solid lines illustrate the plots for classical, and analytical tunnelling (Wigner and Shavitt) behaviours which are quite similar characteristically. The numerical approach (two-dot dashed lines) shows a clear deviation from classical linear descent to flat which resembles a reasonable tunnelling behaviour. On the other hand, the linear behaviour of the Arrhenius plot in Wigner's and Shavitt's methods does not reveal significant deviation from the classical plot, which suggests that those two approaches significantly underestimate the contribution of tunnelling.

The best tunnelling behaviour is observed in the most favourable P-III mechanism where the deviation from linear descent in the plot is more significant. Furthermore, this deviation is larger at higher temperature (around 283.15 K) compared to the other two mechanisms as shown in Table 4.4. On the other hand, the Arrhenius plots corresponding to the TS-4 and SW mechanisms deviate less significantly and the temperature at which they deviate is lower (around 253.15 K).

It must also be noted that additional to the proton, the deviation in the plot is also observed for the deuterium as illustrated by dotted lines in each colour. Even though the curvature for deuterium starts at a lower temperature, it is still an implication of tunnelling for the heavier isotope. The distance between the plots of two isotopes (dotted line and dot and dashed line) is the kinetic isotope effect which indicates the significance of tunnelling for the lighter isotope.

### ***Kinetic Isotope Effect***

Kinetic Isotope Effect (KIE) is described in terms of Arrhenius equation as follows:

$$\ln\left(\frac{k_H}{k_D}\right) = \ln\left(\frac{A_H}{A_D}\right) - \left(\frac{E_a^H - E_a^D}{R}\right) \frac{1}{T} \quad (4.5)$$

Note that this equation is also the experimental expression of classical KIE, similar to Equation 4.1. Figure 4.5 shows the kinetic isotope effect plots of dependence of  $\ln(k_H/k_D)$  versus the inverse temperature ( $1/T$ ) for the main three mechanisms.

In the classical kinetics, the  $A_H$  and  $A_D$  are usually nearly equal and cancel out in the KIE expressions. Furthermore, the activation energy of the two isotopes are almost equal ( $E_a^H \approx E_a^D$ ) which would then cause a zero slope in the plot. Both these effects can

be seen in higher temperature range of Figure 4.5. The lowest level of the classical plot compared to the analytical plots is the expression of the former effect and the slope of almost zero is the expression of the latter effect.

This is rather different when quantum mechanical kinetics is included in the reaction mechanism. The Arrhenius equation of KIE has a tunnelling component which has to be taken into account. Therefore, from Equation 4.2 we will arrive at the following equation:

$$\ln\left(\frac{k_H}{k_D}\right) = \ln\left(\frac{\Gamma_H}{\Gamma_D}\right) + \left(\frac{\Delta G_D^\ddagger - \Delta G_H^\ddagger}{R}\right) \frac{1}{T} \quad (4.6)$$

from which the intercept of the tangent line with the y axis of  $\ln(k_H/k_D)$  at a particular temperature can be obtained (Equation 4.7).

$$\begin{aligned} Y = & \ln\left(\frac{\Gamma_H}{\Gamma_D}\right) + \left(\frac{\Delta G_D^\ddagger - \Delta G_H^\ddagger}{R}\right) \tau \Big|_{\tau=\tau_0} \\ & - \left[ \frac{d}{d(\tau)} \ln(\Gamma_H) \Big|_{\tau=\tau_0} - \frac{d}{d\tau} \ln(\Gamma_D) \Big|_{\tau=\tau_0} \right. \\ & \left. + \frac{\Delta G_D^\ddagger - \Delta G_H^\ddagger}{R} \right] \times \tau_0 \end{aligned} \quad (4.7)$$

The second and fifth terms are negligible if we assume that  $\Delta G_H^\ddagger \approx \Delta G_D^\ddagger$ . Hence, the intercept can be simplified in the form of:

$$Y = \ln\left(\frac{\Gamma_H}{\Gamma_D}\right) - \left[ \frac{d \ln\left(\frac{\Gamma_H}{\Gamma_D}\right)}{d(\tau)} \Big|_{\tau=\tau_0} \right] \tau_0 \quad (4.8)$$

The tangent line on the plot of  $\ln(k_H/k_D)$  versus  $1/T$  is shown at the intercept point of zero for the three aforementioned mechanisms (Figure 4.5). From Equation 4.8, the intercept of zero at y axis of  $\ln(k_H/k_D)$  results in:

$$\ln\left(\frac{\Gamma_H}{\Gamma_D}\right) = \left[ \frac{d \ln\left(\frac{\Gamma_H}{\Gamma_D}\right)}{d(\tau)} \Big|_{\tau=\tau_0} \right] \tau_0 \quad (4.9)$$

$$Y = 0$$

Equation 4.9 exhibits the exponential characteristic of the plot which indicates the tunnelling behaviour at  $\tau=\tau_0$ . This effect is demonstrated in Figure 4.5 where the tunnelling behaviour begins at a point where the intercept of the tangent line to the y axis is zero ( $Y=0$ ); i.e. the plot starts to behave exponentially.

In Figure 4.5, this transition temperature is much lower than the biological temperature, i.e. 113 K for TS-4 and SW mechanisms and 120 K for P-III mechanism. However, relative to one another, the transition temperature is higher for P-III mechanism which further supports the higher tunnelling contribution in this mechanism.

A concave curve (curve down) is observed in low temperature range, which is opposite of the convex curve (curve up) in the high temperature range. In the low temperature part of the plot, as the temperature increases,  $\tau_0$  decreases with which the slope increases (due to the concave shape of the plot at low T). This results in a decrease in the value of the intercept ( $Y$ ). Therefore, the value of  $\ln(\Gamma_H/\Gamma_D)$  must also decrease, while remaining larger than slope since  $Y$  is always positive at low temperature range (according to the plot).

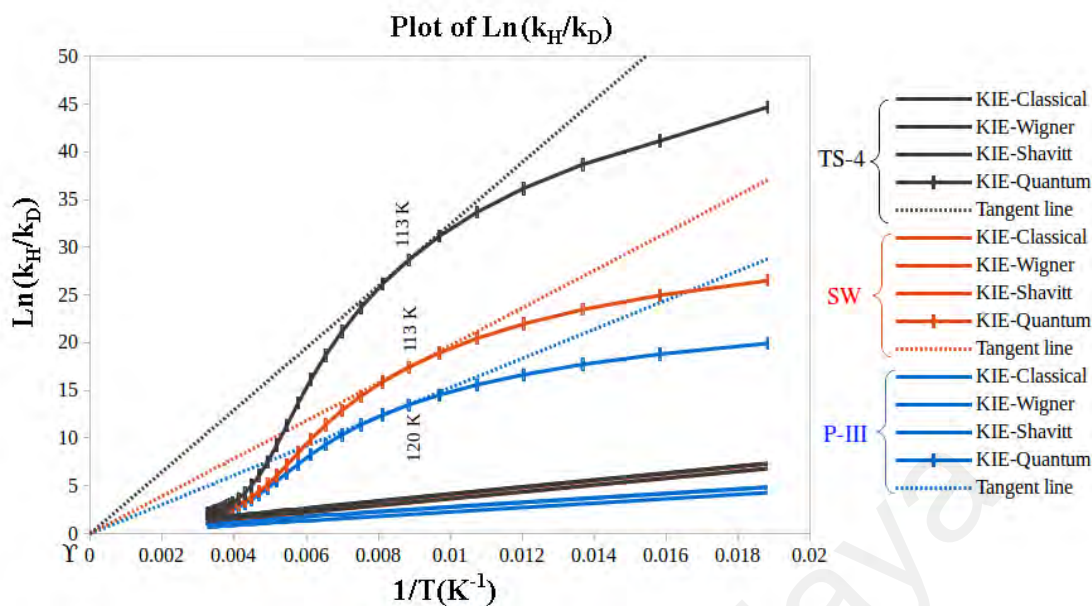


**Figure 4.5: The plot of the kinetic isotope effect for the TS4, SW(TS2-4) and P-III mechanism from 53.15 K to 308.15 K.**

The decrease in  $\ln(\Gamma_H/\Gamma_D)$  as well as the decrease in the ratio of  $\Gamma_H/\Gamma_D$  results in lower KIE (the change is however, minimal due to the logarithmic function). As the temperature passes the tunnelling point (where  $Y=0$ ) and continues to rise, the value of intercept becomes less than zero ( $Y<0$ ) and keeps decreasing to the point where the curvature changes from concave to convex. That is where  $Y$  is at its minimum which can also be regarded as the inflection point.

Mathematically, this is the turning point where the concave shape of the plot changes to the convex shape. The exact position of this point is at the temperature of 193K. It is at this point where the intercept of the tangent line starts to increase due to the convex shape of the plot at higher temperature range until the  $Y>0$ . With further increase in the temperature,  $Y$  starts to elevate back up (due to the convex shape of the plot at higher temperature) with which the value of  $\ln(\Gamma_H/\Gamma_D)$  also increases. Since the slope and  $\tau_0$  is decreasing, the increase in the value of  $\ln(\Gamma_H/\Gamma_D)$  should not be significant for it should always remain less than the slope to retain the negative intercept value.

There is a difference in the tunnelling behaviour of proton transfer reaction between our study and that of Kohen et al. (1999); the intercept of the tangent line in their study never falls below zero, whereas the  $\gamma$  in our study does become negative. As it can be seen in Figure 4.5, this value becomes negative as the temperature increases from the transition temperature to the inflection point.

To have a clearer and closer picture of the high temperature range, we plot the high temperature range of Arrhenius plot in Figure 4.6 and KIE plot in Figure 4.7. These two figures are the magnification of high temperature regions of Figures 4.4 and 4.5.

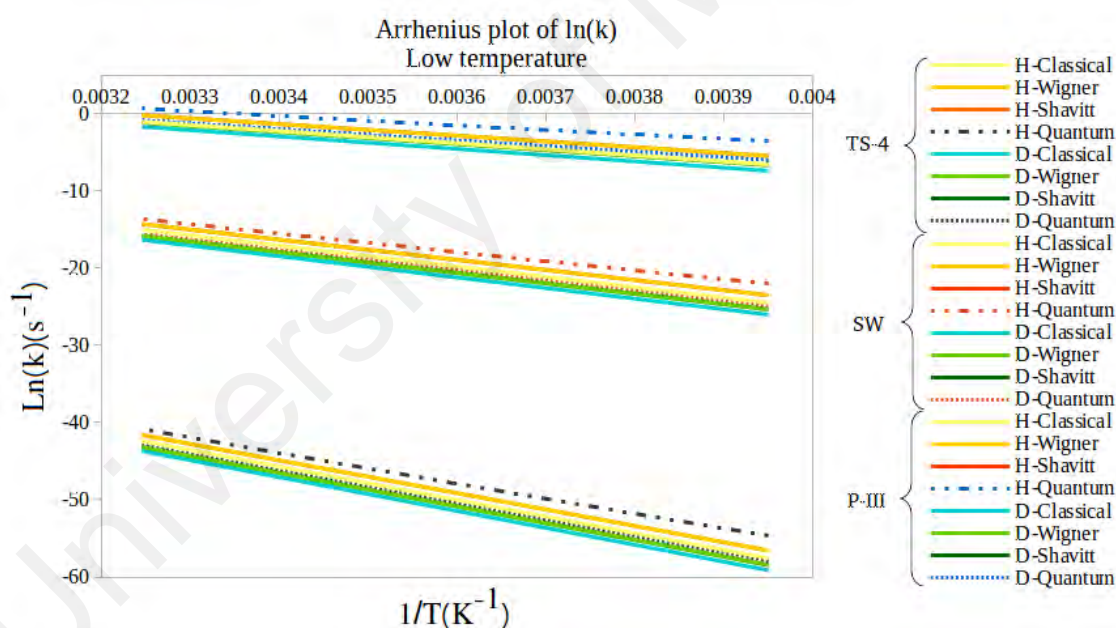


**Figure 4.6: The Arrhenius plot of the reaction rate of TS4, SW(TS2-4) and P-III mechanism from 253.15 K to 308.15 K.**

Due to the small temperature range, only a slight curvature is observed in the plot of hydrogen transfer for the numerical approach. However, the divergence from classical descent is observable (especially in P-III mechanism) which is a clear indication of tunnelling behaviour even at elevated temperatures. This divergence in the plot of KIE

is illustrated as a semi-linear ascent (Figure 4.7). We use the term semi-linear because the plots are slightly curved and are more inclined towards linearity in the three mechanisms. The high temperature range shows a convex behaviour which is also observed in Figure 4.5. At this range,  $\gamma$  is initially negative, but as the temperature rises, it becomes positive again.

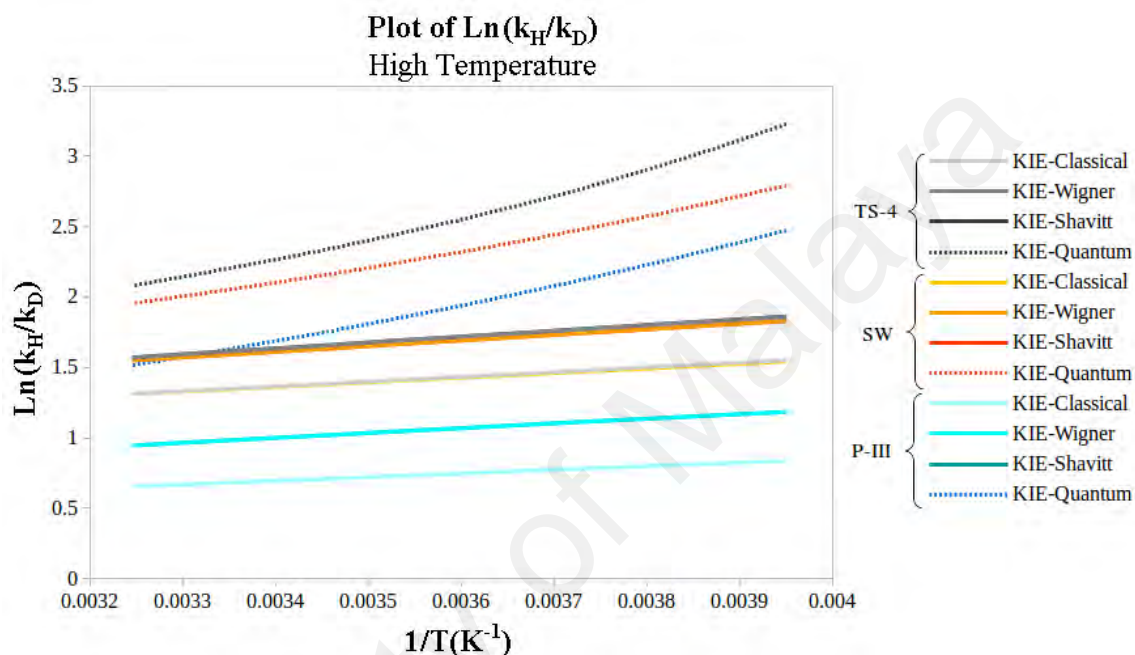


**Figure 4.7: The plot of the kinetic isotope effect of the reaction rate of TS4, SW(TS2-4) and P-III mechanisms from 253.15 K to 308.15 K.**

The intercept point of  $\gamma=0$  cannot be seen in this plot where the minimum of the x axis is not zero. At this temperature range, as the temperature decreases towards the inflection point,  $\gamma$  becomes smaller which is a manifestation of negative slope (Figure 4.5). However, as the temperature increases,  $\tau_0$  decrease while the value of  $\gamma$  increases. This is when the value of  $\ln(\Gamma_H/\Gamma_D)$  must increase to maintain the increment of  $\gamma$ , while still negative. This shows the larger rate of change in the slope of the tangent line which is manifested as a large KIE in TS-4 mechanism. On the other hand, both rate of increment and the value of  $\gamma$  are rather low in P-III mechanism, manifesting a lower KIE.

Comparing the KIE of TS-4 and SW indicates an overall larger tunnelling in TS-4 mechanism. On the other hand, the lower KIE in P-III mechanism with the largest value of  $\Gamma$  does not mean low tunnelling of proton. It indicates the significance of deuterium tunnelling which results in a lower KIE. This is in good agreement with the argument carried out by Klinman and Kohen (Kohen & Klinman, 1998; Kohen et al., 1999) where the negative intercept indicates tunnelling contribution from proton only, with an inflection point on the plot where the plot changes to concave down as the temperature decreases.

In general, the activation energy of different isotopes is almost the same. This is mainly due to the relatively small difference in imaginary frequency of the hydrogen and deuterium compared to the barrier height (Table 4.4). In TS-4 mechanism, the barrier is rather high which gives a large barrier width (see Equation 3.38), resulting in a poor tunnelling behaviour.

The situation is rather different for SW and P-III mechanisms. The barrier height in these two mechanisms, specially in P-III, is relatively low which would result in a thinner barrier width, large tunnelling factor and increased overall reaction rate (Figure 4.7, SW & P-III). The calculated width parameter for all mechanisms in Table 4.4 also confirms this observation where the value of  $\ell$  (Equation 3.33) in  $\Gamma$  (Equation 3.34) is the lowest in P-III mechanism followed by SW and TS-4.

The slight increase in KIE as the temperature increases in this case indicates higher tunnelling contribution of proton and the ratio of  $\Gamma_{\text{H}}/\Gamma_{\text{D}}$  indicates the extent to which proton tunnels at high temperature. This highlights the proficiency of P-III mechanism

in inducing tunnelling which is seen in Table 4.4 (larger tunnelling factor) as well as in Figures 4.4 and 4.6 (higher deviation of Arrhenius plot).

Observing this effect is rather expected in enzymes which are said to promote tunnelling through vibrations. A few arguments on enzymatic tunnelling focus on the protein enzymes and the protein vibrations on promoting tunnelling (Kohen et al., 1999; Longbotham et al., 2016). In the case of ribosome, if there is any tunnelling through enzymatic motion, it should be promoted by the ribosomal bases. This role might be carried out by the A2451 base which is consistently present in the active site of the ribosome.

In this study, the optimized structures are assumed to represent the aftermath of the ribosomal catalysis. In other words, the ribosomal active site groups promote tunnelling by proper positioning of the A2451 base in a location where the proton donor-acceptor distance is suitable for tunnelling. The pre-peptidyl transfer structure in P-III mechanism can be the *tunnelling ready* state of the active site core, which is followed by proton tunnelling and peptidyl transfer. The origin of this tunnelling ready state is still unknown. If there is enough experimental evidence for dynamical motion hypothesis of protein enzymes, it would be necessary to look for origin of ribosomal catalysis from the dynamical effect of ribosomal proteins surrounding the active site.

Additional to its use in medicinal chemistry and drug design, knowing how an enzyme function to increase the rate of reaction can be useful in synthetic chemistry. This study supports the *promoting vibrations hypothesis* which is the base of enzyme induced tunnelling mechanism (Pudney et al., 2009; Hay & Scrutton, 2012).

By mimicking the way enzymes induce tunnelling, one can induce tunnelling in synthetic reactions to achieve a faster reaction rate. An example of such is the esterification reaction of boronic acid with diol containing compounds which is used to design a non-enzymatic glucose sensor. Proton transfer mechanism is also dominant in the rate determining step of this reaction which gives us the advantage of studying the tunnelling phenomenon. Next section elaborates on this chemical reaction and a way to induce tunnelling for a faster reaction rate.

#### **4.2 Mechanistic study of boronic acid's reaction with diols**

Boronic acids are known to be highly reactive towards diol compounds. Upon reaction, they form cyclic boronic or boronate esters (Böeseken, 1949). The majority of mechanistic studies have agreed on a stepwise mechanism for this reaction in which the rate determining step is often attributed to the first step with interaction of diol to boron (Shao et al., 2000; Ito et al., 2003).

Many of the kinetic studies have reported a large negative activation entropy during the first step which indicates an increase in the coordination number of central boron atom (Ishihara et al., 1991; Pizer & Tihal, 1992; Kagawa et al., 1995). There are however a few reports of ring closure being the rate determining step because of the steric strain (Yamamoto et al., 2005). In this research, we are using the kinetic measurements of the reaction rate for boronic acid in interaction with diols to answer three main questions:

- 1- How does electronegativity affect boronic acid's reactivity?
- 2- Is boronic acid reactive in trigonal form or tetrahedral boronate ion form?
- 3- Can we induce proton tunnelling in the reaction of boronic acid with diols?

The first question is explored using a high and low electronegative R-groups,  $-\text{CF}_3$  and  $-\text{CH}_3$  respectively. Both these R-groups are then used on neutral lewis boronic acid ( $\text{CH}_3\text{-B(OH)}_2$  and  $\text{CF}_3\text{-B(OH)}_2$  MI & MII) as well as lewis ( $\text{CH}_3\text{-B}((\text{OH})_2\text{O}(\text{CH}_2)_2\text{OH})$  and  $\text{CF}_3\text{-B}((\text{OH})_2\text{O}(\text{CH}_2)_2\text{OH})$  (MIII-II) and Brønsted ( $\text{CH}_3\text{-B(OOH)}^-$  and  $\text{CF}_3\text{-B(OOH)}^-$  M IV & MV) basic boronate ions to explore the second question. From these initial structures, we proposed five possible reaction pathways (Schemes 4.2 & 4.3). The third question is addressed in Section 4.2.5 by adding the tunnelling contribution to the overall reaction rate.

For simplicity and to avoid confusion, the term *mechanism* which refers to the specific mechanisms from I to V is replaced with M throughout the text. Hence, mechanism I to mechanism V, are named as MI, MII, MIII, MIV and MV.

#### 4.2.1. Kinetic study of $\text{CH}_3\text{-B(OH)}_2$ and $\text{CH}_3\text{-BOOH}^-$ in reaction with diol

The rate determining steps in these five mechanisms differ based on the starting material or the reactant complex. Step 1 of MI for instance has a relatively high activation barrier, resulting in the rate of  $10^{-15}/\text{s}$  (Table 4.5). A significant rate enhancement by the factor of  $10^7$ -fold is observed in step 2 during the chelate ring closure which agrees well with the experiments (Pizer & Tihal, 1992; Shao et al., 2000; Ito et al., 2002). For example in the study done by Pizer & Tihal (1992), a  $10^2$ -fold higher reaction rate was observed in the second step of the reaction between methylboronic acid and polyols compared to that in the first step. The result of this reaction is a trigonal cyclic boronic ester with elimination of two water molecules.

The increased rate during the second step, the chelate ring closure, could be regarded to the stabilizing effect of the eliminated water molecule in step 1 through interaction with the intermediate. This effect is observed even more significantly in MII where the incoming diol lacks an acidic proton. Through the interaction of the OH end of the diol similar to MI, a water molecule gets eliminated which has the stabilizing effect on the transition structure for the second step. Additional to that is the negative charge on the oxygen at the other end of the diol which further stabilizes the structure of the transition state and increases the rate by a factor of  $10^{23}$ -fold for  $\text{CH}_3\text{-B(OH)}_2$  (Table 4.5 & Scheme 4.2).

**Table 4.5: The thermodynamic data of the mechanisms between  $\text{CH}_3\text{-B(OH)}_2$  and 1,2-ethanediol.**

Mechanism/ $\text{CH}_3\text{B(OH)}_2$	Step of reaction	$\Delta G$ (kcalmol <sup>-1</sup> )	$\Delta S$ (kcalmol <sup>-1</sup> K <sup>-1</sup> )	$\Delta G^\ddagger$ (kcalmol <sup>-1</sup> )	$\Delta S^\ddagger$ (kcalmol <sup>-1</sup> K <sup>-1</sup> )	$k$ (s <sup>-1</sup> )
MI/neutral	Step 1	6.621	-0.031	38.110	-0.047	$1.07 \times 10^{-15}$
	Step 2	-4.261	0.014	28.123	-0.010	$2.3 \times 10^{-8}$
	Overall	2.401	-0.017	-	-	<b><math>1.07 \times 10^{-15}</math></b>
MII/acidic	Step 1	0.549	-0.036	47.785	-0.050	$8.5 \times 10^{-23}$
	Step 2	-8.210	-0.007	17.625	-0.006	1.163
	Overall	-7.661	-0.043	-	-	<b><math>8.5 \times 10^{-23}</math></b>
MIII/acidic & basic	Step 1	-4.273	0.042	-	-	-
	Step 2	-3.396	-0.001	8.035	0.003	$1.2 \times 10^7$
	Overall	-7.661	-0.043	-	-	<b><math>1.2 \times 10^7</math></b>
MIV/basic	Step 1	-12.208	-0.044	20.254	-0.042	$1.3 \times 10^{-2}$
	Step 2	-3.396	-0.001	8.035	0.003	$1.2 \times 10^7$
	Overall	-15.590	-0.045	-	-	<b><math>1.3 \times 10^{-2}</math></b>
MV/basic	Step 1	-3.081	-0.032	34.819	-0.047	$2.8 \times 10^{-13}$
	Step 2	0.001	-0.012	0.755	-0.003	$2.79 \times 10^{12}$
	Overall	-3.071	-0.044	-	-	<b><math>2.8 \times 10^{-13}</math></b>

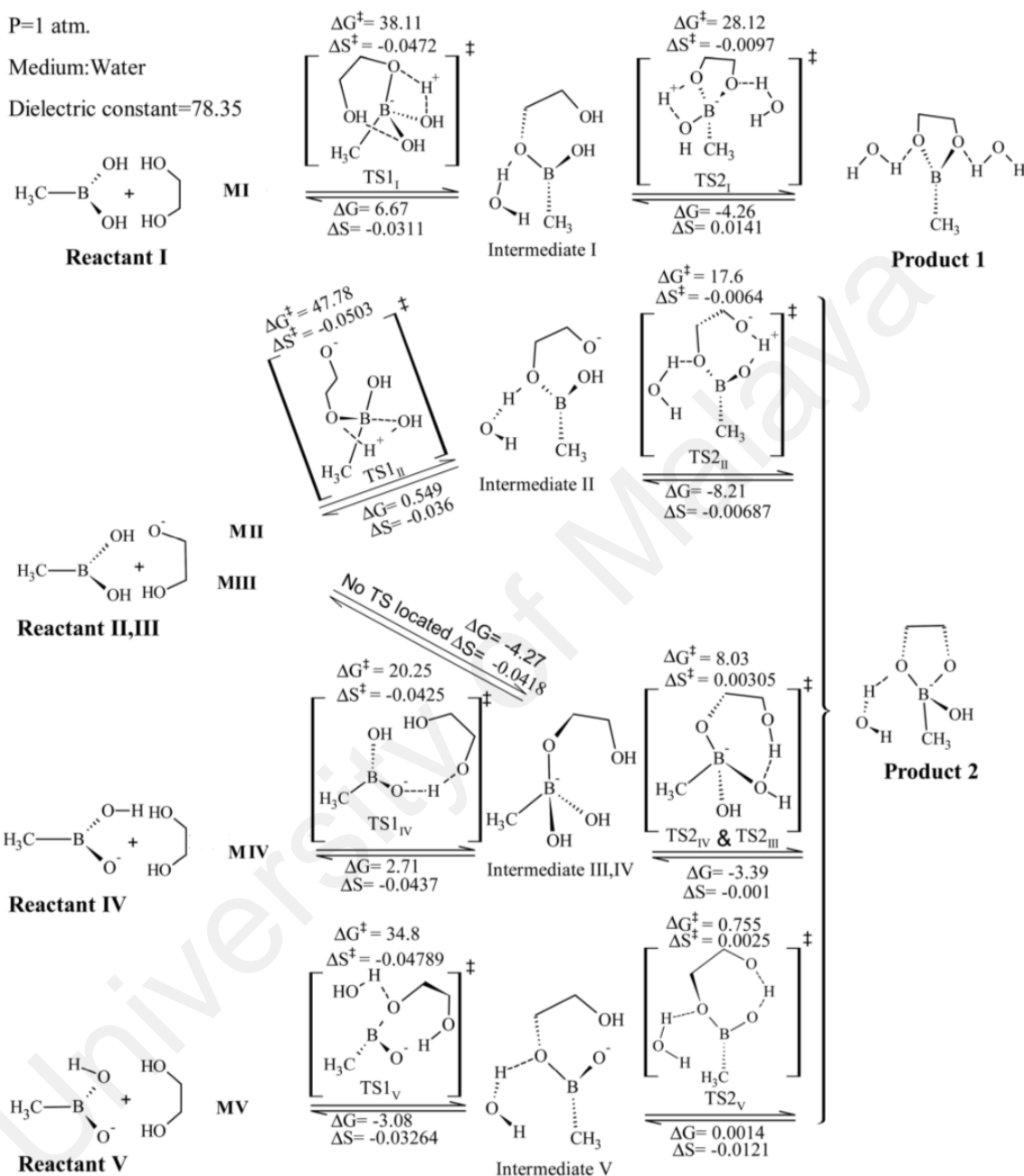
The overall low reaction rate in MII makes its occurrence very unlikely, even though the chelate ring closure occurs quite fast. This agrees well with the lower reactivity of  $\text{HL}^-$  compared to that for  $\text{H}_2\text{L}$  ( $\text{H}_2\text{L}$  being the bidentate ligand) towards boronic acid which was highlighted in the study of Watanabe et al. (2013).

T=298.15 K

P=1 atm.

Medium: Water

Dielectric constant=78.35



\* The units for the free energies and entropies are in kcal/mol and kcal/molK respectively.

\*\* Only mechanism I results in product 1 and mechanisms II, III, IV and V will result in product 2.

**Scheme 4.2: Five stepwise reaction mechanisms for methylboronic acid in interaction with 1,2-ethanediol.**

Additional to this are a few other experimental studies where reduced reactivity of boronic acid was observed upon deprotonation of the ligand (Ishihara et al., 1991; Ito et al., 2002). Ishihara for instance, reported a reduced reaction rate by the factor of  $10^4$ -fold for 4-isopropyltropolone (Hipt) compared to chromotropic acid ( $H_2cht$ ) as ligand. Ito et al. (2003) had also reported a decrease in the reactivity of boronic acid upon deprotonation of  $H_2ipt^+$  to Hipt and  $ipt^-$ . Both their proposed mechanisms however resulted in formation of tetrahedral boronate ion and elimination of a  $H_3O^+$  which is different from MI in our study. Their study was carried out in alkaline solution where boronic acid predominantly exists in its basic form. This would make it more reactive with fully protonated diols.

Another possible reaction mechanism for a deprotonated ligand to react with boronic acid is MIII. In this mechanism, the first step goes through no activation barrier and the reaction occurs with a relatively high rate following the formation of a tetrahedral intermediate. So the rate determining step in this mechanism is the second step since the first step occurs spontaneously.

In fact, the rate of chelate ring closure in the second step of this mechanism is rather high compared to the other mechanisms. This requires further investigation since it can lead towards a better understanding of the reactive form of boronic acid, i.e. either tetrahedral boronate ion or trigonal boronic acid.

This reaction mechanism can provide an explanation for the idea pointed out by Pizer & Tihal stating that trigonal boronic acid would be unreactive if the ligand lacks an acidic proton (Pizer & Tihal, 1992; Pizer & Tihal, 1996). The only way this could happen is if a trigonal intermediate is formed through which, a water molecule is eliminated by a

hydroxide from central boron and a proton from the ligand (MII). Otherwise, one proton transfer from the ligand would suffice for the whole chelation reaction to occur after the direct reaction of negative oxygen of the ligand with boron to form a tetrahedral intermediate. This is only when the starting material is in trigonal form (MIII).

For ligands having no acidic proton, formation of an unchelated tetrahedral intermediate results in an increase in coordination number of boron from 3 ( $sp^2$ ) to 4 ( $sp^3$ ) where the negative boronate ion has a low first energy of ionization. The oxygen attached to boron which is electronegative also makes the B-O bond less stable than that for trigonal boronic acid due to its relative polarity. As a result, an acidic environment could facilitate the formation of chelate ring due to a good leaving hydroxyl group. Lacking one acidic proton does not reduce the reactivity of boronic acid, but it makes it even more efficient.

The MIV and MV represent the reaction in alkaline medium where the dominant species of boronic acid is in trigonal form. MIV step 1 is somehow similar to MV step 2 in terms of the protonation of the basic oxygen of boronate ion from the ligand's OH group. The rates however, significantly differ between these two mechanisms since the former yields a tetrahedral cyclic boronate ester and the latter yields a Lewis basic tetrahedral intermediate.

The lower stability of trigonal boronic acid and its tendency in forming a tetrahedral base shows that the conjugate basic form of boronic acid is in the form of tetrahedral boronate ion. The overall high reaction rates for these mechanisms indicates the importance of fully protonated ligand for increasing the reactivity of boronate ions.

#### 4.2.2. Kinetic study of CF<sub>3</sub>-B(OH)<sub>2</sub> and CF<sub>3</sub>-BOOH in reaction with diol

This section presents the results for the reaction of CF<sub>3</sub>-B(OH)<sub>2</sub> with diol based on the mechanisms presented in Scheme 4.3. The mechanisms are identical with those in previous section, but the significant difference in the electronegativity of the R-group results in different reaction rates altogether. Table 4.6 illustrates the reaction rates for all proposed mechanisms.

**Table 4.6: The thermodynamic data of the five mechanisms between CF<sub>3</sub>-B(OH)<sub>2</sub> and 1,2-ethanediol.**

Mechanism/ CF <sub>3</sub> B(OH) <sub>2</sub>	Step of reaction	$\Delta G$ (kcalmol <sup>-1</sup> )	$\Delta S$ (kcalmol <sup>-1</sup> K <sup>-1</sup> )	$\Delta G^\ddagger$ (kcalmol <sup>-1</sup> )	$\Delta S^\ddagger$ (kcalmol <sup>-1</sup> K <sup>-1</sup> )	$k$ (s <sup>-1</sup> )
MI/neutral	Step 1	4.890	-0.030	29.091	-0.047	4.4×10 <sup>-9</sup>
	Step 2	0.411	0.016	26.862	-0.015	1.9×10 <sup>-7</sup>
	Overall	5.301	-0.014	-	-	<b>4.4×10<sup>-9</sup></b>
MII/acidic	Step 1	-4.780	-0.035	32.161	-0.039	2.5×10 <sup>-11</sup>
	Step 2	-24.160	0.001	9.601	-0.003	0.9×10 <sup>6</sup>
	Overall	-28.940	-0.040	-	-	<b>2.5×10<sup>-11</sup></b>
MIII/acidic & basic	Step 1	-25.601	-0.037	-	-	-
	Step 2	-3.330	-0.003	26.640	-0.009	2.8×10 <sup>-7</sup>
	Overall	-28.940	-0.040	-	-	<b>2.8×10<sup>-7</sup></b>
MIV/basic	Step 1	-5.630	-0.035	24.141	-0.037	1.9×10 <sup>-5</sup>
	Step 2	-3.330	-0.003	26.640	-0.009	2.8×10 <sup>-7</sup>
	Overall	-8.960	-0.038	-	-	<b>2.8×10<sup>-7</sup></b>
MV/basic	Step 1	4.230	-0.024	36.120	-0.042	3.1×10 <sup>-14</sup>
	Step 2	-15.010	-0.007	19.460	-0.011	5.2×10 <sup>-2</sup>
	Overall	-10.780	-0.032	-	-	<b>3.1×10<sup>-14</sup></b>

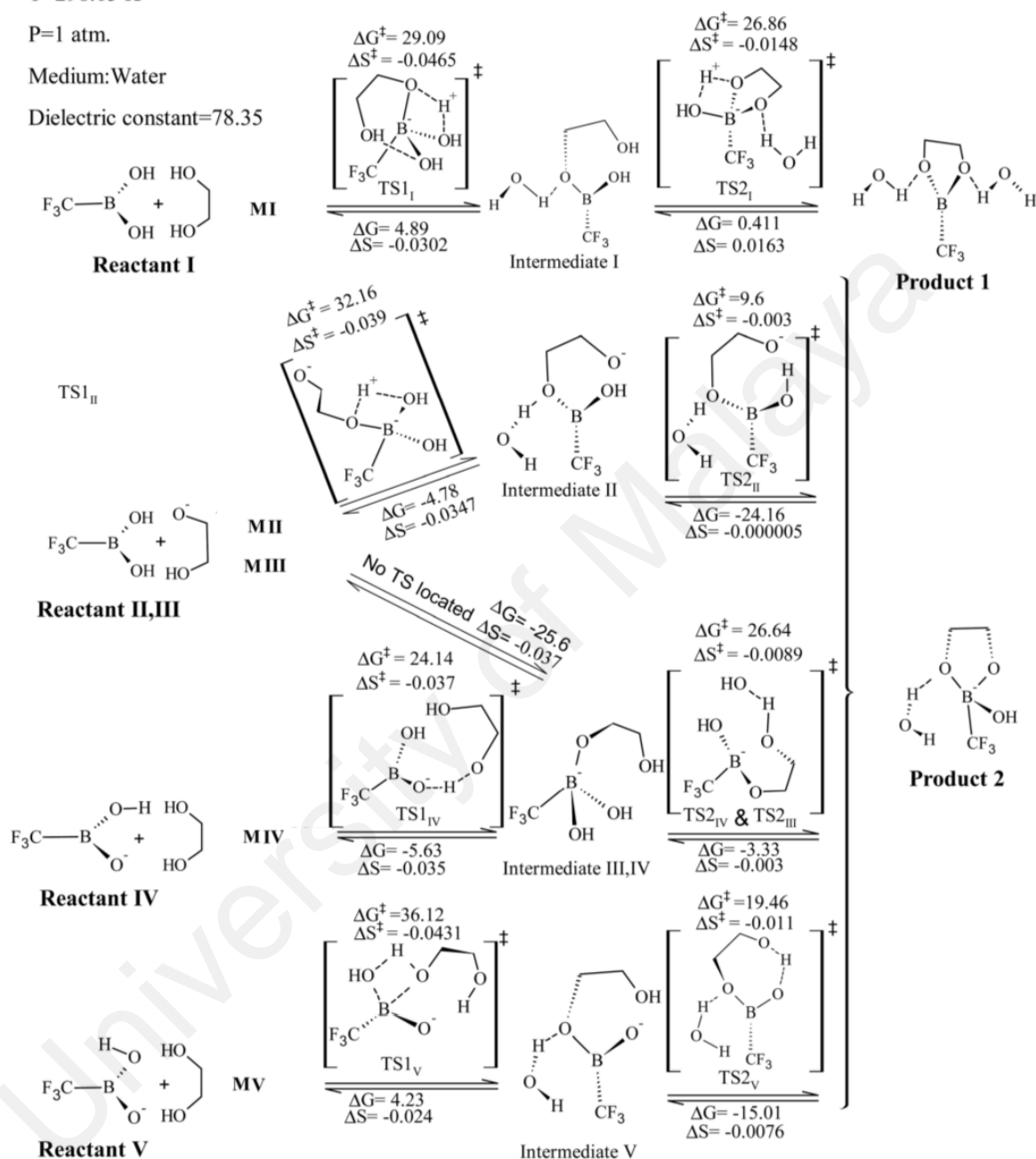
The high electronegative R-group attached to boron enhances the reaction rate by a factor of 10<sup>6</sup>-fold and 10-fold in the first and second steps of MI respectively. These two R-groups however, share an identical transition structures with similar activation entropies in the rate determining step. On the other hand, step 2 of MI in the two R-groups have different transition structures where the activation entropy is slightly higher. This explains the lower activation barrier and higher reaction rate for this mechanism.

T=298.15 K

P=1 atm.

Medium: Water

Dielectric constant=78.35



\* The units for the free energies and entropies are in kcal/mol and kcal/molK respectively.

\*\* Only mechanism I results in product 1 and mechanisms II, III, IV and V will result in product 2.

**Scheme 4.3: Five different reaction mechanisms for trifluoromethylboronic acid in interaction with 1,2-ethanediol.**

The reaction rate for the higher electronegative R-group is also observed in MII, even though the diol lacks an acidic proton. The electronegativity of the R-group results in a slight increase in boron's acidity and electrophilicity which results in increasing its tendency to react with the nucleophilic oxygen of diol. This effect is more precisely observed in the second step of MII where the chelate ring closure does not occur by the deprotonation of the diol.

The MIII in this section occurs at a very low rate compared to that of  $\text{CH}_3\text{-B(OH)}_2$ . The tetrahedral intermediate in general is in a lewis basic form which makes boron a high effective electron donor. The high electronegative R-group lowers this basicity and causes a less effective electron donating boron. This would decrease the rate of reaction by a factor of  $10^{14}$ -fold compared to that of  $\text{CH}_3\text{-B(OH)}_2$ .

Similar behaviour is also observed in the Brønsted basic form of boronic acid. The high electronegativity of  $-\text{CF}_3$  R-group reduces boron's basicity and results in a  $10^3$ -fold and 10-fold reduction in the reaction rate of step 1 in MIV and MV respectively. MIII and MIV are similar in the second step, though this step is rate determining for MIV with  $-\text{CF}_3$  R-group but not the case for the  $-\text{CH}_3$  R-group.

The reaction rate in MV is also lower with a higher electronegativity of the R-group in comparison to that of  $-\text{CH}_3$  R-group. The  $\text{TS-2}_v$  is rather stable for the  $-\text{CH}_3$  R-group due to a simple proton transfer between the basic oxygen of boron and the ligand, but it requires a rather high activation energy with  $-\text{CF}_3$  R-group to proceed with the formation of the final product. It is in fact the high electronegativity of the R-group which destabilizes the transition structure and affects the reaction rate.

These results are consistent with the experimental studies. In the study carried out by Watanabe et al., (2013) for instance, the two different electronegative R-groups i.e. 3-fluorophenylboronic acid (3-FPhB(OH)<sub>2</sub>) and 3-pyridylboronic acid (3-pyB(OH)<sub>2</sub>) were used with the former being more electronegative. They observed 10<sup>4</sup>-fold reduction in the rate of reaction for the tetrahedral 3-fluorophenylboronate ion compared to 3-pyridylboronate ion. These observations indicate the importance of the type of the R-group in affecting the reactive behaviour of boronic acid towards diols. The details of these differences are elaborated in the next section.

#### 4.2.3. Comparing the reactivity of CH<sub>3</sub>-B(OH)<sub>2</sub> and CF<sub>3</sub>-B(OH)<sub>2</sub>

Two different electronegative R-groups can affect the reactivity of boronic acid in different ways. The reactivity of the lewis acidic form of boronic acid for instance, is increased with the higher electronegative R-group (Scheme 4.3, MI and MII), but is decreased with the lower electronegative R-group (Scheme 4.2, MI and MII).

The MIII on the other hand is more favourable with an electropositive R-group compared to that of the electronegative R-group. The nucleophilic attack from the negatively charged oxygen of the incoming diol with boron in MIII yields a tetrahedral intermediate with a lewis basic characteristic. The chelate ring closure in this mechanism is similar to MI step 2 (TS2<sub>1</sub>) which involves the elimination of one water molecule. The rate in this step, the second step, is 10<sup>14</sup>-fold higher for CH<sub>3</sub>-B(OH)<sub>2</sub> compared to CF<sub>3</sub>-B(OH)<sub>2</sub>. This large difference is due to the higher electronegativity of -CF<sub>3</sub> which results in a higher activation barrier through the lower lewis basicity of boronate ion. The enhanced electrophilicity of boron also results in a poorer OH leaving group which is due to the stronger B-O bond.

MIV and MV involve the Brønsted boronate ion as the starting material (Schemes 4.2 and 4.3). The highly electronegative  $-CF_3$  R-group reduces the basicity of boronate ion and as a result, the nucleophilicity of the basic oxygen on boronic acid. This effect causes a delay in proton transfer of the incoming diol to boronic acid's leaving group. The difference can be seen in the activation barrier of  $TS1_{IV}$ ,  $TS2_{III&IV}$ ,  $TS1_V$  and  $TS2_V$ .

The  $TS1_V$  goes through a similar mechanism as  $TS1_I$ . The second step of MV is similar to the first step of MIV, involving a proton transfer from the hydroxyl of the diol to the Brønsted basic oxygen of the boronate ion. This results in a negatively charged oxygen in diol which is now highly reactive towards boron to form a lewis form of tetrahedral boronate ion. This reactivity is increased with a lower electronegative R-group which can be clearly observed in the lower activation barrier in MV with  $-CH_3$  R-group compared to that of  $-CF_3$  R-group (Scheme 4.2).

The comparison between the reactivity of boronic acid and boronate ion with different diols in this study made it quite clear that boronate ion always has lewis characteristic in forming the cyclic boronate ester which is regardless of the properties of the incoming ligand. For lewis base, a water molecule is eliminated and a tetrahedral cyclic boronate ester is formed whereas for Brønsted base, a lewis acid is initially formed by accepting a proton from the ligand. The negatively charged oxygen on the ligand would then form a tetrahedral intermediate with electrophilic boron on boronic acid, ultimately leading towards forming a cyclic boronate ester.

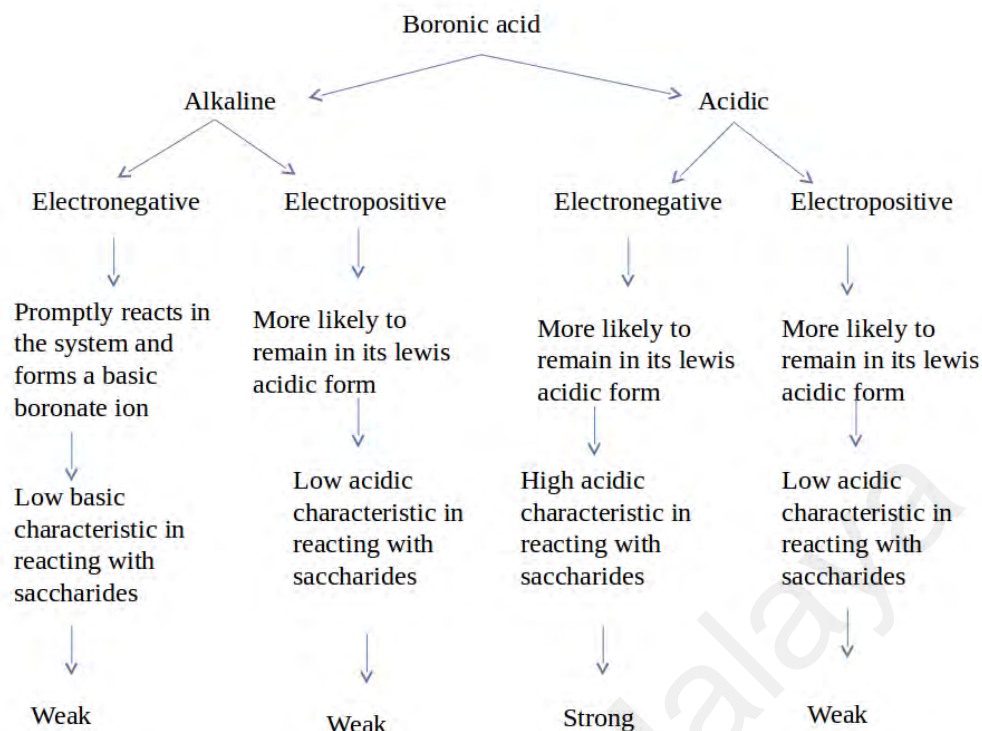
On the other hand, the trigonal boronic acid is more reactive towards bifunctional ligands lacking an acidic proton due to the empty p orbital on boron. The nucleophilic

oxygen of the ligand would then attack the electrophilic boron and form a tetrahedral intermediate without any leaving OH. With the proton transfer from the ligand to the leaving OH the final product is then formed in the form of tetrahedral boronate ion with elimination of one water molecule.

#### **4.2.4. The R-group which results in a better sensor**

The high reactivity of boronic acid in both acidic and basic forms has been evidently observed in this study. Their reactivity depends on the effect of different R-groups on boron as well as the medium in which the boronic acid functions. Based on the results of this study, an electronegative R-group increases the reactivity of boronic acids while decreasing the reactivity of the boronate ion. However, a weak sensor can be resulted by having boronic acid sensors in alkaline medium with electronegative R-group (Scheme 4.4). That is, upon reacting with the bases in the environment, an electrophilic boron can promptly form a tetrahedral boronate ion. The electronegative R-group further decreases the basicity of the newly formed boronate ion base and as a result, its reactivity would also decrease. To have a good sensor, one must use a tetrahedral boronate ion attached to a lower electronegative R-group in alkaline medium since boron's basic characteristic and as a result, its reactivity is enhanced.

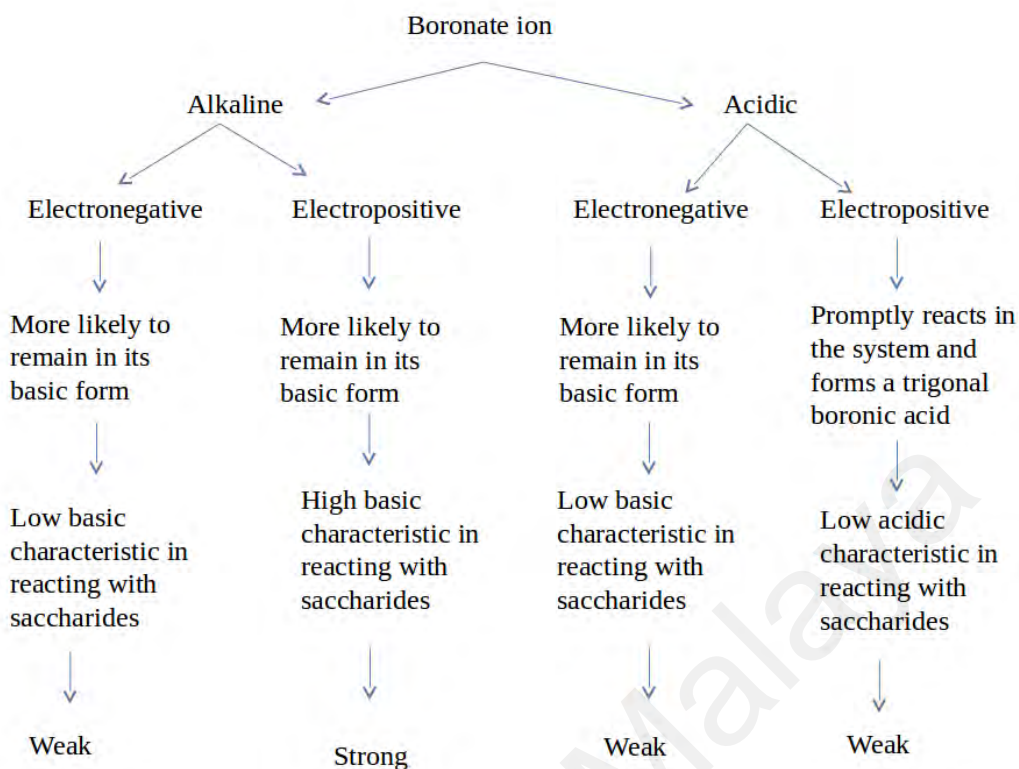
The same argument applies to boronate ions attached to an electropositive R-group in acidic environment (Scheme 4.5). To have a good sensor in acidic environment, one must use a trigonal boronic acid attached to an electronegative R-group in acidic medium. This concludes that boronic acids attached to high electronegative R-groups are more reactive in acidic medium whereas boronate ions attached to high electropositive R-groups are more reactive in alkaline medium.



**Scheme 4.4: Different possibilities of the reactivity of boronic acid with diols in different medium and different electronegative R-groups.**

Since the sensors function better in alkaline media, this study suggests that using a lower electronegative R-group and even an electropositive one attached to a basic boronate ion increases the sensor's reactivity towards diols. Furthermore, from the comparison of different reaction mechanisms and rates of reaction, one can conclude that the boronate ion is more stable in the form of lewis base in alkaline medium and therefore, it predominantly exists in tetrahedral form rather than trigonal form.

In this section, the effect of electronegative R-group on the reactivity of boronic acid was investigated. The conclusion is drawn based on the assumption that the reaction dynamics follows the classical laws of motion. However, when one talks about proton transfer reactions one must also consider the possibility of tunnelling. It would be even better if one can induce tunnelling by controlling external factors such as the type of R-group. We are trying to address this issue in the next section.



**Scheme 4.5: Different possibilities of the reactivity of boronate ion with diols in different mediums and different electronegative R-groups.**

#### 4.2.5. Tunnelling effect in proton transfer reaction of boronic acid with diol

The reaction of boronic acid with diol is dominated by proton transfer which would make the study of proton tunnelling important. The tunnelling corrections have been calculated for each one of the mechanisms with similar methods as mentioned in Section 4.1.4. These values are illustrated in Table 4.7 for methylboronic acid and Table 4.8 for trifluoromethylboronic acid.

The first two mechanisms in Table 4.7 which involve trigonal neutral boronic acid, as well as the first step of MV indicate the highest tunnelling contributions for both  $-\text{CH}_3$  and  $-\text{CF}_3$  R-groups. Almost all mechanisms with  $-\text{CF}_3$  R-group experience higher tunnelling contribution compared to the less electronegative  $-\text{CH}_3$  R-group. The only

difference is that the rate determining step in MI which is CF<sub>3</sub>-I-I has a larger tunnelling contribution compared to CF<sub>3</sub>-I-II. This is exactly the opposite for MI involving the -CH<sub>3</sub> R-group (Tables 4.8 & 4.9). In addition, mechanism CF<sub>3</sub>-I-I is also classically more favourable than the CH<sub>3</sub>-I-I. The higher electronegativity of the -CF<sub>3</sub> R-group can explain the classical rate enhancement as elaborated in Section 4.2.3.

Not all of the rates of these mechanisms are affected by tunnelling since the energy barrier is rather high to be affected by the tunnelling correction. Furthermore, those mechanisms with low energy barrier which are classically favourable are also not affected by tunnelling due to the small or lack of tunnelling coefficient.

Among all, the only mechanism with a reasonable barrier height as well as barrier width relative to other mechanisms, is MI. We therefore selected this mechanism to further investigate the tunnelling effect. Since the rate determining step is the first step, the tunnelling behaviour is calculated mainly for this step. Two factors are taken as variable in this calculation, the temperature and the R-group electronegativity.

The temperature dependant reaction rate is calculated over the temperature range of 53.15 K to 308.15 K. Additional to -CH<sub>3</sub> and -CF<sub>3</sub> which are the two extremes in terms of electronegativity, the same types of calculations have been carried out for the -CCl<sub>3</sub>, -CBr<sub>3</sub> and -CI<sub>3</sub> R-groups with electronegativities in between -CF<sub>3</sub> and -CH<sub>3</sub>. By substituting the transferring proton with the heavier isotope, deuterium, we have performed the kinetic isotope effect study for each of these reactions.

**Table 4.7: The tunnelling correction ( $\Gamma$ ), width parameter ( $\ell$ ) and tunnelling rate for reaction of  $\text{CH}_3\text{B}(\text{OH})_2$  with 1,2-ethanediol.**

Mechanism	$\Delta G^\ddagger$ (kcal/mol)	$k$ classical ( $\text{s}^{-1}$ )	$E_0$ (kcal/mol)	$\ell$ (Å)	$\sigma$ ( $\text{cm}^{-1}$ )	$\Gamma$			$k_{Q\text{-tunnelling}}$ ( $\text{s}^{-1}$ )		
						(Wigner)	(Shavitt)	(Numerical)	(Wigner)	(Shavitt)	(Numerical)
CH <sub>3</sub> -I-I	38.110	1.08E-15	23.65	1.98	1181.26	2.35	2.35	6.20	2.54E-15	2.54E-15	6.69E-15
CH <sub>3</sub> -I-II	28.123	2.30E-08	26.50	1.81	1364.37	2.81	2.81	16.37	6.45E-08	6.45E-08	3.77E-07
CH <sub>3</sub> -II-I	47.785	8.57E-23	33.95	2.04	1376.39	2.84	2.84	21.38	2.43E-22	2.43E-22	1.83E-21
CH <sub>3</sub> -II-II	17.625	1.16	16.18	5.87	329.57	1.11	1.11	1.12	1.29	1.29	1.30
CH <sub>3</sub> -III-I	-	-	-	-	-	-	-	-	-	-	-
CH <sub>3</sub> -III-II	8.035	1.27E+07	8.89	63.80	22.46	1.00	1.00	1.00	1.27E+07	1.27E+07	1.27E+07
CH <sub>3</sub> -IV-I	20.254	1.37E-02	8.19	7.28	188.957	1.03	1.03	1.04	1.42E-02	1.42E-02	1.42E-02
CH <sub>3</sub> -IV-II	8.035	1.27E+07	8.89	63.80	22.46	1.00	1.00	1.00	1.27E+07	1.27E+07	1.27E+07
CH <sub>3</sub> -V-I	34.819	2.81E-13	21.50	2.10	1063.01	2.10	2.10	3.97	5.88E-13	5.88E-13	1.11E-12
CH <sub>3</sub> -V-II	0.755	2.79E+12	0.07	10.60	12.19	1.00	1.00	1.00	2.79E+12	2.79E+12	2.79E+12

**Table 4.8: The tunnelling correction ( $\Gamma$ ), width parameter ( $\ell$ ) and tunnelling rate for reaction of  $\text{CF}_3\text{B}(\text{OH})_2$  with 1,2-ethanediol.**

Mechanism	$\Delta G^\ddagger$ (kcal/mol)	$k$ classical ( $\text{s}^{-1}$ )	$E_0$ (kcal/mol)	$\ell$ (Å)	$\sigma$ ( $\text{cm}^{-1}$ )	$\Gamma$			$k_{Q\text{-tunnelling}}$ ( $\text{s}^{-1}$ )		
						(Wigner)	(Shavitt)	(Numerical)	(Wigner)	(Shavitt)	(Numerical)
CF <sub>3</sub> -I-I	29.091	4.48E-09	28.48	1.94	1319.60	2.64	2.64	11.80	1.18E-08	1.184E-08	5.29E-08
CF <sub>3</sub> -I-II	26.862	1.94E-07	11.70	1.43	1152.53	2.29	2.29	4.74	4.43E-07	4.43E-07	9.18E-07
CF <sub>3</sub> -II-I	32.161	2.5E-11	30.56	1.88	1415.68	2.94	2.94	26.01	7.37E-11	7.37E-11	6.51E-10
CF <sub>3</sub> -II-II	9.601	9E+05	9.081	4.71	307.42	1.09	1.09	1.10	9.83E+05	9.83E+05	9.93E+05
CF <sub>3</sub> -III-I	-	-	-	-	-	-	-	-	-	-	-
CF <sub>3</sub> -III-II	26.640	2.82E-07	24.96	8.26	290.73	1.08	1.08	1.09	3.05E-07	3.05E-07	3.07E-07
CF <sub>3</sub> -IV-I	24.141	1.92E-05	13.02	6.48	267.77	1.07	1.07	1.08	2.06E-05	2.06E-05	2.07E-05
CF <sub>3</sub> -IV-II	26.640	2.82E-07	24.96	8.26	290.73	1.08	1.08	1.09	3.05E-07	3.05E-07	3.07E-07
CF <sub>3</sub> -V-I	36.120	3.11E-14	20.99	1.76	1253.25	2.52	2.52	8.14	7.86E-14	7.86E-14	2.53E-13
CF <sub>3</sub> -V-II	19.460	5.23E-02	31.35	8.78	306.48	1.09	1.09	1.10	5.71E-02	5.71E-02	5.75E-02

The Arrhenius plots are shown in Figure 4.8 for five different R-groups. The curved lines indicate the tunnelling corrected rate which is calculated using the numerical algorithm for proton and deuterium transfer reactions respectively. The straight lines indicate the linear descent of the log of classical reaction rates as well as the tunnelling corrected reaction rates (calculated using Wigner's and Shavitt's approaches), all of which follow the Arrhenius law.

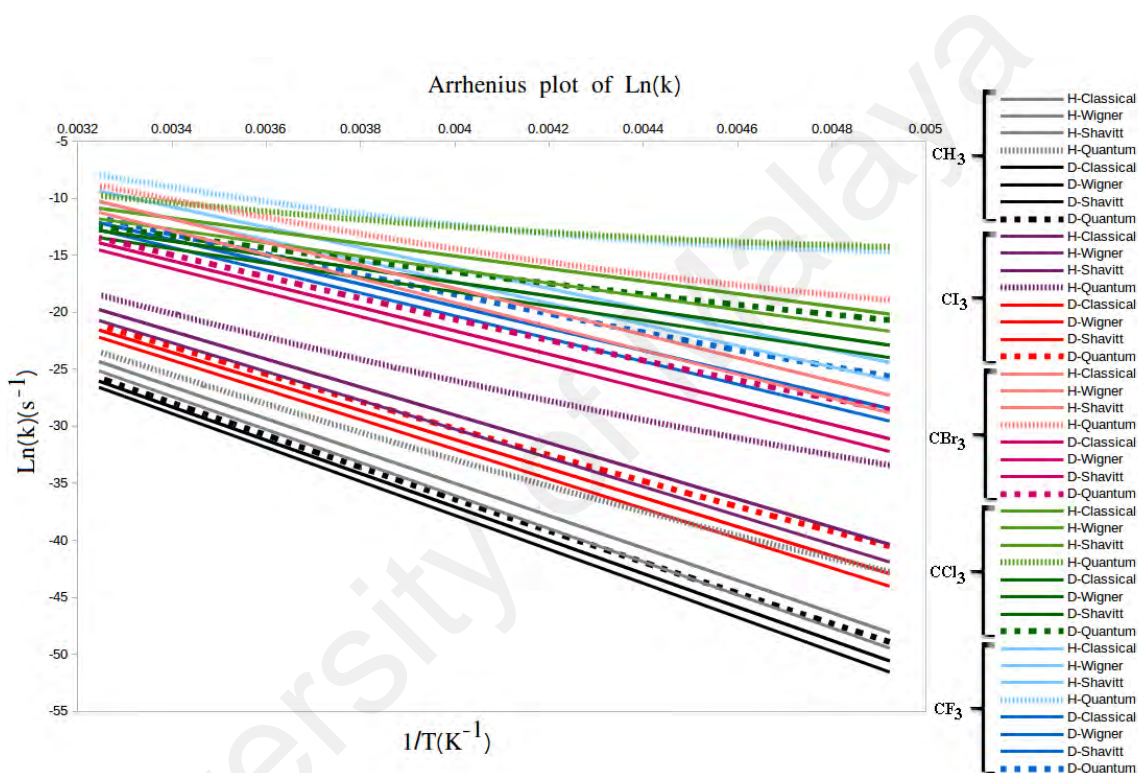


**Figure 4.8: The Arrhenius plot of reaction rate for the proton and deuterium transfer reaction of  $\text{CH}_3\text{-B}(\text{OH})_2$ ,  $\text{Cl}_3\text{-B}(\text{OH})_2$ ,  $\text{CBr}_3\text{-B}(\text{OH})_2$ ,  $\text{CCl}_3\text{-B}(\text{OH})_2$ , and  $\text{CF}_3\text{-B}(\text{OH})_2$  with diol from 203.15 K to 308.15 K.**

The analytical approaches of Wigner and Shavitt in this system (similar to those in Section 4.1.4) also show classical linear behaviour in the plot. The numerical approach however, shows quantum behaviour with a significant deviation from linear descent as the electronegativity of the R-groups increases. Hence, it is a good approach for studying the tunnelling phenomenon in this reaction and our discussion in this section would be based on the numerical plot.

The best quantum behaviour is observed for the  $-\text{CF}_3$  R-group where the deviation from classical linear behaviour is more significant compared to the other R-groups. The same tunnelling behaviour is also observed in deuterium transfer reaction, but it deviates at lower temperature compared to proton. As the electronegativity of the R-group decreases, the deviation also decreases where in the  $-\text{CH}_3$  R-group, the plot is slightly deviated starting at the low temperature of around 263.15 K.

There is one peculiarity which can be clearly observed in this plot and that is the change in the tunnelling behaviour in two different temperature ranges. The low temperature range shows a slightly higher tunnelling behaviour for the  $-\text{CCl}_3$  R-group (green dashed line) than  $-\text{CF}_3$  R-group (blue dashed line) due to a slightly higher rate. However, the high temperature range shows otherwise.

Before the deviation from linear descent, the  $-\text{CF}_3$  R-group has a higher rate and appears higher on the plot than the  $-\text{CCl}_3$  R-group. The reason for this sudden change can be attributed to the sensitivity of the high electronegativity to the temperature change. In other words, as the electronegativity decreases, the sensitivity to the temperature change also decreases. Hence, at a certain temperature, the rate of change in the plot of  $-\text{CF}_3$  R-group is enhanced and results in that difference whereas the plots for the other R-groups are closer to linear with less curvature.

To have a better view of the plot at high temperature range, we zoom in at the range from 253.15 K to 308.15 K (Figure 4.9). This temperature range is of particular importance in this study since we are modelling a sensor which should function in biological environment and high temperature.

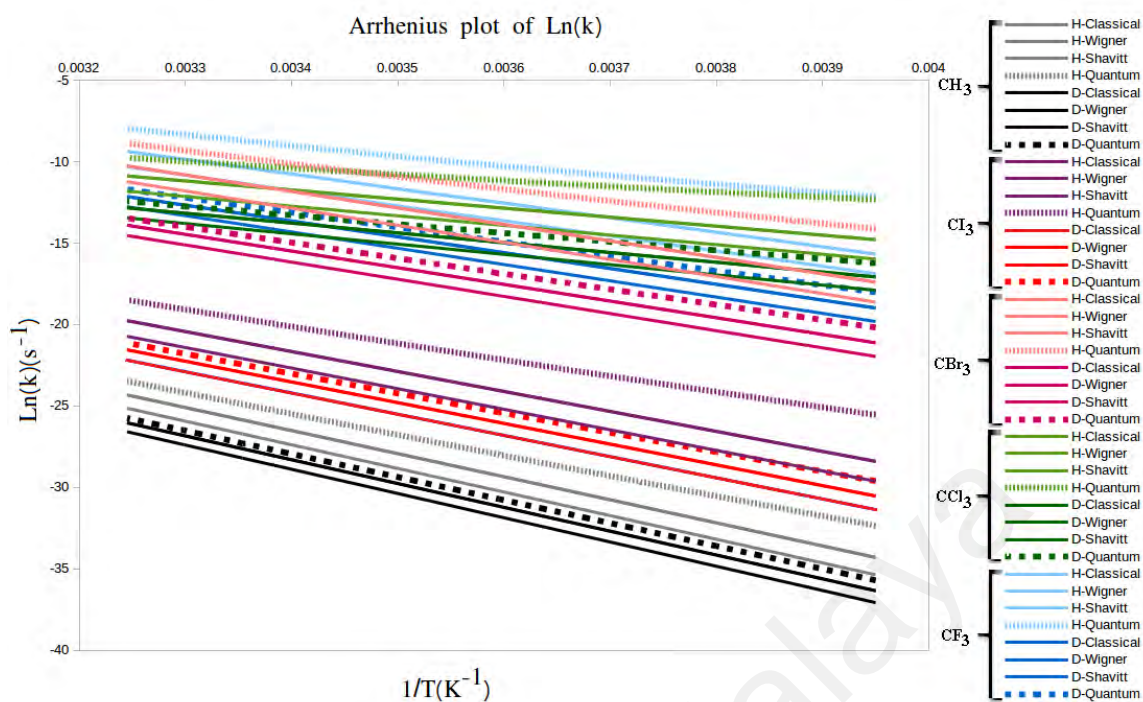


**Figure 4.9:** The Arrhenius plot of reaction rate for the proton and deuterium transfer reaction of  $\text{CH}_3\text{-B}(\text{OH})_2$ ,  $\text{Cl}_3\text{-B}(\text{OH})_2$ ,  $\text{CBr}_3\text{-B}(\text{OH})_2$ ,  $\text{CCl}_3\text{-B}(\text{OH})_2$ , and  $\text{CF}_3\text{-B}(\text{OH})_2$  with diol from 253.15 K to 308.15 K.

Due to the short range, no significant curvature is observed at low electronegativity. However, as the electronegativity of the R-group increases, the divergence from linear descent becomes more apparent and a slight curvature appears in the  $-\text{CF}_3$  R-group. The tunnelling for proton would also become more significant compared to deuterium which is observed from the increase in KIE. The plot of KIE in Figure 4.10 indicates the hyper-exponential growth of the ratio between  $k_{\text{H}}$  over  $k_{\text{D}}$ . The increase in the discrepancy between H and D as the electronegativity increases can be clearly observed with the  $-\text{CCl}_3$  and  $-\text{CF}_3$  having the largest ones (Figure 4.10).

The tangent line of the inflection point at which  $Y=0$  is plotted for each R-group. As it had been mentioned earlier in Section 4.1.4 (Equation 4.9), at this point the tunnelling behaviour begins due to the exponential behaviour of the function. The increase in the slope of numerical plot can be seen at higher electronegative R-groups which implies

increase in KIE. In the high temperature range the intercept of the tangent line ( $\gamma$ ) is negative at any point of the graph, similar to what we observed in Section 4.1.4.

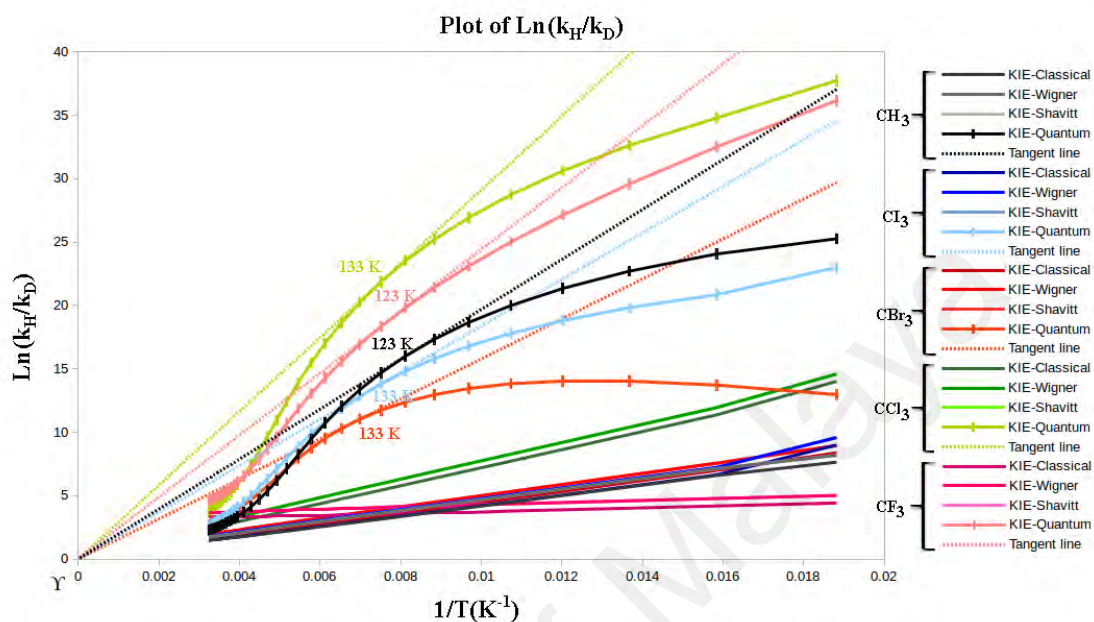


**Figure 4.10:** The plot of kinetic isotope effect for the proton and deuterium transfer reaction of  $\text{CH}_3\text{-B(OH)}_2$ ,  $\text{Cl}_3\text{-B(OH)}_2$ ,  $\text{CBr}_3\text{-B(OH)}_2$ ,  $\text{CCl}_3\text{-B(OH)}_2$ , and  $\text{CF}_3\text{-B(OH)}_2$  with diol from 53.15 K to 308.15 K.

At low electronegativity for  $-\text{CH}_3$  and  $-\text{Cl}_3$  R-groups, the change in  $\gamma$  is lower with respect to increase in temperature. As the electronegativity of the R-group increases, much larger change is observed in  $\gamma$  where it tends to move towards zero with a higher rate. This indicates a higher ratio of  $\Gamma_{\text{H}}/\Gamma_{\text{D}}$  (the  $\ln(\Gamma_{\text{H}}/\Gamma_{\text{D}})$  is increased). Observing Figure 4.8, we can conclude that this higher ratio is due to the significance of proton tunnelling.

Similar to Figure 4.8, different tunnelling behaviour between the high and low temperature range is also observed in Figure 4.10. It can be clearly seen in this figure that the increase in KIE is completely independent of the order of electronegativity of the R-group at low temperature range. However, as the plot moves towards higher

temperature after the inflection point, the increment of the KIE becomes consistent with the increment of the electronegativity (Figure 4.11).

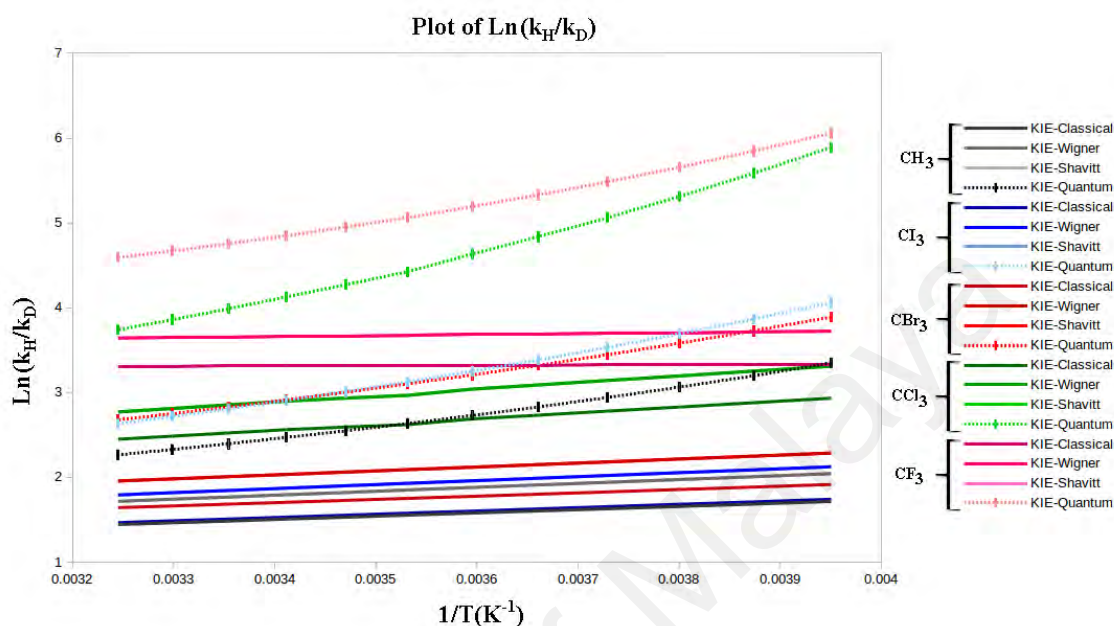


**Figure 4.11:** The plot of the kinetic isotope effect for proton and deuterium transfer reactions of  $\text{CH}_3\text{-B(OH)}_2$ ,  $\text{CI}_3\text{-B(OH)}_2$ ,  $\text{CBr}_3\text{-B(OH)}_2$ ,  $\text{CCl}_3\text{-B(OH)}_2$ , and  $\text{CF}_3\text{-B(OH)}_2$  with diol from 253.15 K to 308.15 K.

The difference in tunnelling behaviour between low and high temperature range is rather obvious. In the former (Figure 4.10) the KIE is the largest for  $-\text{CCl}_3$  R-group and decreases in the following order:  $-\text{CCl}_3 > -\text{CF}_3 > -\text{CH}_3 > -\text{CI}_3 > -\text{CBr}_3$ . This order does not follow the change in the electronegativity, nor does it follow the van der Waals radius of the R-group. In the higher temperature range on the other hand, the increase in the KIE is consistent with the increase in the electronegativity of the R-group. The occurrence of this predictability at higher temperature range makes it in our favour since we are mainly interested in reactions at biological temperatures.

The trend where the increase in the electronegativity of the R-group results in a better tunnelling behaviour is not seen in the width parameter. There is no significant difference between the calculated values of  $\ell$  for  $-\text{CH}_3$  and  $-\text{CF}_3$  R-groups as observed in

Tables 4.7 and 4.8 respectively. Furthermore, the calculated values of  $\ell$  for other three R-groups also does not show any particular trend (Table 4.9).

**Table 4.9: The calculated barrier width for the energy barrier of mechanism M-I-I for all five R-groups.**

R-group	$E_0$ (kcal/mol)	$\sigma$ (cm <sup>-1</sup> )	$\ell$ (Å)
-CH <sub>3</sub>	23.65	1181.28	1.98
-Cl <sub>3</sub>	21.65	1331.40	1.68
-CBr <sub>3</sub>	21.28	1339.68	1.66
-CCl <sub>3</sub>	21.08	1301.30	1.70
-CF <sub>3</sub>	28.48	1319.60	1.94

The fact that the width parameter is independent of temperature and that there is no proper trend observed between different electronegativity and barrier width is a clear indication of high sensitivity of the tunnelling to the temperature. This is specially so at higher temperatures where the tunnelling behaviour differs from that in lower temperatures. Based on these results, we can conclude that the best R-group for inducing tunnelling at higher temperature is the one with the highest electronegativity.

#### 4.2.6. The R-group which results in a better tunnelling

As argued in Section 4.2.4, boronate ion with low electronegative R-group has higher reactivity in alkaline environment and overall, the -CH<sub>3</sub> R-group performed better in terms of reaction rate. However, a higher tunnelling contribution was observed for the reaction with boronic acid rather than boronate ion. This made us to further investigate the tunnelling effect on the reaction for the first step of MI. Adding more R-group variation to the calculations results in a more detailed and thorough comparison. Thus,

we added three more R-groups with electronegativities between those of  $-\text{CH}_3$  and  $-\text{CF}_3$  to the calculations (Figure 4.12).

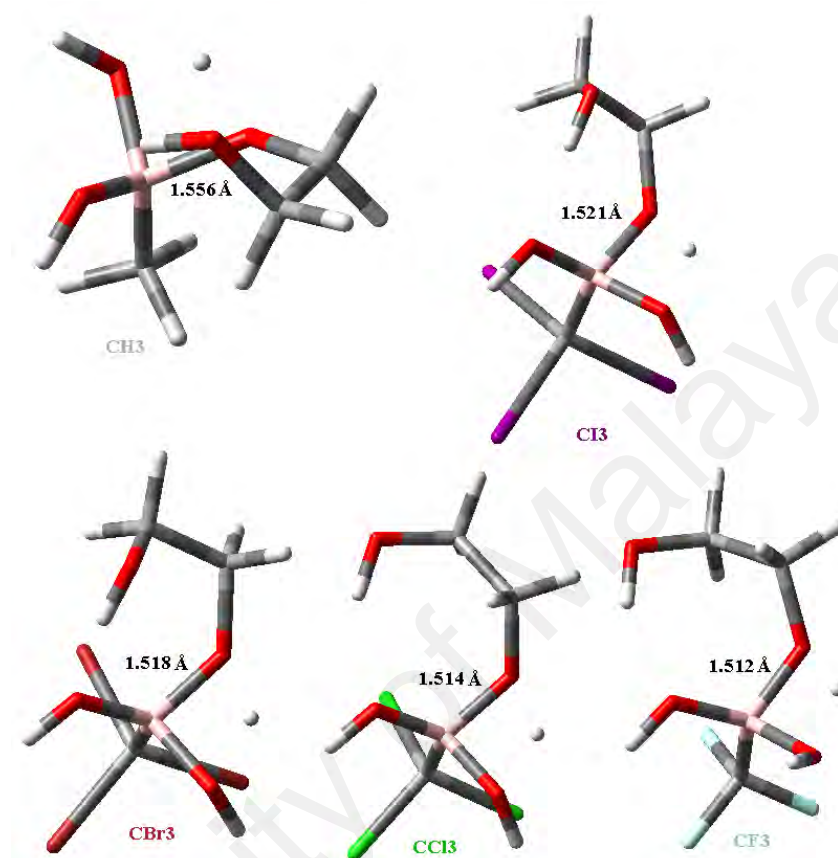


**Figure 4.12: The transition structure of boronic acid in reaction with diol in five different R-groups at room temperature. The numbers represent the distance between boron and the oxygen of incoming diol at the first step of reaction.**

At high temperature range, a consistent change is observed in Arrhenius plot of reaction rate and KIE as the electronegativity of the R-group increases. The higher electronegative R-group induces a better tunnelling behaviour on the proton transfer mechanism. This can be explained by the effect of the R-group on boron and its interaction with the diol. A highly electrophile boron resulted from an electronegative R-group forms a stronger bond with the oxygen which would make it rather difficult to

dissociate. Even though this results in a high classical activation barrier, it has one advantage in that it induces tunnelling.

We have learned in Section 4.1.4 that enzymes can induce tunnelling by positioning the substrate in an orientation where the donor-acceptor distance is reduced. Based on our observations in this section, the high electronegative R-group in boronic acid does exactly that. The high electrophilicity of boron results in a shorter hydrogen bond between boron and the oxygen of diol (Figure 4.12). That brings the proton of diol closer to the OH group of boronic acid, resulting in a high tunnelling contribution during proton transfer reaction of boronic acid with diol.

The basic boronate ion would not have such characteristic since the boron is less electrophilic. It is however important to study the tunnelling behaviour of basic boronate ion with different electronegative R-groups as comparison, which is part of our planned future studies.

## CHAPTER 5

### PROTON TUNNELLING IN BIOCHEMISTRY-A CONCLUSION

In this thesis the kinetics of both the enzymatic and non-enzymatic proton transfer reactions have been thoroughly studied. In general, we emphasized three main aspects, namely the electronic structure treatment of atoms involved in the chemical reactions, the calculation of the classical rate constant using transition state theory, and the incorporation of quantum mechanical effects in the transition state theory to calculate the tunnelling correction factor via the numerical integration method.

The first aspect is handled by searching for the stationary points on the PES. This involves the structures of reactant, product and transition state. The second aspect is handled by calculating the energy that the system requires to surmount the classical trajectory of the reaction mechanism, via the saddle point. The third aspect can only be studied when the transferring particle is light enough to bypass the saddle point and tunnel through the energy barrier without gaining the classical energy of activation. This can occur if the system is in the *tunnelling ready* state, that is, the quantum transition state, where the quantum state energies of the reactant and product becomes degenerate. At biological temperatures, this degeneracy can only be achieved through thermal fluctuations which makes it is necessary to incorporate quantum mechanical effects in biological proton transfer reactions.

This concept has enabled us to explain the tunnelling phenomenon during ribosomal peptide bond formation. Despite the unknown reaction mechanism, what is known for sure is that proton transfer directly determines the reaction rate. That makes the incorporation of quantum effects in the peptide bond formation necessary, the effects of

which had been neglected in all ribosomal studies carried out so far, leading towards the total acceptance of the conventional ribosomal catalysis. This acceptance causes stagnation in understanding the exact mechanism of peptide bond formation. This study provides new insights in the catalytic role of the ribosome by looking beyond the common knowledge of ribosomal catalysis via tunnelling induced peptide bond formation to the reaction path. To do this, we need to investigate the movement of atoms in the molecule during the reaction which itself requires a known reaction mechanism.

To know the mechanism, one must ascertain whether there is quantum tunnelling in the reaction. To study whether quantum tunnelling occurs in the reaction, one needs to know the mechanism. To get out of this loop, we made some approximations to the reaction mechanism by proposing and comparing many different possible mechanisms. This will help us to get closer to the real one.

Among all these mechanisms, three show promising tunnelling contribution, one of which is a novel mechanism proposed in this study which highlights the importance of the A76-2'-OH moiety in handing over the growing polypeptide chain to the nascent amino acid. In this mechanism (P-III), the A2451-3'-OH hydrogen bonds with the P-site 2'-O, facilitating the release of polypeptide chain from the P-site tRNA. This is where this base assists in shortening the donor acceptor distance by pushing the 2'-O towards the attacking nucleophile to promote tunnelling. This is a plausible reaction mechanism which suggests that the ribosome provides the necessary conditions for inducing tunnelling.

Nevertheless, more thorough investigation is required to understand how the ribosomal rRNA residues in the active site of the ribosome are affected by ribosomal proteins. For

this to be carried out, we need to work inside out, meaning that we should zoom out from the active site core of the enzyme and reactive species to the rRNA bases and eventually to the surrounding proteins. So far we have proposed a mechanism with a plausibility which is confirmed through valid theoretical methods and is backed by crystallographic structures of the reactant and product species. From this point, a larger portion of the enzyme which involves the surrounding proteins need to be simulated for studying the motion of the active site groups in inducing tunnelling (shortening the donor-acceptor distance).

The understanding of how an enzyme catalyses a reaction can be helpful in improving the efficiency of synthetic reactions by mimicking the way the enzyme catalysis works. In a more specific way, we tried to understand whether shortening the donor-acceptor distance also induces tunnelling in other proton transfer reactions. To do this, we studied the reactivity of boronic acid towards diol with different electronegative R-groups. Our results show that as the electronegativity of the R-group increases, the tunnelling contribution to the reaction rate increases. By analysing the transition structures of all the R-groups we have found a correlation between the electronegativity and the distance between the transferring proton from the diol to the OH group of the boron. With the increase in the electronegativity of the R-group, the donor acceptor distance decreases, which results in the enhancement of the tunnelling contribution to the reaction rate.

The sensitivity of the tunnelling rate to the temperature and the electronegativity of the R-group can be very useful in controlling the interaction between a boronic acid sensor and glucose. A well-known challenge with non-enzymatic glucose sensors is the lack of selectivity due to the presence of fructose in blood, affecting the accuracy of these sensors. Even though there is a slight difference in the orientation of the OH groups

between glucose and fructose, they have a negligible difference in their classical energy barriers during the reaction with boronic acid (Norrild & Eggert, 1996). Hence, the sensor reacts with fructose as well as the glucose and results in a wrong reading of blood glucose concentration. Inducing the tunnelling conditions to the system can make a large difference between the reaction rate of glucose and fructose. The different orientation of the OH groups in these two structures can result in a different donor-acceptor distance which significantly affects the tunnelling rate. This gives us the idea of designing a tunnelling induced glucose sensor with high sensitivity and as a result selectivity towards glucose in the future studies.

By fine-tuning the proper conditions to bring the system to the tunnelling ready state, we were able to induce tunnelling conditions in biological temperatures. However, the occurrence of quantum phenomena in biological systems is still not widely accepted, despite the fact that Niels Bohr, Werner Heisenberg and Erwin Schrödinger, the founders of quantum physics, all share the viewpoint which states that quantum physics is a key to understanding life. It is understood without doubt that biological phenomenon is reducible to quantum mechanical effects which is what was meant by those great physicists. Whether or not these quantum laws (e.g. coherent wavelike nature of the matter) guide biological phenomena (e.g. tunnelling in biochemical reactions) is still debatable. However, this ambiguity is fading away since the general understanding of this subject area, which involves deep knowledge of quantum mechanics and its application to the biochemical world is advancing at a staggering speed. With the tremendous improvement and advancement in computational resources and by performing immense calculations on the enzymatic active site and implementing quantum mechanical laws to the reaction kinetics, we are at the beginning of the path towards understanding the mysteries of quantum biology.

## REFERENCES

- Acosta-Silva, C., Bertran, J., Branchadell, V., & Oliva, A. (2012). Quantum-mechanical study on the mechanism of peptide bond formation in the ribosome. *Journal of the American Chemical Society*, *134*(13), 5817-5831.
- Agirrezabala, X., & Frank, J. (2010). From DNA to proteins via the ribosome: structural insights into the workings of the translation machinery. *Human Genomics*, *4*(4), 226.
- Alecu, I. M., Zheng, J., Papajak, E., Yu, T., & Truhlar, D. G. (2012). Biofuel combustion. Energetics and kinetics of hydrogen abstraction from carbon-1 in n-butanol by the hydroperoxyl radical calculated by coupled cluster and density functional theories and multistructural variational transition-state theory with multidimensional tunnelling. *The Journal of Physical Chemistry A*, *116*(50), 12206-12213.
- Al-Khalili, J., & McFadden, J. (2014). *Life on the edge: the coming of age of quantum biology*. Random House.
- Alsallaq, R., & Zhou, H. X. (2007). Prediction of protein-protein association rates from a transition-state theory. *Structure*, *15*(2), 215-224.
- Andersson, S., Goumans, T. P. M., & Arnaldsson, A. (2011). Tunnelling in hydrogen and deuterium atom addition to CO at low temperatures. *Chemical Physics Letters*, *513*(1), 31-36.
- Åqvist, J., Lind, C., Sund, J., & Wallin, G. (2012). Bridging the gap between ribosome structure and biochemistry by mechanistic computations. *Current Opinion in Structural Biology*, *22*(6), 815-823.
- Arabi, A. A., & Matta, C. F. (2011). Effects of external electric fields on double proton transfer kinetics in the formic acid dimer. *Physical Chemistry Chemical Physics*, *13*(30), 13738-13748.
- Arrhenius, S. (1889). On the reaction velocity of the inversion of cane sugar by acids. *Journal of Physical Chemistry*, *4*, 226.
- Atkins, P., Friedman, R. (2005). *Molecular quantum mechanics*. Oxford University Press.
- Ball, P. (2004). Enzymes: by chance, or by design?. *Nature*, *431*(7007), 396-397.
- Ban, N., Nissen, P., Hansen, J., Moore, P. B., & Steitz, T. A. (2000). The complete atomic structure of the large ribosomal subunit at 2.4 Å resolution. *Science*, *289*(5481), 905-920.

- Basran, J., Patel, S., Sutcliffe, M. J., & Scrutton, N. S. (2001). Importance of barrier shape in enzyme-catalysed reactions. *Journal of Biological Chemistry*, 276(9), 6234-6242.
- Basran, J., Harris, R. J., Sutcliffe, M. J., & Scrutton, N. S. (2003). H-tunnelling in the multiple H-transfers of the catalytic cycle of morphinone reductase and in the reductive half-reaction of the homologous pentaerythritol tetranitrate reductase. *Journal of Biological Chemistry*, 278(45), 43973-43982.
- Becke, A. D. (1988). Density-functional exchange-energy approximation with correct asymptotic behaviour. *Physical Review A*, 38(6), 3098.
- Becke, A. D. (1993-a). A new mixing of Hartree-Fock and local density-functional theories. *The Journal of Chemical Physics*, 98(2), 1372-1377.
- Becke, A. D. (1993-b). Density-functional thermochemistry. III. The role of exact exchange. *The Journal of Chemical Physics*, 98(7), 5648-5652.
- Becke, A. D., & Johnson, E. R. (2007). Exchange-hole dipole moment and the dispersion interaction revisited. *The Journal of Chemical Physics*, 127(15), 154108.
- Becke, A. D. (2012). Kohn-Sham density-functional approach to strong correlations. In *Abstracts of Papers, 243rd American Chemical Society National Meeting & Exposition, San Diego, CA, United States, March 25-29, 2012*.
- Becke, A. D. (2014). Perspective: Fifty years of density-functional theory in chemical physics. *The Journal of Chemical Physics*, 140(18), 18A301.
- Bell, R. P. (1973). *The proton in chemistry* (Vol. 1). London: Chapman and Hall.
- Benkovic, S. J., & Hammes-Schiffer, S. (2003). A perspective on enzyme catalysis. *Science*, 301(5637), 1196-1202.
- Bhat, K. L., Hayik, S., Corvo, J. N., Marycz, D. M., & Bock, C. W. (2004). A computational study of the formation of 1, 3, 2-dioxaborolane from the reaction of dihydroxy borane with 1, 2-ethanediol. *Journal of Molecular Structure: THEOCHEM*, 673(1), 145-154.
- Blaha, G., Stanley, R. E., & Steitz, T. A. (2009). Formation of the first peptide bond: the structure of EF-P bound to the 70S ribosome. *Science*, 325(5943), 966-970.
- Bothma, J. P., Gilmore, J. B., & McKenzie R. H. (2010). The role of quantum effects in proton transfer reactions in enzymes: Quantum tunnelling in a noisy environment?. *New Journal of Physics*, 12, 1367-2630.
- Böeseken, J. (1949). The use of boric acid for the determination of the configuration of carbohydrates. *Advances in Carbohydrate Chemistry*, 4, 189-210.

- Braun-Sand, S., Olsson, M. H., Mavri, J., & Warshel, A. (2007). Computer Simulations of Proton Transfer in Proteins and Solutions. *Hydrogen-Transfer Reactions*, 1171-1205.
- Brovarets, O. H. O., Zhurakivsky, R. O., & Hovorun, D. M. (2013). The physico-chemical mechanism of the tautomerisation via the DPT of the long Hyp...Hyp Watson-Crick base pair containing rare tautomer: A QM and QTAIM detailed look. *Chemical Physics Letters*, 578, 126-132.
- Brovarets, O. H. O., & Hovorun, D. M. (2015). How many tautomerization pathways connect Watson-Crick-like G\*· T DNA base mispair and wobble mismatches?. *Journal of Biomolecular Structure and Dynamics*, 33(11), 2297-2315.
- Brunelle, J. L., Shaw, J. J., Youngman, E. M., & Green, R. (2008). Peptide release on the ribosome depends critically on the 2' OH of the peptidyl-tRNA substrate. *RNA*, 14(8), 1526-1531.
- Bruno, W. J., & Bialek, W. (1992). Vibrationally enhanced tunnelling as a mechanism for enzymatic hydrogen transfer. *Biophysical Journal*, 63(3), 689.
- Bull, S. D., Davidson, M. G., Van den Elsen, J. M., Fossey, J. S., Jenkins, A. T. A., Jiang, Y. B., ... & James, T. D. (2012). Exploiting the reversible covalent bonding of boronic acids: recognition, sensing, and assembly. *Accounts of Chemical Research*, 46(2), 312-326.
- Burke, K. (2012). Perspective on density functional theory. *The Journal of Chemical Physics*, 136(15), 150901.
- Byun, B. J., & Kang, Y. K. (2013). A mechanistic study supports a two-step mechanism for peptide bond formation on the ribosome. *Physical Chemistry Chemical Physics*, 15(36), 14931-14935.
- Chuang, Y. Y., & Truhlar, D. G. (1998). Reaction-path dynamics in redundant internal coordinates. *The Journal of Physical Chemistry A*, 102(1), 242-247.
- Cohen, A. J., Mori-Sánchez, P., & Yang, W. (2011). Challenges for density functional theory. *Chemical Reviews*, 112(1), 289-320.
- Cramer, C. J., & Truhlar, D. G., (2009). Density functional theory for transition metals and transition metal chemistry. *Physical Chemistry Chemical Physics*, 11, 10757-10816.
- Davis, A. P., & Wareham, R. S. (1999). Carbohydrate recognition through noncovalent interactions: a challenge for biomimetic and supramolecular chemistry. *Angewandte Chemie International Edition*, 38(20), 2978-2996.
- Ditchfield, R. H. W. J., Hehre, W. J., & Pople, J. A. (1971). Self-consistent molecular-orbital methods. IX. An extended Gaussian-type basis for molecular-orbital studies of organic molecules. *The Journal of Chemical Physics*, 54(2), 724-728.

- Dix, E. J., Herman, M. S., & Goodman, J. L. (1993). The 1, 2-hydrogen rearrangement of methylchlorocarbene: contribution of quantum mechanical tunnelling. *Journal of the American Chemical Society*, 115(22), 10424-10425.
- Dorner, S., Panuschka, C., Schmid, W., & Barta, A. (2003). Mononucleotide derivatives as ribosomal P-site substrates reveal an important contribution of the 2'-OH to activity. *Nucleic Acids Research*, 31(22), 6536-6542.
- Dybala-Defratyka, A., Paneth, P., Banerjee, R., & Truhlar, D. G. (2007). Coupling of hydrogenic tunnelling to active-site motion in the hydrogen radical transfer catalysed by a coenzyme B12-dependent mutase. *Proceedings of the National Academy of Sciences*, 104(26), 10774-10779.
- Eckart, C. (1930). The penetration of a potential barrier by electrons. *Physical Review*, 35(11), 1303.
- Edwards, J. O., Morrison, G. C., Ross, V. F., & Schultz, J. W. (1955). The structure of the aqueous borate ion. *Journal of the American Chemical Society*, 77(2), 266-268.
- Erlacher, M. D., Lang, K., Shankaran, N., Wotzel, B., Hüttenhofer, A., Micura, R., ... & Polacek, N. (2005). Chemical engineering of the peptidyl transferase center reveals an important role of the 2'-hydroxyl group of A2451. *Nucleic Acids Research*, 33(5), 1618-1627.
- Evans, M. G., & Polanyi, M. (1935). Some applications of the transition state method to the calculation of reaction velocities, especially in solution. *Transactions of the Faraday Society*, 31, 875-894.
- Eyring, H. (1935). The activated complex in chemical reactions. *The Journal of Chemical Physics*, 3(2), 107-115
- Fernández-Ramos, A., Ellingson, B. A., Garrett, B. C., & Truhlar, D. G. (2007). Variational transition state theory with multidimensional tunnelling. *Reviews in Computational Chemistry*, 23, 125.
- Frisch, M. J., Trucks, G. W., Schlegel, H. B., Scuseria, G. E., Robb, M. A., Cheeseman, J. R., ... & Nakatsuji, H. (2010). Gaussian development version. *Revision h, 1*.
- Gagnon, M. G., Lin, J., Bulkley, D., & Steitz, T. A. (2014). Crystal structure of elongation factor 4 bound to a clockwise ratcheted ribosome. *Science*, 345(6197), 684-687.
- Gao, J., & Truhlar, D. G. (2002). Quantum mechanical methods for enzyme kinetics. *Annual Review of Physical Chemistry*, 53(1), 467-505.
- Garrett, B. C., & Truhlar, D. G. (1979a). Accuracy of tunnelling corrections to transition state theory for thermal rate constants of atom transfer reactions. *Journal of Physical Chemistry*, 83(1), 200-203.

- Garrett, B. C., & Truhlar, D. G. (1979b). Generalized transition state theory. Quantum effects for collinear reactions of hydrogen molecules and isotopically substituted hydrogen molecules. *Journal of Physical Chemistry*, 83(8), 1079-1112.
- Gil, M., & Waluk, J. (2007). Vibrational gating of double hydrogen tunnelling in porphycene. *Journal of the American Chemical Society*, 129(5), 1335-1341.
- Gindulyte, A., Bashan, A., Agmon, I., Massa, L., Yonath, A., & Karle, J. (2006). The transition state for formation of the peptide bond in the ribosome. *Proceedings of the National Academy of Sciences*, 103(36), 13327-13332.
- Glasstone, S., Eyring, H., & Laidler, K. J. (1941). *The theory of rate processes*. McGraw-Hill.
- Goerigk, L., & Grimme, S. (2011). A thorough benchmark of density functional methods for general main group thermochemistry, kinetics, and noncovalent interactions. *Physical Chemistry Chemical Physics*, 13(14), 6670-6688.
- Gray, S. K., Miller, W. H., Yamaguchi, Y., & Schaefer III, H. F. (1981). Tunnelling in the unimolecular decomposition of formaldehyde: a more quantitative study. *Journal of the American Chemical Society*, 103(8), 1900-1904.
- Gregory, J. K., Clary, D. C., Liu, K., Brown, M. G., & Saykally, R. J. (1997). The water dipole moment in water clusters. *Science*, 275(5301), 814-817.
- Grimme, S., Antony, J., Ehrlich, S., & Krieg, H. (2010). A consistent and accurate ab initio parametrization of density functional dispersion correction (DFT-D) for the 94 elements H-Pu. *The Journal of Chemical Physics*, 132(15), 154104.
- Hall, G. G. (1951). The molecular orbital theory of chemical valency. VIII. A method of calculating ionization potentials. In *Proceedings of the Royal Society of London A: Mathematical, Physical and Engineering Sciences* (Vol. 205, No. 1083, pp. 541-552). The Royal Society.
- Hansen, J. L., Schmeing, T. M., Moore, P. B., & Steitz, T. A. (2002). Structural insights into peptide bond formation. *Proceedings of the National Academy of Sciences*, 99(18), 11670-11675.
- Hansen, J. S., Christensen, J. B., Solling, T. I., Jakobsen, P., & Hoeg-Jensen, T. (2011). Ortho-substituted aryl monoboronic acids have improved selectivity for d-glucose relative to d-fructose and l-lactate. *Tetrahedron*, 67(6), 1334-1340.
- Hasnip, P. J., Refson, K., Probert, M. I., Yates, J. R., Clark, S. J., & Pickard, C. J. (2014). Density functional theory in the solid state. *Philosophical Transactions of the Royal Society of London A: Mathematical, Physical and Engineering Sciences*, 372(2011), 20130270.
- Hay, S., Pudney, C. R., McGrory, T. A., Pang, J., Sutcliffe, M. J., & Scrutton, N. S. (2009). Barrier compression enhances an enzymatic hydrogen-transfer reaction. *Angewandte Chemie*, 121(8), 1480-1482.

- Hay, S., Johannissen, L. O., Sutcliffe, M. J., & Scrutton, N. S. (2011). Barrier compression and its contribution to both classical and quantum mechanical aspects of enzyme catalysis. *Biophysical Journal*, 98(1), 121-128.
- Hay, S., & Scrutton, N. S. (2012). Good vibrations in enzyme-catalysed reactions. *Nature Chemistry*, 4(3), 161-168.
- Hele, T. J. H., 2014. 'Quantum transition state theory', Doctor of Philosophy, University of Cambridge, The Old Schools, Trinity Lane, Cambridge CB2 1TN, United Kingdom.
- Hiller, D. A., Singh, V., Zhong, M., & Strobel, S. A. (2011). A two-step chemical mechanism for ribosome-catalysed peptide bond formation. *Nature*, 476(7359), 236-239.
- Hohenberg, P. C., Kohn, W., & Sham, L. J. (1990). The beginnings and some thoughts on the future. *Advances in Quantum Chemistry*, 21, 7-26.
- Hohenberg, P., & Kohn, W. (1964). Inhomogeneous electron gas. *Physical Review*, 136(3B), B864.
- Horsewill, A. J., Jones, N. H., & Caciuffo, R. (2001). Evidence for coherent proton tunnelling in a hydrogen bond network. *Science*, 291(5501), 100-103.
- Horsewill, A. J. (2010). How quantum tunnelling can contribute to proton transfer at biologically relevant temperatures. *Journal of Physical Organic Chemistry*, 23(7), 580-585.
- Hu, H., & Dibble, T. S. (2013). Quantum chemistry, reaction kinetics, and tunnelling effects in the reaction of Methoxy radicals with O<sub>2</sub>. *The Journal of Physical Chemistry A*, 117(51), 14230-14242.
- Hu, W. P., Liu, Y. P., & Truhlar, D. G. (1994). Variational transition-state theory and semiclassical tunnelling calculations with interpolated corrections: a new approach to interfacing electronic structure theory and dynamics for organic reactions. *Journal of the Chemical Society, Faraday Transactions*, 90(12), 1715-1725.
- Ishihara, K., Mouri, Y., Funahashi, S., & Tanaka, M. (1991). Mechanistic study of the complex formation of boric acid. *Inorganic Chemistry*, 30(10), 2356-2360.
- Ito, H., Kono, Y., Machida, A., Mitsumoto, Y., Omori, K., Nakamura, N., ... & Ishihara, K. (2003). Kinetic study of the complex formation of boric and boronic acids with mono-and diprotonated ligands. *Inorganica Chimica Acta*, 344, 28-36.
- Iwatsuki, S., Kanamitsu, Y., Ohara, H., Watanabe, E., & Ishihara, K. (2012). Higher reactivity of 3-pyridinium boronic acid compared with 3-pyridinium boronate ion toward 4-isopropyltropolone in acidic aqueous solution: fundamental reaction analyses for an effective organoboron-based chemosensor. *Journal of Physical Organic Chemistry*, 25(9), 760.

- Iwatsuki, S., Nakajima, S., Inamo, M., Takagi, H. D., & Ishihara, K. (2007). Which is reactive in alkaline solution, boronate ion or boronic acid? Kinetic evidence for reactive trigonal boronic acid in an alkaline solution. *Inorganic Chemistry*, 46(2), 354-356.
- Jensen, F. (2013). *Introduction to computational chemistry*. John Wiley & Sons.
- Jones, R. O. (2015). Density functional theory: Its origins, rise to prominence, and future. *Reviews of Modern Physics*, 87(3), 897.
- Kagawa, S., Sugimoto, K. I., & Funahashi, S. (1995). Kinetic study on complexation of boric acid with 4-isopropyltropolone in non-aqueous solvents. *Inorganica Chimica Acta*, 231(1), 115-119.
- Kamerlin, S. C. L., Mavri, J., & Warshel, A. (2010). Examining the case for the effect of barrier compression on tunneling, vibrationally enhanced catalysis, catalytic entropy and related issues. *FEBS letters*, 584(13), 2759-2766.
- Keck, J. C. (1960). Variational Theory of Chemical Reaction Rates Applied to Three-Body Recombinations. *The Journal of Chemical Physics*, 32(4), 1035-1050.
- Kiefer, P. M., & Hynes, J. T. (2010). Theoretical aspects of tunnelling proton transfer reactions in a polar environment. *Journal of Physical Organic Chemistry*, 23(7), 632-646.
- Klimeš, J., & Michaelides, A. (2012). Perspective: Advances and challenges in treating van der Waals dispersion forces in density functional theory. *The Journal of Chemical Physics*, 137(12), 120901.
- Klinman, J. P. (1989). Quantum mechanical effects in enzyme-catalysed hydrogen transfer reactions. *Trends in Biochemical Sciences*, 14(9), 368-373.
- Klinman, J. P., & Kohen, A. (2013). Hydrogen tunnelling links protein dynamics to enzyme catalysis. *Annual Review of Biochemistry*, 82, 471.
- Klinman, J. P. (2014). Dynamically achieved active site precision in enzyme catalysis. *Accounts of Chemical Research*, 48(2), 449-456.
- Klippenstein, S. J., Pande, V. S., & Truhlar, D. G. (2014). Chemical kinetics and mechanisms of complex systems: A perspective on recent theoretical advances. *Journal of the American Chemical Society*, 136(2), 528-546.
- Knapp, M. J., & Klinman, J. P. (2002). Environmentally coupled hydrogen tunnelling. *European Journal of Biochemistry*, 269(13), 3113-3121.
- Knowles, P., Schutz, M., & Werner, H. J. (2000). Ab initio methods for electron correlation in molecules. *Modern Methods and Algorithms of Quantum Chemistry*, 3, 97-179.
- Kohen, A., & Klinman, J. P. (1998). Enzyme catalysis: beyond classical paradigms. *Accounts of Chemical Research*, 31(7), 397-404.

- Kohen, A., Cannio, R., Bartolucci, S., & Klinman, J. P. (1999). Enzyme dynamics and hydrogen tunnelling in a thermophilic alcohol dehydrogenase. *Nature*, 399(6735), 496-499.
- Kohen, A. (2014). Role of dynamics in enzyme catalysis: substantial versus semantic controversies. *Accounts of Chemical Research*, 48(2), 466-473.
- Kohn, W., & Sham, L. J. (1965). Self-consistent equations including exchange and correlation effects. *Physical Review*, 140(4A), A1133.
- Kohn, W., & Sherrill, C. D. (2014). Editorial: Reflections on fifty years of density functional theory. *The Journal of Chemical Physics*, 140(18), 18A201.
- Kuhlenkoetter, S., Wintermeyer, W., & Rodnina, M. V. (2011). Different substrate-dependent transition states in the active site of the ribosome. *Nature*, 476(7360), 351-354.
- Kuivila, H. G., Keough, A. H., & Soboczenski, E. J. (1954). Areneboronates from diols and polyols. *The Journal of Organic Chemistry*, 19(5), 780-783.
- Kuppermann, A., & Truhlar, D. G. (1971). Exact tunnelling calculations. *Journal of the American Chemical Society*, 93(8), 1840-1851.
- Lacina, K., Skládál, P., & James, T. D. (2014). Boronic acids for sensing and other applications-a mini-review of papers published in 2013. *Chemistry Central Journal*, 8(1), 60.
- Laidler, K. J. (1977). *Chemical Kinetics*. McGraw-Hill.
- Laidler, K. J., & King, M. C. (1983). Development of transition-state theory. *The Journal of Physical Chemistry*, 87(15), 2657-2664.
- Laidler, K. J. (1984). The development of the Arrhenius equation. *Journal of Chemical Education* 61(6), 494-498.
- Lambert, T. (2012). Antibiotics that affect the ribosome. *Revue Scientifique et Technique (International Office of Epizootics)*, 31(1), 57-64.
- Landau, L. D., Lifshitz, E. M., Sykes, J. B., Bell, J. S., & Rose, M. E. (1958). Quantum mechanics, non-relativistic theory. *Physics Today*, 11, 56.
- Lang, K., Erlacher, M., Wilson, D. N., Micura, R., & Polacek, N. (2008). The role of 23S ribosomal RNA residue A2451 in peptide bond synthesis revealed by atomic mutagenesis. *Chemistry & Biology*, 15(5), 485-492.
- Langreth, D. C., & Perdew, J. P. (1982). Exchange-correlation energy of a metallic surface: Wave-vector analysis. II. *Physical Review B*, 26(6), 2810.
- Lee, C., Yang, W., & Parr, R. G. (1988). Development of the Colle-Salvetti correlation-energy formula into a functional of the electron density. *Physical Review B*, 37(2), 785.

- Lee, T. H., Blanchard, S. C., Kim, H. D., Puglisi, J. D., & Chu, S. (2007). The role of fluctuations in tRNA selection by the ribosome. *Proceedings of the National Academy of Sciences*, *104*(34), 13661-13665.
- Levine, I. N. (2009). *Quantum chemistry* (Vol. 6). Upper Saddle River, NJ: Pearson Prentice Hall.
- Ley, D., Gerbig, D., & Schreiner, P. R. (2012). tunnelling control of chemical reactions—the organic chemist's perspective. *Organic & Biomolecular Chemistry*, *10*(19), 3781-3790.
- Longbotham, J. E., Hardman, S. J., Görlich, S., Scrutton, N. S., & Hay, S. (2016). Untangling heavy protein and cofactor isotope effects on enzyme-catalysed hydride transfer. *Journal of the American Chemical Society* *138*(41), 13693-13699.
- Lorand, J. P., & Edwards, J. O. (1959). Polyol complexes and structure of the benzenboronate ion. *The Journal of Organic Chemistry*, *24*(6), 769-774.
- Löwdin, P. O. (1963). Proton tunnelling in DNA and its biological implications. *Reviews of Modern Physics*, *35*(3), 724.
- Löwdin, P. O. (1965). Quantum genetics and the aperiodic solid: Some aspects on the biological problems of heredity, mutations, aging, and tumors in view of the quantum theory of the DNA molecule. In *Advances in Quantum Chemistry* (Vol. 2, pp. 213-360). Academic Press.
- Manthe, U. (2011). Accurate calculations of reaction rates: predictive theory based on a rigorous quantum transition state concept. *Molecular Physics*, *109*(11), 1415-1426.
- Marcus, R. A. (1952). Unimolecular dissociations and free radical recombination reactions. *The Journal of Chemical Physics*, *20*(3), 359-364.
- Marcus, R. A., & Coltrin, M. E. (1977). A new tunnelling path for reactions such as  $H^+ + H_2 \rightarrow H_2^+ + H$ . *The Journal of Chemical Physics*, *67*(6), 2609-2613.
- Marcus, R. A. (1993). Electron transfer reactions in chemistry. Theory and experiment. *Reviews of Modern Physics*, *65*(3), 599.
- Marenich, A. V., Cramer, C. J., & Truhlar, D. G. (2009). Universal solvation model based on solute electron density and on a continuum model of the solvent defined by the bulk dielectric constant and atomic surface tensions. *The Journal of Physical Chemistry B*, *113*(18), 6378-6396.
- Marenich, A. V., Olson, R. M., Kelly, C. P., Cramer, C. J., & Truhlar, D. G. (2007). Self-consistent reaction field model for aqueous and nonaqueous solutions based on accurate polarized partial charges. *Journal of Chemical Theory and Computation*, *3*(6), 2011-2033.
- Martínez-Aguirre, M. A., Villamil-Ramos, R., Guerrero-Alvarez, J. A., & Yatsimirsky, A. K. (2013). Substituent effects and pH profiles for stability constants of

arylboronic acid diol esters. *The Journal of Organic Chemistry*, 78(10), 4674-4684.

Masgrau, L., Roujeinikova, A., Johannissen, L. O., Hothi, P., Basran, J., Ranaghan, K. E., ... & Leys, D. (2006). Atomic description of an enzyme reaction dominated by proton tunnelling. *Science*, 312(5771), 237-241.

Masgrau, L., & Truhlar, D. G. (2014). The importance of ensemble averaging in enzyme kinetics. *Accounts of Chemical Research*, 48(2), 431-438.

Massa, L., Matta, C. F., Yonath, A., & Karle, J. (2010). Quantum transition state for peptide bond formation in the ribosome. *Quantum Biochemistry*, 499-515.

Matta, C. F. (Ed.). (2010). *Quantum biochemistry*. John Wiley & Sons.

Matsumura, T., Iwatsuki, S., & Ishihara, K. (2005). Direct kinetic measurements for the fast interconversion process between trigonal boronic acid and tetragonal boronate ion at low temperatures. *Inorganic Chemistry Communications*, 8(8), 713-716.

Mavri, J., Liu, H., Olsson, M. H., & Warshel, A. (2008). Simulation of tunneling in enzyme catalysis by combining a biased propagation approach and the quantum classical path method: application to lipoxygenase. *The Journal of Physical Chemistry B*, 112(19), 5950-5954.

McFadden, J., & Al-Khalili, J. (1999). A quantum mechanical model of adaptive mutation. *Biosystems*, 50(3), 203-211.

Meana-Pañeda, R., & Fernández-Ramos, A. (2010). Tunnelling Transmission Coefficients: Toward More Accurate and Practical Implementations. In *Kinetics and Dynamics* (pp. 481-500). Springer Netherlands.

Miller, W. H. (1974). Quantum mechanical transition state theory and a new semiclassical model for reaction rate constants. *The Journal of Chemical Physics*, 61(5), 1823-1834.

Miller, W. H. (1975a). Semiclassical limit of quantum mechanical transition state theory for nonseparable systems. *The Journal of Chemical Physics*, 62(5), 1899-1906.

Miller, W. H. (1975b). Path integral representation of the reaction rate constant in quantum mechanical transition state theory. *The Journal of Chemical Physics*, 63(3), 1166-1172.

Miller, W. H. (1976). Importance of nonseparability in quantum mechanical transition-state theory. *Accounts of Chemical Research*, 9(8), 306-312.

Miller, W. H., Handy, N. C., & Adams, J. E. (1980). Reaction path Hamiltonian for polyatomic molecules. *The Journal of Chemical Physics*, 72(1), 99-112.

- Miller, W. H., Schwartz, S. D., & Tromp, J. W. (1983). Quantum mechanical rate constants for bimolecular reactions. *The Journal of Chemical Physics*, 79(10), 4889-4898.
- Miller, W. H. (1998). Spiers memorial lecture quantum and semiclassical theory of chemical reaction rates. *Faraday Discussions*, 110, 1-21.
- Mincer, J. S., & Schwartz, S. D. (2003). A computational method to identify residues important in creating a protein promoting vibration in enzymes. *The Journal of Physical Chemistry B*, 107(1), 366-371.
- Miyamoto, C., Suzuki, K., Iwatsuki, S., Inamo, M., Takagi, H. D., & Ishihara, K. (2008). Kinetic evidence for high reactivity of 3-nitrophenylboronic acid compared to its conjugate boronate ion in reactions with ethylene and propylene glycols. *Inorganic Chemistry*, 47(5), 1417-1419.
- Monajemi, H., Omar, N. Y., Daud, M. N., Zain, S. M., & Abdullah, W. A. T. W. (2011-a). The role of initiator tRNA<sub>i</sub><sup>met</sup> in fidelity of initiation of protein synthesis. *Nucleosides, Nucleotides and Nucleic Acids*, 30(9), 726-739.
- Monajemi, H., Zain, S. M., & Abdullah, W. A. T. W. (2011-b). Computational outlook on the ribosome as an entropy trap. *Computational and Theoretical Chemistry*, 976(1), 148-152.
- Monajemi, H., Daud, M. N., Mohd. Zain, S., & Wan Abdullah, W. A. T. (2012). ONIOM and ab-initio calculations on the mechanism of uncatalysed peptide bond formation. *Biochemistry and Cell Biology*, 90(6), 691-700.
- Monajemi, H., Cheah, M. H., Lee, V. S., Zain, S. M., & Wan Abdullah, W. A. T. (2014). On the kinetics and reaction mechanisms of boronic acid in interaction with diols for non-enzymatic glucose monitoring applications: a hybrid DFT study. *RSC Advances*, 4(21), 10505-10513.
- Monajemi, H., Zain, S. M., & Wan Abdullah, W. A. T. (2015). The P-site A76 2'-OH acts as a peptidyl shuttle in a stepwise peptidyl transfer mechanism. *RSC Advances*, 5(32), 25489-25503.
- Moore, P. B., & Steitz, T. A. (2003). After the ribosome structures: How does peptidyl transferase work? *RNA*, 9(2), 155-159.
- Moore, P. B. (2009). The ribosome returned Peter B Moore. *Journal of Biology*, 8, 8.
- Muth, G. W., Ortoleva-Donnelly, L., & Strobel, S. A. (2000). A single adenosine with a neutral pKa in the ribosomal peptidyl transferase center. *Science*, 289(5481), 947-950.
- Nguyen, T. L., Stanton, J. F., & Barker, J. R. (2010). A practical implementation of semi-classical transition state theory for polyatomics. *Chemical Physics Letters*, 499(1), 9-15.

- Nishiyabu, R., Kubo, Y., James, T. D., & Fossey, J. S. (2011-a). Boronic acid building blocks: tools for sensing and separation. *Chemical Communications*, 47(4), 1106-1123.
- Nishiyabu, R., Kubo, Y., James, T. D., & Fossey, J. S. (2011-b). Boronic acid building blocks: tools for self assembly. *Chemical Communications*, 47(4), 1124-1150.
- Nissen, P., Hansen, J., Ban, N., Moore, P. B., & Steitz, T. A. (2000). The structural basis of ribosome activity in peptide bond synthesis. *Science*, 289(5481), 920-930.
- Noller, H. F., Hoffarth, V., & Zimniak, L. (1992). Unusual resistance of peptidyl transferase to protein extraction procedures. *Science*, 256(5062), 1416-1419.
- Norrild, J. C., & Eggert, H. (1996). Boronic acids as fructose sensors. Structure determination of the complexes involved using  $^1\text{J}$  CC coupling constants. *Journal of the Chemical Society, Perkin Transactions 2*(12), 2583-2588.
- Ohmine, I., & Saito, S. (1999). Water dynamics: Fluctuation, relaxation, and chemical reactions in hydrogen bond network rearrangement. *Accounts of Chemical Research*, 32(9), 741-749.
- Olsson, M. H., Siegbahn, P. E., & Warshel, A. (2004). Simulations of the large kinetic isotope effect and the temperature dependence of the hydrogen atom transfer in lipoxygenase. *Journal of the American Chemical Society*, 126(9), 2820-2828.
- Olsson, M. H., Mavri, J., & Warshel, A. (2006). Transition state theory can be used in studies of enzyme catalysis: lessons from simulations of tunnelling and dynamical effects in lipoxygenase and other systems. *Philosophical Transactions of the Royal Society B: Biological Sciences*, 361(1472), 1417-1432.
- Park, K., Pak, Y., & Kim, Y. (2012). Large tunnelling effect on the hydrogen transfer in bis ( $\mu$ -oxo) dicopper enzyme: A theoretical study. *Journal of the American Chemical Society*, 134(7), 3524-3531.
- Peng, C., Ayala, P. Y., Schlegel, H. B., & Frisch, M. J. (1996). Using redundant internal coordinates to optimize equilibrium geometries and transition states. *Journal of Computational Chemistry*, 17(1), 49-56.
- Peng, C., & Bernhard Schlegel, H. (1993). Combining Synchronous Transit and Quasi-Newton Methods to Find Transition States. *Israel Journal of Chemistry*, 33(4), 449-454.
- Perdew, J. P., & Yue, W. (1986). Accurate and simple density functional for the electronic exchange energy: Generalized gradient approximation. *Physical Review B*, 33(12), 8800.
- Perdew, J. P., & Wang, Y. (1992). Accurate and simple analytic representation of the electron-gas correlation energy. *Physical Review B*, 45(23), 13244.
- Peeverati, R., & Truhlar, D. G. (2011-a). M11-L: a local density functional that provides improved accuracy for electronic structure calculations in chemistry and physics. *The Journal of Physical Chemistry Letters*, 3(1), 117-124.

- Peeverati, R., & Truhlar, D. G. (2011-b). Improving the accuracy of hybrid meta-GGA density functionals by range separation. *The Journal of Physical Chemistry Letters*, 2(21), 2810-2817.
- Peeverati, R., & Truhlar, D. G. (2012-a). Exchange–correlation functional with good accuracy for both structural and energetic properties while depending only on the density and its gradient. *Journal of Chemical Theory and Computation*, 8(7), 2310-2319.
- Peeverati, R., & Truhlar, D. G. (2012-b). An improved and broadly accurate local approximation to the exchange–correlation density functional: The MN12-L functional for electronic structure calculations in chemistry and physics. *Physical Chemistry Chemical Physics*, 14(38), 13171-13174.
- Peeverati, R., & Truhlar, D. G. (2012-c). Screened-exchange density functionals with broad accuracy for chemistry and solid-state physics. *Physical Chemistry Chemical Physics*, 14(47), 16187-16191.
- Piecuch, P., Włoch, M., Gour, J. R., Li, W., & Lutz, J. J. (2015, January). Dealing with chemical reaction pathways and electronic excitations in molecular systems via renormalized and active-space coupled-cluster methods. In *Proceedings Of The International Conference Of Computational Methods In Sciences And Engineering 2010 (ICCMSE-2010)* (Vol. 1642, pp. 172-175). AIP Publishing.
- Pietro, W. J., Francl, M. M., Hehre, W. J., DeFrees, D. J., Pople, J. A., & Binkley, J. S. (1982). Self-consistent molecular orbital methods. 24. Supplemented small split-valence basis sets for second-row elements. *Journal of the American Chemical Society*, 104(19), 5039-5048.
- Pizer, R., & Tihal, C. (1992). Equilibria and reaction mechanism of the complexation of methylboronic acid with polyols. *Inorganic Chemistry*, 31(15), 3243-3247.
- Pizer, R. D., & Tihal, C. A. (1996). Mechanism of boron acid/polyol complex formation. Comments on the trigonal/tetrahedral interconversion on boron. *Polyhedron*, 15(19), 3411-3416.
- Polacek, N., Gaynor, M., Yassin, A., & Mankin, A. S. (2001). Ribosomal peptidyl transferase can withstand mutations at the putative catalytic nucleotide. *Nature*, 411(6836), 498-501.
- Polikanov, Y. S., Steitz, T. A., & Innis, C. A. (2014). A proton wire to couple aminoacyl-tRNA accommodation and peptide-bond formation on the ribosome. *Nature Structural & Molecular Biology*, 21(9), 787-793.
- Pollak, E. (2012). Quantum variational transition state theory for hydrogen tunnelling in enzyme catalysis. *The Journal of Physical Chemistry B*, 116(43), 12966-12971.
- Pople, J. A. (1999). Nobel lecture: Quantum chemical models. *Reviews of Modern Physics*, 71(5), 1267.
- Pribram-Jones, A., Gross, D. A., & Burke, K. (2014). Dft: A theory full of holes?. *arXiv preprint arXiv:1408.4826*.

- Pu, J., Gao, J., & Truhlar, D. G. (2006). Multidimensional tunnelling, recrossing, and the transmission coefficient for enzymatic reactions. *Chemical Reviews*, 106(8), 3140-3169.
- Pudney, C. R., Hay, S., Sutcliffe, M. J., & Scrutton, N. S. (2006).  $\alpha$ -secondary isotope effects as probes of “tunnelling-ready” configurations in enzymatic H-tunnelling: Insight from environmentally coupled tunnelling models. *Journal of the American Chemical Society*, 128(43), 14053-14058.
- Pudney, C. R., Johannissen, L. O., Sutcliffe, M. J., Hay, S., & Scrutton, N. S. (2010). Direct Analysis of Donor– Acceptor Distance and Relationship to Isotope Effects and the Force Constant for Barrier Compression in Enzymatic H-tunnelling Reactions. *Journal of the American Chemical Society*, 132(32), 11329-11335.
- Pullman, B., & Pullman, A. (1963). *Quantum biochemistry* (No. QP521 P8 1963).
- Ramakrishnan, V. (2008). What we have learned from ribosome structures. *Biochemical Society Transactions*, 36(Pt 4), 567-574.
- Ramakrishnan, V. (2010). Unraveling the structure of the ribosome (Nobel Lecture). *Angewandte Chemie International Edition*, 49(26), 4355-4380.
- Rangelov, M. A., Vayssilov, G. N., Yomtova, V. M., & Petkov, D. D. (2006). The syn-oriented 2-OH provides a favorable proton transfer geometry in 1, 2-diol monoester aminolysis: implications for the ribosome mechanism. *Journal of the American Chemical Society*, 128(15), 4964-4965.
- Rassolov, V. A., Ratner, M. A., Pople, J. A., Redfern, P. C., & Curtiss, L. A. (2001). 6-31G\* basis set for third-row atoms. *Journal of Computational Chemistry*, 22(9), 976-984.
- Rhodes, M. M., Réblová, K., Šponer, J., & Walter, N. G. (2006). Trapped water molecules are essential to structural dynamics and function of a ribozyme. *Proceedings of the National Academy of Sciences*, 103(36), 13380-13385.
- Robinson, J. B., & Knowles, P. J. (2012-a). Benchmark quasi-variational coupled cluster calculations of multiple bond breaking. *Journal of Chemical Theory and Computation*, 8(8), 2653-2660.
- Robinson, J. B., & Knowles, P. J. (2012-b). Breaking multiple covalent bonds with Hartree–Fock-based quantum chemistry: Quasi-Variational Coupled Cluster theory with perturbative treatment of triple excitations. *Physical Chemistry Chemical Physics*, 14(19), 6729-6732.
- Rodnina, M. V., Kuhlenkotter, S., Wohlgemuth, I., & Wintermeyer, W. (2012). Different substrate-dependent transition states in the active site of the ribosome. *The FASEB Journal*, 26(1\_MeetingAbstracts), 544-1.
- Roothaan, C. C. J. (1951). New developments in molecular orbital theory. *Reviews of Modern Physics*, 23(2), 69.

- Rucker, J., Cha, Y., Jonsson, T., Grant, K. L., & Klinman, J. P. (1992). Role of internal thermodynamics in determining hydrogen tunnelling in enzyme-catalysed hydrogen transfer reactions. *Biochemistry*, 31(46), 11489-11499.
- Samish, I., Bourne, P. E., & Najmanovich, R. J. (2015). Achievements and challenges in structural bioinformatics and computational biophysics. *Bioinformatics*, 31(1), 146-150.
- Sanbonmatsu, K. Y., Joseph, S., & Tung, C. S. (2005). Simulating movement of tRNA into the ribosome during decoding. *Proceedings of the National Academy of Sciences of the United States of America*, 102(44), 15854-15859.
- Sanbonmatsu, K. Y. (2012). Computational studies of molecular machines: the ribosome. *Current Opinion in Structural Biology*, 22(2), 168-174.
- Schlegel, H. B. (1982). Optimization of equilibrium geometries and transition structures. *Journal of Computational Chemistry*, 3(2), 214-218.
- Schmeing, T. M., Huang, K. S., Kitchen, D. E., Strobel, S. A., & Steitz, T. A. (2005-a). Structural insights into the roles of water and the 2' hydroxyl of the P site tRNA in the peptidyl transferase reaction. *Molecular Cell*, 20(3), 437-448.
- Schmeing, T. M., Huang, K. S., Strobel, S. A., & Steitz, T. A. (2005-b). An induced-fit mechanism to promote peptide bond formation and exclude hydrolysis of peptidyl-tRNA. *Nature*, 438(7067), 520-524.
- Schmeing, T. M., & Ramakrishnan, V. (2009). What recent ribosome structures have revealed about the mechanism of translation. *Nature*, 461(7268), 1234-1242.
- Schrödinger, E. (1944). *What Is Life? the physical aspect of the living cell and mind*. Cambridge University Press, Cambridge.
- Schwinger, J. (1962). Gauge invariance and mass. II. *Physical Review*, 128(5), 2425.
- Scott, A. P., & Radom, L. (1996). Harmonic vibrational frequencies: an evaluation of Hartree-Fock, Møller-Plesset, quadratic configuration interaction, density functional theory, and semiempirical scale factors. *The Journal of Physical Chemistry*, 100(41), 16502-16513.
- Scuseria, G. E., & Staroverov, V. N. (2005). Progress in the development of exchange-correlation functionals. *Theory and Application of Computational Chemistry: The First 40 Years*, 669.
- Seila, A. C., Okuda, K., Núñez, S., Seila, A. F., & Strobel, S. A. (2005). Kinetic isotope effect analysis of the ribosomal peptidyl transferase reaction. *Biochemistry*, 44(10), 4018-4027.
- Sen, A., & Kohen, A. (2010). Enzymatic tunnelling and kinetic isotope effects: chemistry at the crossroads. *Journal of Physical Organic Chemistry*, 23(7), 613-619.

- Shao, C., Matsuoka, S., Miyazaki, Y., Yoshimura, K., Suzuki, T. M., & Tanaka, D. P. (2000). Equilibrium and kinetic studies on the complexation of boric acid with chromotropic acid. *Journal of the Chemical Society, Dalton Transactions*, (18), 3136-3142.
- Shavitt, I. (1959). A Calculation of the Rates of the Ortho-Para Conversions and Isotope Exchanges in Hydrogen. *The Journal of Chemical Physics*, 31(5), 1359-1367.
- Sholl, D., & Steckel, J. A. (2011). *Density functional theory: a practical introduction*. John Wiley & Sons.
- Sievers, A., Beringer, M., Rodnina, M. V., & Wolfenden, R. (2004). The ribosome as an entropy trap. *Proceedings of the National Academy of Sciences of the United States of America*, 101(21), 7897-7901.
- Simonović, M., & Steitz, T. A. (2009). A structural view on the mechanism of the ribosome-catalysed peptide bond formation. *Biochimica et Biophysica Acta (BBA)-Gene Regulatory Mechanisms*, 1789(9), 612-623.
- Slater, J. C. (1951). A simplification of the Hartree-Fock method. *Physical Review*, 81(3), 385.
- Small, M. S., Predescu, C., & Miller, W. H. (2006). Quantifying the extent of recrossing flux for quantum systems. *Chemical Physics*, 322(1), 151-159.
- Šponer, J., Banáš, P., Jurečka, P., Zgarbová, M., Kührová, P., Havrila, M., ... & Otyepka, M. (2014). Molecular dynamics simulations of nucleic acids. From tetranucleotides to the ribosome. *The Journal of Physical Chemistry Letters*, 5(10), 1771-1782.
- Springsteen, G., & Wang, B. (2002). A detailed examination of boronic acid–diol complexation. *Tetrahedron*, 58(26), 5291-5300.
- Staib, A., Borgis, D., & Hynes, J. T. (1995). Proton transfer in hydrogen-bonded acid–base complexes in polar solvents. *The Journal of Chemical Physics*, 102(6), 2487-2505.
- Steinfeld, J. I., Francisco, J. S., & Hase, W. L. (1999). *Chemical kinetics and dynamics*. Prentice Hall.
- Steitz, T. A. (2010). From the structure and function of the ribosome to new antibiotics (Nobel Lecture). *Angewandte Chemie International Edition*, 49(26), 4381-4398.
- Still, W. C., Tempczyk, A., Hawley, R. C., & Hendrickson, T. (1990). Semianalytical treatment of solvation for molecular mechanics and dynamics. *Journal of the American Chemical Society*, 112(16), 6127-6129.
- Stojković, V., & Kohen, A. (2009). Enzymatic H transfers: Quantum tunnelling and coupled motion from kinetic isotope effect studies. *Israel Journal of Chemistry*, 49(2), 163-173.

- Świderek, K., Tuñón, I., Martí, S., Moliner, V., & Bertrán, J. (2013). Role of solvent on nonenzymatic peptide bond formation mechanisms and kinetic isotope effects. *Journal of the American Chemical Society*, 135(23), 8708-8719.
- Świderek, K., Martí, S., Tuñón, I., Moliner, V., & Bertran, J. (2015). Peptide bond formation mechanism catalysed by ribosome. *Journal of the American Chemical Society*, 137(37), 12024-12034.
- Szalay, P. G., Müller, T., Gidofalvi, G., Lischka, H., & Shepard, R. (2011). Multiconfiguration self-consistent field and multireference configuration interaction methods and applications. *Chemical Reviews*, 112(1), 108-181.
- Tantillo, D. J., Jiangang, C., & Houk, K. N. (1998). Theozymes and compuzymes: theoretical models for biological catalysis. *Current Opinion in Chemical Biology*, 2(6), 743-750.
- Tautermann, C. S., Voegelé, A. F., Loerting, T., & Liedl, K. R. (2002). The optimal tunnelling path for the proton transfer in malonaldehyde. *The Journal of Chemical Physics*, 117(5), 1962-1966.
- Thompson, W. H. (1999). Quantum mechanical transition state theory and tunnelling corrections. *The Journal of Chemical Physics*, 110(9), 4221-4228.
- Tirado-Rives, J., & Jorgensen, W. L. (2008). Performance of B3LYP density functional methods for a large set of organic molecules. *Journal of Chemical Theory and Computation*, 4(2), 297-306.
- Toghill, K. E., & Compton, R. G. (2010). Electrochemical non-enzymatic glucose sensors: a perspective and an evaluation. *International Journal of Electrochemical Science*, 5(9), 1246-1301.
- Tomasi, J., Mennucci, B., & Cammi, R. (2005). Quantum mechanical continuum solvation models. *Chemical Reviews*, 105(8), 2999-3094.
- Tomasi, J., Mennucci, B., & Cancès, E. (1999). The IEF version of the PCM solvation method: an overview of a new method addressed to study molecular solutes at the QM ab initio level. *Journal of Molecular Structure: THEOCHEM*, 464(1), 211-226.
- Torres, E., & DiLabio, G. A. (2012). A (nearly) universally applicable method for modeling noncovalent interactions using B3LYP. *The Journal of Physical Chemistry Letters*, 3(13), 1738-1744.
- Trapp, K., Mathew, M. A., & Joseph, S. (2014). Thermodynamic and kinetic insights into stop codon recognition by release factor 1. *PLOS ONE*, 9(4), e94058.
- Trobro, S., & Åqvist, J. (2005). Mechanism of peptide bond synthesis on the ribosome. *Proceedings of the National Academy of Sciences of the United States of America*, 102(35), 12395-12400.
- Trobro, S., & Åqvist, J. (2006). Analysis of predictions for the catalytic mechanism of ribosomal peptidyl transfer. *Biochemistry*, 45(23), 7049-7056.

- Truhlar, D. G., & Garrett, B. C. (1980). Variational transition-state theory. *Accounts of Chemical Research*, 13(12), 440-448.
- Truhlar, D. G., & B. C. (1984). Variational transition state theory. *Annual Review of Physical Chemistry*, 35(1), 159-189.
- Truhlar, D. G., Isaacson, A. D., & Garrett, B. C. (1985). Generalized transition state theory. *Theory of Chemical Reaction Dynamics*, 4, 65-137.
- Truhlar, D. G., Garrett, B. C., & Klippenstein, S. J. (1996). Current status of transition-state theory. *The Journal of Physical Chemistry*, 100(31), 12771-12800.
- Truhlar, D. G. (2010). Tunnelling in enzymatic and nonenzymatic hydrogen transfer reactions. *Journal of Physical Organic Chemistry*, 23(7), 660-676.
- Truhlar, D. G. (2015). Transition state theory for enzyme kinetics. *Archives of Biochemistry and Biophysics*.
- Valley, M. P., & Fitzpatrick, P. F. (2004). Comparison of enzymatic and non-enzymatic nitroethane anion formation: thermodynamics and contribution of tunnelling. *Journal of the American Chemical Society*, 126(20), 6244-6245.
- Van't Hoff, M. J. H. (1884). Etudes de dynamique chimique. *Recueil des Travaux Chimiques des Pays-Bas*, 3(10), 333-336.
- Varandas, A. J. C. (2012). Ab initio treatment of bond-breaking reactions: accurate course of HO<sub>3</sub> dissociation and revisit to isomerization. *Journal of Chemical Theory and Computation*, 8(2), 428-441.
- Vilčiauskas, L., Tuckerman, M. E., Bester, G., Paddison, S. J., & Kreuer, K. D. (2012). The mechanism of proton conduction in phosphoric acid. *Nature Chemistry*, 4(6), 461-466.
- Voorhees, R. M., & Ramakrishnan, V. (2013). Structural Basis of the Translational Elongation Cycle. *Annual Review of Biochemistry*, 82, 203-236.
- Voorhees, R. M., Weixlbaumer, A., Loakes, D., Kelley, A. C., & Ramakrishnan, V. (2009). Insights into substrate stabilization from snapshots of the peptidyl transferase center of the intact 70S ribosome. *Nature Structural & Molecular Biology*, 16(5), 528-533.
- Voth, G. A., Chandler, D., & Miller, W. H. (1989). Rigorous formulation of quantum transition state theory and its dynamical corrections. *The Journal of Chemical Physics*, 91(12), 7749-7760.
- Wallin, G., & Åqvist, J. (2010). The transition state for peptide bond formation reveals the ribosome as a water trap. *Proceedings of the National Academy of Sciences*, 107(5), 1888-1893.

- Walter, D., Carter, E. A. (2001). Multi-reference weak pairs local configuration interaction: efficient calculations of bond breaking. *Chemical Physics Letters* 346, 177-185.
- Wang, Q., Gao, J., Liu, Y., & Liu, C. (2010). Validating a new proton shuttle reaction pathway for formation of the peptide bond in ribosomes: A theoretical investigation. *Chemical Physics Letters*, 501(1), 113-117.
- Wang, Q., Gao, J., Zhang, D., & Liu, C. (2015). A theoretical model investigation of peptide bond formation involving two water molecules in ribosome supports the two-step and eight membered ring mechanism. *Chemical Physics*, 450, 1-11.
- Warshel, A., & Bora, R. P. (2016). Perspective: Defining and quantifying the role of dynamics in enzyme catalysis. *The Journal of Chemical Physics*, 144(18), 180901.
- Watanabe, E., Miyamoto, C., Tanaka, A., Iizuka, K., Iwatsuki, S., Inamo, M., ... & Ishihara, K. (2013). Relative kinetic reactivity of boronic acid and boronate ion towards Tiron, 2, 2'-biphenol, and propylene glycol. *Dalton Transactions*, 42(23), 8446-8453.
- Watson, J. D., & Crick, F. H. (1953). Molecular structure of nucleic acids. *Nature*, 171(4356), 737-738.
- Weinger, J. S., Parnell, K. M., Dorner, S., Green, R., & Strobel, S. A. (2004). Substrate-assisted catalysis of peptide bond formation by the ribosome. *Nature Structural & Molecular Biology*, 11(11), 1101-1106.
- Wigner, E. (1932). On the quantum correction for thermodynamic equilibrium. *Physical Review*, 40(5), 749.
- Wigner, E. (1932). On the Presentation of Potential Barriers in Chemical Reactions. *Zeitschrift für Physikalische Chemie*, B19, 203.
- Wilson, S. (2014). *Electron correlation in molecules*. Courier Corporation.
- Whitman, D. W., & Carpenter, B. K. (1982). Limits on the activation parameters for automerization of cyclobutadiene-1, 2-d2. *Journal of the American Chemical Society*, 104(23), 6473-6474.
- Wohlgemuth, I., Beringer, M., & Rodnina, M. V. (2006). Rapid peptide bond formation on isolated 50S ribosomal subunits. *EMBO Reports*, 7(7), 699-703.
- Wright, M. R. (1999). *Fundamental chemical kinetics: an explanatory introduction to the concepts*. Elsevier.
- Wu, X., Li, Z., Chen, X. X., Fossey, J. S., James, T. D., & Jiang, Y. B. (2013). Selective sensing of saccharides using simple boronic acids and their aggregates. *Chemical Society Reviews*, 42(20), 8032-8048.

- Wynne-Jones, W. F. K., & Eyring, H. (1935). The absolute rate of reactions in condensed phases. *The Journal of Chemical Physics*, 3(8), 492-502.
- Xu, S. Y., Ruan, Y. B., Luo, X. X., Gao, Y. F., Zhao, J. S., Shen, J. S., & Jiang, Y. B. (2010). Enhanced saccharide sensing based on simple phenylboronic acid receptor by coupling to Suzuki homocoupling reaction. *Chemical Communications*, 46(32), 5864-5866.
- Xu, X., Yu, T., Papajak, E., & Truhlar, D. G. (2012-a). Multistructural variational transition state theory: kinetics of the hydrogen abstraction from carbon-2 of 2-methyl-1-propanol by hydroperoxyl radical including all structures and torsional anharmonicity. *The Journal of Physical Chemistry A*, 116(43), 10480-10487.
- Xu, J., Zhang, J. Z., & Xiang, Y. (2012-b). Ab initio QM/MM free energy simulations of peptide bond formation in the ribosome support an eight-membered ring reaction mechanism. *Journal of the American Chemical Society*, 134(39), 16424-16429.
- Yamamoto, T., & Miller, W. H. (2005). Path integral evaluation of the quantum instanton rate constant for proton transfer in a polar solvent. *The Journal of Chemical Physics*, 122(4), 044106.
- Yamamoto, Y., Matsumura, T., Takao, N., Yamagishi, H., Takahashi, M., Iwatsuki, S., & Ishihara, K. (2005). Fast trigonal/tetragonal interconversion followed by slow chelate-ring closure in the complexation of boronic acids. *Inorganica Chimica Acta*, 358(12), 3355-3361.
- Yonath, A. (2010). Hibernating Bears, Antibiotics, and the Evolving Ribosome (Nobel Lecture). *Angewandte Chemie International Edition*, 49(26), 4340-4354.
- Young, L., & Post, C. B. (1996). Catalysis by entropic guidance from enzymes. *Biochemistry*, 35(48), 15129-15133.
- Zaher, H. S., & Green, R. (2009). Quality control by the ribosome following peptide bond formation. *Nature*, 457(7226), 161-166.
- Zaher, H. S., Shaw, J. J., Strobel, S. A., & Green, R. (2011). The 2'-OH group of the peptidyl-tRNA stabilizes an active conformation of the ribosomal PTC. *The EMBO Journal*, 30(12), 2445-2453.
- Zangwill, A. (2013). Hartree and Thomas: the forefathers of density functional theory. *Archive for History of Exact Sciences*, 67(3), 331-348.
- Zhai, W., Sun, X., James, T. D., & Fossey, J. S. (2015). Boronic acid-based carbohydrate sensing. *Chemistry—An Asian Journal*.
- Zhang, F., & Dibble, T. S. (2011). Impact of tunnelling on hydrogen-migration of the n-propylperoxy radical. *Physical Chemistry Chemical Physics*, 13(40), 17969-17977.
- Zhang, Y., Stecher, T., Cvitaš, M. T., & Althorpe, S. C. (2014). Which is better at predicting quantum-tunnelling rates: Quantum transition-state theory or free-

energy instanton theory?. *The Journal of Physical Chemistry Letters*, 5(22), 3976-3980.

Zhao, Y., Schultz, N. E., & Truhlar, D. G. (2005). Exchange-correlation functional with broad accuracy for metallic and nonmetallic compounds, kinetics, and noncovalent interactions. *The Journal of Chemical Physics*, 123(16), 161103.

Zhao, Y., & Truhlar, D. G. (2005). Benchmark databases for nonbonded interactions and their use to test density functional theory. *Journal of Chemical Theory and Computation*, 1(3), 415-432.

Zhao, Y., & Truhlar, D. G. (2006-a). A new local density functional for main-group thermochemistry, transition metal bonding, thermochemical kinetics, and noncovalent interactions. *The Journal of Chemical Physics*, 125(19), 194101.

Zhao, Y., & Truhlar, D. G. (2006-b). Density functional for spectroscopy: no long-range self-interaction error, good performance for Rydberg and charge-transfer states, and better performance on average than B3LYP for ground states. *The Journal of Physical Chemistry A*, 110(49), 13126-13130.

Zhao, Y., & Truhlar, D. G. (2008-a). Density functionals with broad applicability in chemistry. *Accounts of Chemical Research*, 41(2), 157-167.

Zhao, Y., & Truhlar, D. G. (2008-b). The M06 suite of density functionals for main group thermochemistry, thermochemical kinetics, noncovalent interactions, excited states, and transition elements: two new functionals and systematic testing of four M06-class functionals and 12 other functionals. *Theoretical Chemistry Accounts: Theory, Computation, and Modeling (Theoretica Chimica Acta)*, 120(1), 215-241.

Zhao, Y., & Truhlar, D. G. (2008-c). Exploring the limit of accuracy of the global hybrid meta density functional for main-group thermochemistry, kinetics, and noncovalent interactions. *Journal of Chemical Theory and Computation*, 4(11), 1849-1868.

Zheng, J., Meana-Pañeda, R., & Truhlar, D. G. (2014). Including tunnelling in Non-Born–Oppenheimer Simulations. *The Journal of Physical Chemistry Letters*, 5(11), 2039-2043.

## LIST OF PUBLICATIONS AND PAPERS PRESENTED

- Monajemi, H., Daud, M. N., Mohd. Zain, S., & Wan Abdullah, W. A. T. (2012). ONIOM and ab-initio calculations on the mechanism of uncatalysed peptide bond formation. *Biochemistry and Cell Biology*, 90(6), 691-700.
- Monajemi, H., Cheah, M. H., Lee, V. S., Zain, S. M., & Wan Abdullah, W. A. T. (2014). On the kinetics and reaction mechanisms of boronic acid in interaction with diols for non-enzymatic glucose monitoring applications: a hybrid DFT study. *RSC Advances*, 4(21), 10505-10513.
- Monajemi, H., Zain, S. M., & Wan Abdullah, W. A. T. (2015). The P-site A76 2'-OH acts as a peptidyl shuttle in a stepwise peptidyl transfer mechanism. *RSC Advances*, 5(32), 25489-25503.

University of Malaysia